



**EFFECTS OF PRIOR AGING ON THE CREEP RESPONSE OF CARBON
FIBER REINFORCED PMR-15 NEAT RESIN AT 288°C IN AN AIR
ENVIRONMENT**

THESIS

Christopher A. Back, Ensign, USN

AFIT/GAE/ENY/07-J02

**DEPARTMENT OF THE AIR FORCE
AIR UNIVERSITY**

AIR FORCE INSTITUTE OF TECHNOLOGY

Wright-Patterson Air Force Base, Ohio

APPROVED FOR PUBLIC RELEASE; DISTRIBUTION UNLIMITED

The views expressed in this thesis are those of the author and do not reflect the official policy or position of the United States Air Force, Department of Defense, or the U.S. Government.

AFIT/GAE/ENY/07-J02

**EFFECTS OF PRIOR AGING ON THE CREEP RESPONSE OF CARBON FIBER
REINFORCED PMR-15 NEAT RESIN AT 288°C IN AN AIR ENVIRONMENT**

THESIS

Presented to the Faculty

Department of Aeronautical and Astronautical Engineering

Graduate School of Engineering and Management

Air Force Institute of Technology

Air University

Air Education and Training Command

In Partial Fulfillment of the Requirements for the
Degree of Master of Science in Aeronautical Engineering

Christopher A. Back, BS

Ensign, USN

June 2007

APPROVED FOR PUBLIC RELEASE; DISTRIBUTION UNLIMITED

AFIT/GAE/ENY/07-J02

**EFFECTS OF PRIOR AGING ON THE CREEP RESPONSE OF CARBON
FIBER REINFORCED PMR-15 NEAT RESIN AT 288°C IN AN AIR
ENVIRONMENT**

Christopher A. Back, BS

Ensign, USN

Approved:

//SIGNED//
Dr. Marina Ruggles-Wrenn, (Chairman)

Date

//SIGNED//
Dr. Richard Hall, (Member)

Date

//SIGNED//
Dr. Greg. Schoeppner, (Member)

Date

Abstract

The mechanical response of carbon fiber reinforced PMR-15 neat resin with a ± 45 fiber orientation was investigated at 288°C. Mechanical testing was performed on unaged specimens and specimens that were aged up to 1000 hours in an air environment. Tensile tests were performed to determine Young's modulus of elasticity and Ultimate Tensile Strength. Creep tests were performed at creep stress levels of 30 and 60 MPa. Creep periods of at least 25 h in duration were followed by recovery at zero stress. Duration of the recovery period was at least twice the time of the creep period. Oxidation layer growth and weight loss measurements were also taken as a function of aging time. Unaged test specimens accumulated creep strains of ~1.7% at 60 MPa and ~1.1% at 30 MPa. After 1000 h of aging the test specimens accumulated creep strains of ~0.5% at 60 MPa and ~0.1% at 30 MPa. It is clear that with prior aging time, there is a reduction in creep strain accumulation. Prior aging did not appear to significantly influence recovery at zero stress. The experimental data revealed that weight loss and oxidation layer growth increase with increasing aging time at elevated temperature. After 500 h of aging, the rectangular ± 45 carbon fiber reinforced PMR-15 composite had ~0.95% weight loss compared to ~0.5% at 250 h. The oxidation layer growth at 500 h was ~0.97 mm for the cut surface and ~0.32 mm for the molded surface. After 1000 h the oxidation layer growth was ~1.5 mm for the cut surface and ~0.33 mm for the molded surface. It is apparent that the cut side of the specimen with the fibers exposed to the oxidizing environment experiences a thicker oxidation layer growth.

Acknowledgments

I would like to express my sincere appreciation to my wonderful faculty advisor, Dr. Marina Ruggles-Wrenn, for always providing her time to help guide and support me throughout this thesis effort. She provided me with advice and created a path that I could follow in order to complete the mission. I would also like to thank the following individuals for their assistance: the support staff in the Structures and Materials Testing Laboratory for their experience and technical assistance, the AFRL/MLBC staff for their support, Dr. Greg Schoeppner (AFRL/MLBCM), Dr. Charles Y-C Lee (AFOSR/NE), and Dr. Richard Hall (AFRL/MLBCM) for their sponsorship of my thesis. It was also nice to have the support of my family, my friends, and my fellow classmates. Without all of you this thesis would not have been such a great experience.

Christopher A. Back

Table of Contents

	Page
Abstract.....	iv
Acknowledgments.....	v
Table of Contents.....	vi
List of Figures.....	x
List of Tables.....	xvi
I. Introduction	1
Background.....	1
Thesis Objective	5
Assumptions/Limitations.....	6
Methodology.....	7
Implications	7
II. Literature Review	8
Chapter Overview.....	8
Synthesis and Processing of PMR-15 Resin	8
Different Forms of Degradation and their Effect on Mechanical Behavior.....	9
Thermal Oxidative Stability and Degradation.....	11
Summary.....	26
III. Material and Specimen	27
Chapter Overview.....	27
CYCOM 2237/PMR-15.....	27
<i>Specimen Fabrication</i>	27
Material Processing.....	27

	Page
Specimen Geometry	29
Specimen Tabbng	30
Aging.....	31
Relative Humidity	33
IV. Experimental Setup and Testing Procedures	34
Chapter Overview.....	34
<i>Test Equipment</i>	34
Servo Hydraulic Machine	34
Cooling System.....	35
Extensometer.....	36
Computer Software	38
High Temperature Equipment.....	39
<i>Experimental Procedures</i>	41
Determining Test Temperature	41
Test Procedures.....	42
<i>Test Descriptions</i>	43
Initial Elastic Modulus Measurements.....	43
Monotonic Tensile Test	44
Creep Tests.....	44
Weight Measurements and Oxidation Layer Growth	45
Summary.....	48

	Page
V. Results and Discussion.....	49
Chapter Overview.....	49
Weight Loss Measurements	49
Oxidation Layer Thickness.....	53
<i>Elastic Modulus</i>	57
Initial Room Temperature Modulus.....	57
Aged Modulus versus Initial Modulus.....	59
Elastic Modulus upon Loading and Unloading	61
Elastic Modulus Ratios	65
<i>Monotonic Tensile Tests</i>	70
Tensile Tests for Aged and Unaged Test Specimens.....	70
<i>Creep Tests</i>	73
Creep Tests of Unaged Specimens	73
Creep Tests at 60 MPa	75
Creep Tests at 30 MPa	76
Recovery at Zero Stress after 60 MPa Creep Test.....	79
VI. Concluding Remarks	84
Chapter Overview.....	84
Concluding Remarks	84
Bibliography	88
Appendix A – Fracture micrographs for test specimens subjected to tensile testing at 288°C	91

	Page
Appendix B – Oxidation Layer Growth on Cut and Uncut Surfaces of Test Specimens Aged in Air at 288°C	101

List of Figures

Page

Figure 1: Elevated and room-temperature mechanical properties of DMBZ and PMR-15 composites (left - interlaminar strength, center – flexural modulus, right – flexural strength). Figure from Ref. [13].	3
Figure 2: Structures of PMR polyimides. Figure from Ref. [27].	4
Figure 3: Synthesis and Processing of PMR-15. Figure from Ref. [12].	9
Figure 4: Weight loss as a function of short aging times at 288°C for T-650-35/PMR-15 composite. Figure from Ref. [7].	14
Figure 5: Weight loss as a function of long aging times at 288°C for T-650-35/PMR-15 composite. Figure from Ref. [7].	14
Figure 6: Shrinkage of T-650-35/PMR-15 composite specimens with aging at 288°C. Figure from Ref. [7].	15
Figure 7: Surface layer thickness of T-650-35/PMR-15 composite specimens as a function of aging at 288°C. Figure from Ref [7].	15
Figure 8: Oxidation measurement procedures. Figure from Ref. [22].	17
Figure 9: Oxidation of unidirectional G30-500/PMR-15 composites at 288°C. Figure from Ref. [22].	18
Figure 10: A close-up view of an oxidized fiber end. Figure from Ref. [22].	18
Figure 11: Surface area types for unidirectional and woven composites. Figure from Ref. [22].	19
Figure 12: Comparison of oxidation growth in S_1 and S_3 directions of unidirectional composites. Figure from Ref. [22].	20
Figure 13: Comparison of oxidation growth in transverse direction S_1 of composite and in neat resin PMR-15. Figure from Ref. [22].	21
Figure 14: Surface oxidation of T650-35/PMR-15 composite specimens aged in air. (a) Aged 1000 hours at 316°C. (b) Aged 10,000 hours at 204°C. Figure from Ref. [4].	23

Figure 15: Photo micrographs of the axial surface of a unidirectional specimen aged for 1,864 hours at 288°C showing (a) matrix cracking perpendicular to fiber ends, (b) close-up view of a matrix crack providing a pathway for enhanced diffusion. Figure from Ref. [22].	24
Figure 16: Compression strengths and moduli of T650-35/PMR-15 sections cut from a single specimen. Figure from Ref. [6].	25
Figure 17: Stored moduli of a T650-35/PMR-15 composite aged in air at 360°C for 2,090 hours as a function of temperature for different depth cuts. Figure from Ref. [6].	26
Figure 18: Dog bone test specimen with nominal dimensions. Figure from Ref. [14].	29
Figure 19: A test specimen before being tabbed.	30
Figure 20: A test specimen after being tabbed.	31
Figure 21: Aging chamber	32
Figure 22: 3 KIP MTS hydraulic machine.	35
Figure 23: MTS High temperature axial extensometer assembly with heat shield	37
Figure 24: MTS High Temperature Axial Extensometer Attached to the Test Specimen	37
Figure 25: MPT creep test procedure. Figure from Ref. [14].	38
Figure 26: Temperature controller	40
Figure 27: Furnace	40
Figure 28: Temperature calibration specimen with two attached k-type thermocouples.	42
Figure 29: ZEISS Discovery.V12 Model Stereo Microscope	45
Figure 30: Metler Toledo AG245 Microbalance	46
Figure 31: Buehler PowerPro 5000 Variable Speed Grinder-Polisher	47
Figure 32: Sections of test specimens ready to be analyzed for oxidation growth after being mounted, sanded, and polished.	47
Figure 33: Weight loss factor as a function of aging time for carbon fiber reinforced PMR-15 neat resin at 288°C in air.	50
Figure 34: Percent weight loss as a function of aging time for carbon fiber reinforced PMR-15 neat resin aged in air at 288°C.	52

Figure 35: Optical micrograph showing the oxidation layer on the cut surface with the exposed fiber edges for the carbon fiber reinforced PMR-15 composite aged for 500 h at 288°C in air.	54
Figure 36: Optical micrograph showing the oxidation layer on the molded outer surface of a carbon fiber reinforced PMR-15 composite aged for 1000 h in air at 288°C.....	55
Figure 37: Oxidation layer thickness measure on both cross sectional cut and uncut surfaces as a function of aging time in air at 288°C for carbon fiber reinforced PMR-15 neat resin.	56
Figure 38: Initial room temperature elastic modulus data as a function of test specimens from a single panel, with a 95% confidence interval for each test specimen. This figure was produced using the MiniTab program.	58
Figure 39: Elastic modulus of aged samples measured at 288°C versus initial room temperature elastic modulus for carbon fiber reinforced PMR-15 neat resin.....	60
Figure 40: Tensile stress-strain curves during loading obtained in all tests at 288°C.	61
Figure 41: Elastic modulus upon loading versus aging time in air at 288°C for carbon fiber reinforced PMR-15 neat resin.	62
Figure 42: Elastic modulus obtained upon unloading versus aging time in air at various creep stress levels where carbon fiber reinforced PMR-15 composites were tested at 288°C.	63
Figure 43: Change in elastic modulus between loading and unloading moduli as a function of aging time.....	64
Figure 44: Elastic modulus ratios versus aging time in air for carbon fiber reinforced PMR-15 composites aged at 288°C and tested in creep at 60 MPa at 288°C.....	66
Figure 45: Ratio of elastic modulus measured upon loading to the initial room temperature elastic modulus as a function of aging time for carbon fiber reinforced PMR-15 composites tested in creep at 30 and 60 MPa.	67

Figure 46: Ratio of elastic modulus measured upon unloading to the elastic modulus measured upon loading as a function of aging time for carbon fiber reinforced PMR-15 composites tested in creep at 30 and 60 MPa.	68
Figure 47: Ratio of elastic modulus measured upon unloading to the initial room temperature elastic modulus as a function of aging time for carbon fiber reinforced PMR-15 composites tested in creep at 30 and 60 MPa.	69
Figure 48: Stress-strain curves for aged and unaged specimens at 288°C during tensile testing.	71
Figure 49: The strain as a function of time that it took the aged and unaged carbon fiber reinforced PMR-15 neat resin specimens to fracture at 288°C.	73
Figure 50: Creep stress versus strain curves for the unaged (as-processed) carbon fiber reinforced PMR-15 neat resin at 288°C.	74
Figure 51: Creep stress versus strain curves for carbon fiber reinforced PMR-15 neat resin aged in air at 288°C at a creep stress level of 60 MPa.	76
Figure 52: Creep stress versus strain curves for carbon fiber reinforced PMR-15 neat resin aged in air at 288°C at a creep stress level of 30 MPa.	77
Figure 53: Creep strain accumulated in 25 h as a function of aging time for carbon fiber reinforced PMR-15 neat resin.	78
Figure 54: Recovery curves for carbon fiber reinforced PMR-15 neat resin aged in air at 288°C with a prior creep stress of 60 MPa at 288°C.	79
Figure 55: Schematic stress-strain curve for a constant stress creep period followed by recovery period at zero stress. Figure from Ref. [10].	80
Figure 56: Recovered Strain versus time curves for carbon fiber reinforced PMR-15 neat resin aged in air at 288°C and exposed to a prior creep stress of 60 MPa at 288°C.	81
Figure 57: Creep recovery curves for carbon fiber reinforced PMR-15 neat resin aged in air at 288°C with a prior creep stress of 60 MPa.	83
Figure 58: Carbon fiber reinforced PMR-15 neat resin unaged specimen 1	91
Figure 59: Carbon fiber reinforced PMR-15 neat resin unaged specimen 1 (top view)...	92

Figure 60: Carbon fiber reinforced PMR-15 neat resin unaged specimen 4 (side view).	93
Figure 61: Carbon fiber reinforced PMR-15 neat resin unaged specimen 4 (top view)...	94
Figure 62: Carbon fiber reinforced PMR-15 neat resin specimen 7 aged in air for 50 h at 288°C (side view).	95
Figure 63: Carbon fiber reinforced PMR-15 neat resin specimen 7 aged in air for 50 h at 288°C (top view).....	96
Figure 64: Carbon fiber reinforced PMR-15 neat resin specimen 9 aged in air for 100 h at 288°C (side view).	97
Figure 65: Carbon fiber reinforced PMR-15 neat resin specimen 9 aged in air for 100 h at 288°C (top view).....	98
Figure 66: Carbon fiber reinforced PMR-15 neat resin specimen 17 aged in air for 1000 h at 288°C (side view).	99
Figure 67: Carbon fiber reinforced PMR-15 neat resin specimen 17 aged in air for 1000 h at 288°C (top view).....	100
Figure 68: Oxidation layer growth on a specimen aged for 1000 h at 288°C (cut surface). This shows an average oxidation layer of 1.58 mm thick.....	101
Figure 69: Oxidation layer growth on a specimen aged for 1000 h at 288°C (uncut surface).....	101
Figure 70: Oxidation layer growth on a specimen aged for 500 h at 288°C (cut surface). This shows an average oxidation layer of 1.04 mm thick.....	102
Figure 71: Oxidation layer growth on a specimen aged for 500 h at 288°C (uncut surface).....	102
Figure 72: Oxidation layer growth on a specimen aged for 100 h at 288°C (cut surface). This shows an average oxidation layer of 0.42 mm thick.....	103
Figure 73: Oxidation layer growth on a specimen aged for 100 h at 288°C (uncut surface).....	103
Figure 74: Oxidation layer growth on a specimen aged for 50 h at 288°C (cut surface). This shows an oxidation layer of 0.28 mm thick.	104

Figure 75: Oxidation layer growth on a specimen aged for 50 h at 288°C (uncut surface).	
.....	104
Figure 76: Oxidation layer growth on a specimen aged for 50 h at 288°C (uncut surface).	
.....	105

List of Tables

Page

Table 1	12
from TGA Kinetics	12
Table 2: T650-35/PMR-15 composite compression test specimen nominal dimensions. Table from Ref. [7].	13
Table 3: Dimensions of the four specimen geometries. Table from Ref. [24].	16
Table 4: Steps for HyComps laminate cure cycle.....	28
Table 5: Steps for HyComps free-standing post-cure cycle	28
Table 6: Elastic modulus and UTS measurements for test specimens subjected to tensile testing at 288°C.....	72

EFFECTS OF PRIOR AGING ON THE CREEP RESPONSE OF CARBON FIBER REINFORCED PMR-15 NEAT RESIN AT 288°C IN AN AIR ENVIRONMENT

I. Introduction

Background

Advanced polymer matrix composites (PMCs) are used for their many advantages including: light weight, high specific strength and stiffness, increased flexibility of design, and their property tailorability. For the last 50 years, PMCs have been manufactured in the United States and have become very important applications in both military and civilian aircraft structural components [9]. During the 1970s, fighter aircraft such as the Navy's F-14 Tomcat and the Air Forces F-15 Eagle had about 2 to 4 percent by weight carbon-epoxy composites. In the 1990s, the usage of PMCs on military fighters increased from 15 to 30 percent by weight for the A-6 Intruder, Curtiss A-8, Navy F/A-18 Hornet, and the Air Force F/A-22 Raptor. Today, PMCs make up the whole airframe of the Marine Corps V-22 Osprey [9]. In the 1980s, PMCs became major players in constructing the next generation of civilian aircraft to include the Boeing 757 and the Airbus A310. Polymer matrix composite applications to these commercial airliners included secondary structures such as fairings and empennage cover panels, as well as flight controls such as elevators, ailerons, and rudders [16].

When designing aeronautical vehicles, compliance of the PMCs with the surrounding environment is a major consideration in material selection. Applications for PMCs are categorized based on operation temperature. PMCs on both air and land

vehicles encounter extreme temperatures ranging from -150°C to 550°C [9]. The need for lightweight High Temperature Polymer Matrix Composites (HTPMCs) has become very important in the aerospace community.

PMR-15 (Polymerization of Monomeric Reactants-15), developed in the 1970s at the National Air and Space Administration (NASA) Lewis Research Center, is one of the most widely used thermosetting polyimide resins for high-temperature polymer-matrix composite applications. Of the many high-temperature resins, PMR-15 has good overall thermo-oxidative stability (TOS), processing, behavior, and retention of mechanical properties up to temperatures around 316°C [17]. PMR-15 polyimide composites have a glass transition temperature (T_g) of 348°C. Composite materials must be used below their T_g . After multiple studies the long-term temperature use of PMR-15 composites is 288°C [14]. PMR-15 has good stability and performance at temperatures up to 288°C [13]. Carbon/PMR-15 composites are excellent for structural components such as jet engine housings, wings, and nose cones [17]. PMR-15 is also being used in the development of a variety of engine components such as compression molded bearings and structural autoclave-molded engine ducts used on the F404 engine for the Navy F/A-18 Hornet [18].

Unfortunately, PMR-15 is made with methylene dianiline (MDA), a known animal mutagen and a suspected human carcinogen. Safety and economic concerns have caused some airlines to eliminate PMR-15 components from engines in their fleets [13]. The search for a less-toxic MDA replacement monomer has been difficult because of the requirement to match the properties offered by MDA in production, and in the ultimate

properties of the PMR-15 resin [19]. One material that the NASA Lewis Research Center is working on is T650-35 carbon fiber reinforced laminates with thermosetting DMBZ-15 polyimides. The glass transition temperatures of these laminates are about 50°C higher than those of the T650-35/PMR-15 composites (400°C versus 348°C). Moreover, DMBZ-15 polyimide composites had weight loss measurements close to those of PMR-15 polyimide composites (0.9% versus 0.7%). In Figure 1, one can see that T650-35 reinforced PMR-15 and DMBZ-15 polyimide laminates have comparable mechanical properties at elevated (288°C) and room temperature [13]. The chemical structures of DMBZ-15 and PMR-15 can be seen in Figure 2.

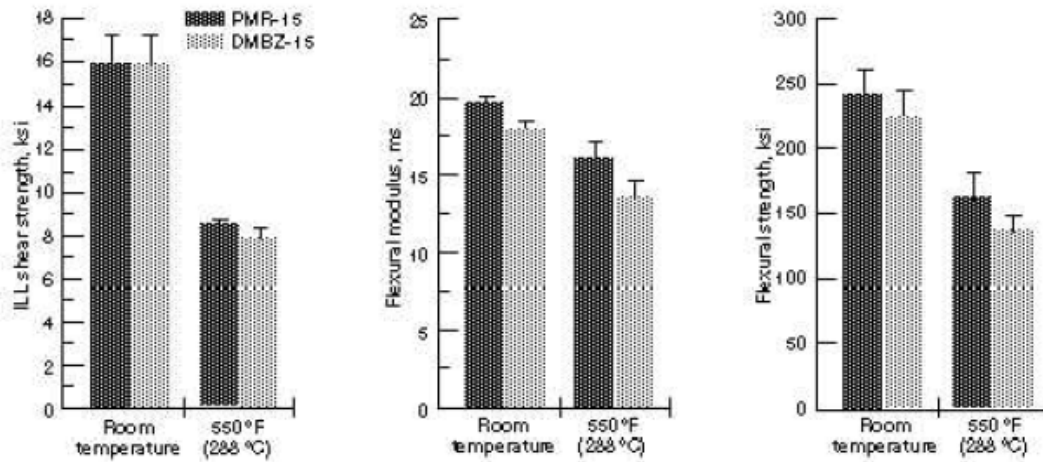


Figure 1: Elevated and room-temperature mechanical properties of DMBZ and PMR-15 composites (left - interlaminar strength, center – flexural modulus, right – flexural strength). Figure from Ref. [13].

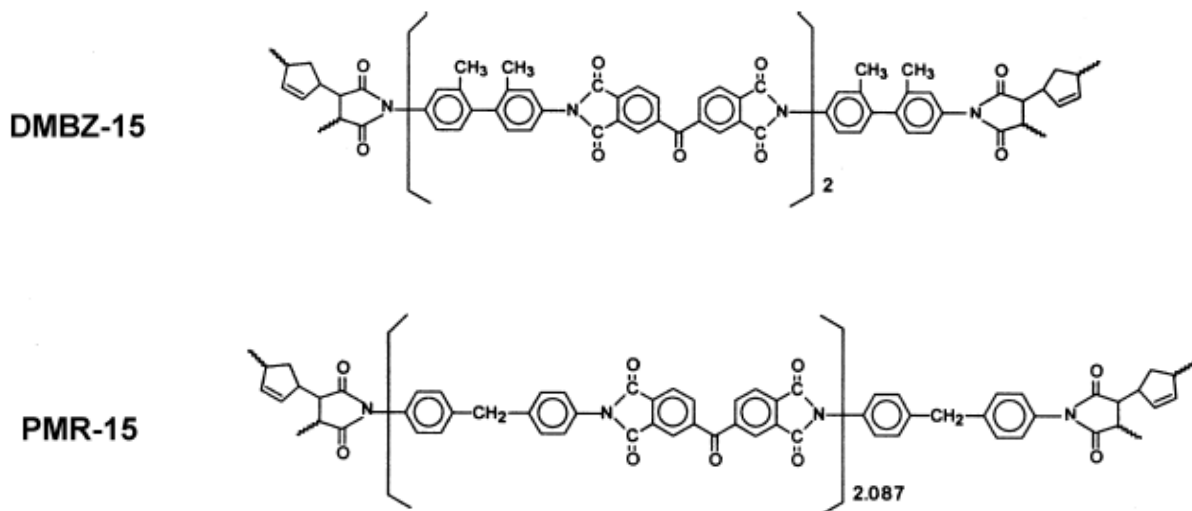


Figure 2: Structures of PMR polyimides. Figure from Ref. [27]

With a growing need for stronger aerospace applications, HTPMCs reinforced with fibers are being increasingly utilized [8]. The usage of these composites should allow for the replacement of heavy metal engine components to provide a greater thrust to weight ratio [15]. Furthermore, the overall oxidative stability of PMR-15 composites might be improved by the use of a more thermal oxidatively stable fiber [25]. With fiber reinforcement, researchers hope that this could lead to higher operating temperatures and a more stable material. Current interests in aircraft engine structures applications are focused on HTPMCs with use temperatures in air at 371°C, and eventually in temperatures as high as 416°C [8].

The use of HTPMCs in turbine engine and high speed aircraft skin applications requires durable materials that can be exposed to oxidizing high temperature environments while maintaining their thermo-mechanical properties and long term structural integrity. Aging due to oxidation refers to chemical changes as a result of the

polyimide reacting with oxygen at elevated temperatures. Oxidation is characterized by the reduction in molecular weight as a result of breaking chemical bonds, and weight loss associated with out gassing of oxidation by-products. The oxidation reaction rate is diffusion controlled rather than reaction controlled [21]. Severe surface oxidation degradation results in the formation of transverse surface cracks which not only reduce strength, but also create pathways for oxygen to penetrate deeper into the polymer matrix. It is typical for the tensile strength, strain to failure, flexural strength, density, and toughness to decrease while the modulus increases within the oxidized layer of the polymer [23]. The oxidation layers formed on the carbon fiber reinforced PMR-15 composite due to aging at 288°C will be analyzed in this study.

This thesis research explores the effects of thermal oxidative degradation on the mechanical properties and creep response on carbon fiber reinforced PMR-15 composites at 288°C. The results gathered from this research will add to the information already known for the thermo-oxidative stability, mechanical properties, and creep response behavior of carbon fiber reinforced PMR-15 composites. These results will be critical in determining the safe use of carbon fiber reinforced PMR-15 components in high performance applications such as aircraft engines.

Thesis Objective

The objective of this research is to characterize the mechanical properties and creep response behavior of carbon fiber reinforced PMR-15 neat resin that was exposed (aged) for different lengths of time in air at an elevated temperature of 288°C. This study will explain the evolution of Young's Elastic Modulus and creep response behavior with

prior aging time. Furthermore, weight loss and oxidized layer growth of carbon fiber reinforced PMR-15 composites are analyzed as functions of aging time at elevated temperature. The results of this study will further help us to understand the mechanical property degradation of the carbon fiber reinforced PMR-15 neat resin at high temperature and extended periods of prior exposure to air. The collected data will help to determine if carbon fiber reinforced PMR-15 composites can be reliable in aerospace structural applications.

Assumptions/Limitations

There were many assumptions made in this thesis research. Most importantly, the oxidation of the carbon fiber reinforced PMR-15 is negligible at ambient temperatures. This assumption is common in many studies since the material is exposed to air immediately after the manufacturing process and prior to actual testing. Oxidation present on the surface of the specimens is determined to be unavoidable and will have negligible effects on the mechanical properties of the specimens. The aging chamber was open for specimen removal and weight measurements, and to put the specimens into the dessicator. Common to many aging studies, it is assumed that the thermal cycling of the specimens during heating and cooling periods does not introduce factors contributing to the degradation of carbon fiber reinforced PMR-15. Lastly, it is also assumed that all testing was done in a moisture free (dry) environment.

Methodology

This study was completed in many different stages. The first stage was to find the elastic modulus of the as-processed carbon fiber reinforced PMR-15 neat resin to analyze the specimen-to-specimen variability in the elastic modulus. The second step was to expose the specimens to air for various durations of time at an elevated temperature of 288°C. After aging, some of the specimens were subjected to axial tensile testing. Loading and unloading elastic moduli, creep response, weight loss, and oxidation layer growth were also characterized.

Implications

The results that are gathered from the mechanical testing in this study will have implications on future applications of this material. With the growing need for high strength, low weight, high temperature materials for aerospace structures, PMCs reinforced with carbon fibers will be needed. This research will help to expand the knowledge of carbon fiber reinforced PMR-15 composites for use in structural components.

II. Literature Review

Chapter Overview

This section will discuss published material that addresses the issues pertinent to this thesis. Much of this literature addresses the assumptions that make this work possible, and in many cases have proven the assumptions to be true. The literature that was reviewed covers the current knowledge on the effects of prior exposure time in air at elevated temperatures on the mechanical properties and thermal-oxidative degradation of fiber reinforced PMR-15 neat resin. First, the basic chemical make-up of PMR-15 and the general theories of polymer degradation will be discussed.

Synthesis and Processing of PMR-15 Resin

PMR stands for the polymerization of monomer reactants. PMR-15, the most used PMR polyimide is processed using 3 monomers. It is formulated from a monoalkyl ester of 5-norbornene-2,3-dicarboxylic acid (nadic ester, NE), 4,4'-methylene dianiline (MDA) and dimethyl ester of 3,3',4,4'-benzophenonetetracarboxylic acid (BTDE) which is dissolved in a low-boiling alkyl alcohol (methyl or ethyl alcohol). The monomers are combined in a 2.00 : 3.087 : 2.087 molar ratio which corresponds to a 1500 average molecular weight for the imidized prepolymer. Once dissolved, the monomeric solution is used to impregnate the reinforcing fibers. Mentioned above, a norbene end-capped low molecular weight imide prepolymer is formed when the monomers undergo *in situ* cyclodehydration. A composite material with excellent thermal and mechanical properties is formed after addition polymerization through the nadic endcaps occurs directly on the fiber surfaces. An attractive feature of the synthesis process is the fact that there is little

evolution of volatile materials during the final curing step [12]. The synthesis process for PMR-15 is shown in Figure 3.

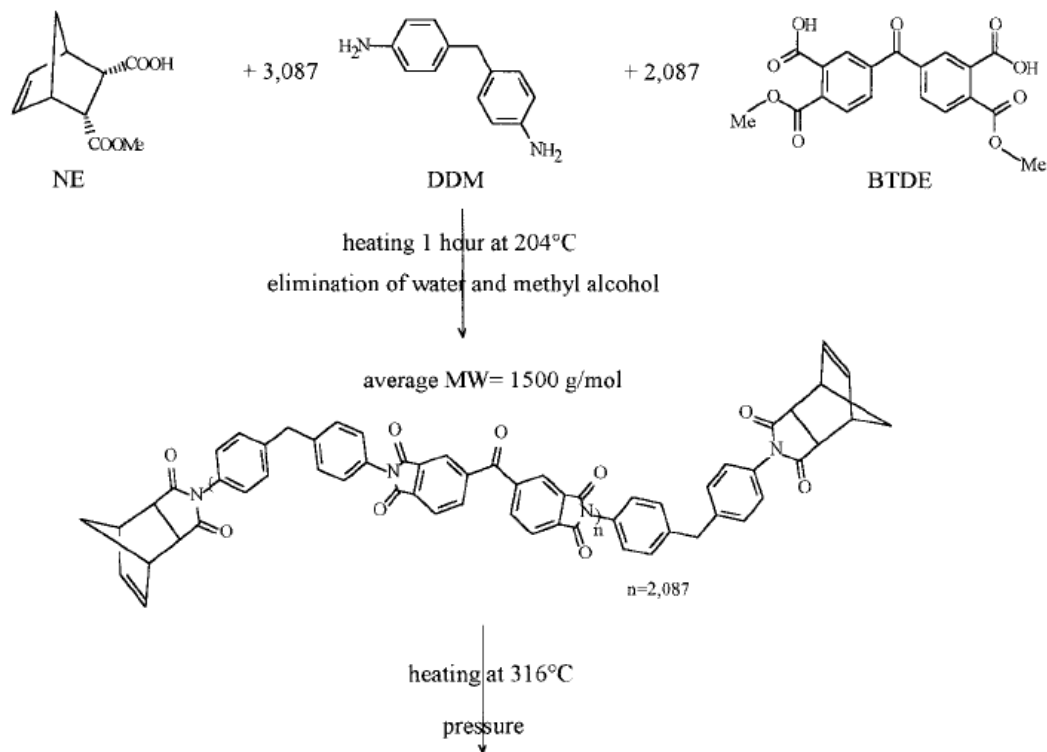


Figure 3: Synthesis and Processing of PMR-15. Figure from Ref. [12].

Different Forms of Degradation and their Effect on Mechanical Behavior

The importance of understanding the general theories behind polymer degradation is important to this study. Although this is not the focus of this research, it will help to realize the effects that physical, chemical, and oxidation degradation changes have due to the environment and temperature changes over an extended period of time.

Physical aging is defined as the thermodynamically reversible volumetric response due to slow evolution toward thermodynamic equilibrium. Physical aging is very dependent on the polymer's glass transition temperature. When below a polymer systems glass transition temperature, the material is in a non-equilibrium state and undergoes a time-dependent rearrangement toward thermodynamic equilibrium. While the system is rearranging (relaxing) toward a state of equilibrium, there are changes in enthalpy, entropy, volume, and mechanical properties. HTPMCs generally operate at temperatures near their initial design T_g , and any changes in the local T_g can have severe effects on performance. Physical aging is typically characterized by changes in yield stress, density, viscosity, stiffness, fracture energy (toughness), diffusivity, and embrittlement in some polymer systems. Physical aging may also affect the time-dependent mechanical properties (creep and stress relaxation) and rate dependent failure processes [24].

Chemical aging, unlike physical aging, is generally defined as the nonreversible volumetric response due to chain scission reactions, additional cross linking, or reduction in cross-link density, hydrolysis (chemical reaction of polymer with water), depolymerization, and plasticization. In this research, the dominant chemical aging process is thermo-oxidative aging, which is the nonreversible surface diffusion response and chemical changes occurring during oxidation of a polymer [24]. Typical effects of chemical aging include lower molecular weight, etching of the surface, discoloration, voids, and hardening [10].

Finally, oxidation aging refers to the chemical changes as a result of the polyimide reacting with oxygen at elevated temperatures. Oxidation is generally characterized by the reduction in molecular weight as a result of chemical bond breakage, and the loss in weight associated with out gassing of oxidation by-products [21]. The rate of oxidation can be greater than the rate of oxygen into the polymer, for which, the oxidative process is diffusion rate limited. It is typical that the tensile strength, strain to failure, flexural strength, toughness, and density decrease while the modulus increases within the oxidized region of the polymer [24]. Severe surface oxidation degradation results in the formation of transverse surface cracks that not only reduce strength, but also create enhanced pathways for oxygen to penetrate deeper into the polymer system [23]. The size of the crack opening width typically increases with aging time due to material loss as a consequence of the oxidation process [20].

Thermal Oxidative Stability and Degradation

Sheppard [25] carried out an investigation of the thermal oxidative stability of a number of PMR-15 composites made with different carbon fibers and fiber finishes. In an attempt to develop specifications for the use of this material, it was observed that the thermal oxidative stability of PMR-15 composites was not only influenced by the curing conditions, but also significantly with the kind of fiber. Because isothermal aging is expensive and time consuming, Sheppard used thermal gravimetric analysis (TGA) to supplement isothermal aging. Five types of fibers were used in this investigation: Cleanese G40 X – Modulus 40M psi, Hitco Hites 46 – Modulus 46M psi, Union Carbide

T40 – Modulus 40M psi, Hercules IM6 – Modulus 40M psi, and Celanese 6000 – Modulus 32M psi.

The fibers were screened by TGA kinetics, using the method of Flynn and Wall as incorporated into the computer software of the DuPont 1090 Thermal Analyzer. This thermal gravimetric analysis decomposition kinetics program was used to make a number of TGA runs with different rates and converting the resulting data to a kinetic equation representing the systems overall decomposition kinetics. The software calculates a 60 minute half-life temperature and plots an estimated lifetime, a particular degree of conversion (5% weight loss) versus reciprocal temperature. The estimated lifetimes at 288°C are shown in Table 1.

Table 1 Predicted Aging of Fibers at 550°F (288°C) from TGA Kinetics			
Fiber	Time to Lose 5% Weight (h)	Activation Energy	Pre-exponential Factor
Celanese G40X	180,000	176	2.37×10^8
Hitco Hitex 46	65,000	177	4.87×10^8
Union Carbide T40B	28,000	128	2.7×10^4
Hercules IM6	650	133	2.84×10^6
Celion 6000	550	99	2.6×10^3

Bowles et. al. [7] preformed a study on the effects of long-term aging at elevated temperatures on compression and thermal durability properties of T650-35 fabric-reinforced PMR-15 composites. The aging temperatures were 204, 260, 288, 316, and 343°C. However, the main focus of this review will be on the changes that occurred at 288°C. Specimens with different dimensions were evaluated. All property changes were

thickness dependent in this study, and weight loss, degraded surface layer growth, thickness changes, and failure modes were monitored and recorded. The composite materials were aged in air-circulating ovens at the specified temperatures, and were conditioned at 125°C for 16 hours before compression testing. During testing, no tabs were used and strain was measured with an extensometer, and moduli were measured using strains and loads at 500 and 1500 microstrain. Thickness changes were calculated prior to aging and at the end of the aging period. Oxidation layer thickness measurements were made from photomicrographs that were taken using differential interference contrast (DIC) to accent the difference in gray tones at the damage surface interface with the visibly undamaged core. In Table 2, the nominal test specimen dimensions are shown. Results of this study at 288°C can be seen in the Figures 4, 5, 6, and 7 below.

Specimen	Length, cm	Width, cm	Thickness, cm	Edge area, percent
T-3	8.94	10.83	0.13	2.7
T-5	8.94	10.83	.25	5.4
T-12	8.94	10.83	.75	11.9
T-50	4.61	1.80	1.30	50.3

Table 2: T650-35/PMR-15 composite compression test specimen nominal dimensions. Table from Ref. [7].

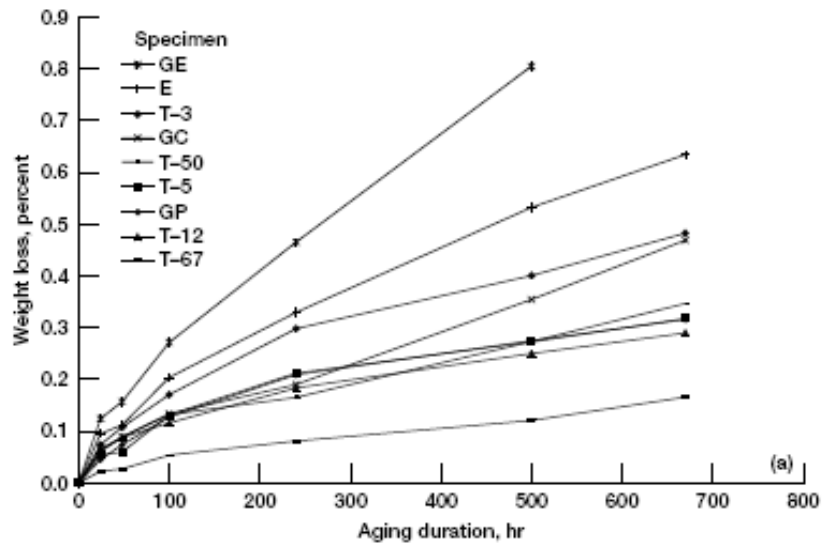


Figure 4: Weight loss as a function of short aging times at 288°C for T-650-35/PMR-15 composite. Figure from Ref. [7].

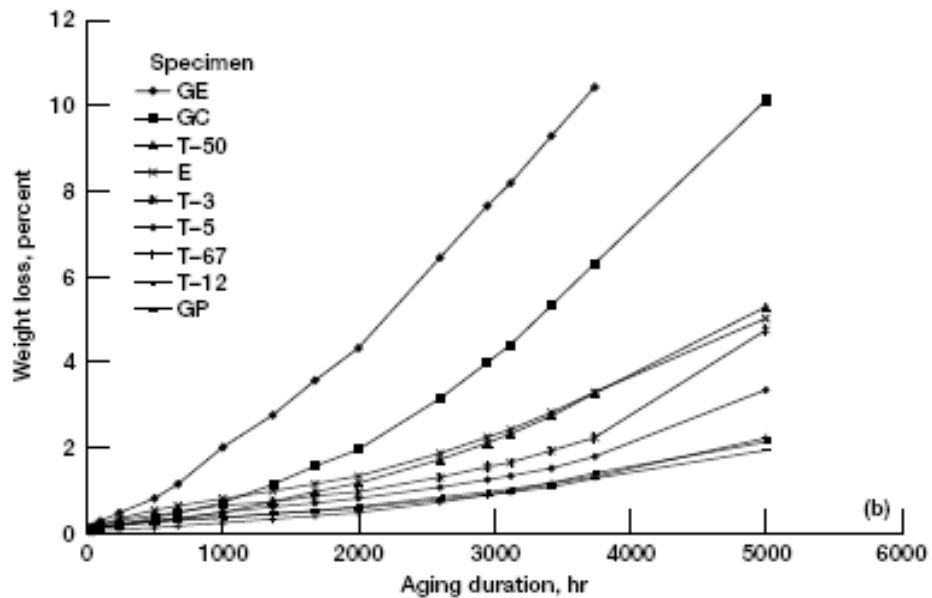


Figure 5: Weight loss as a function of long aging times at 288°C for T-650-35/PMR-15 composite. Figure from Ref. [7].

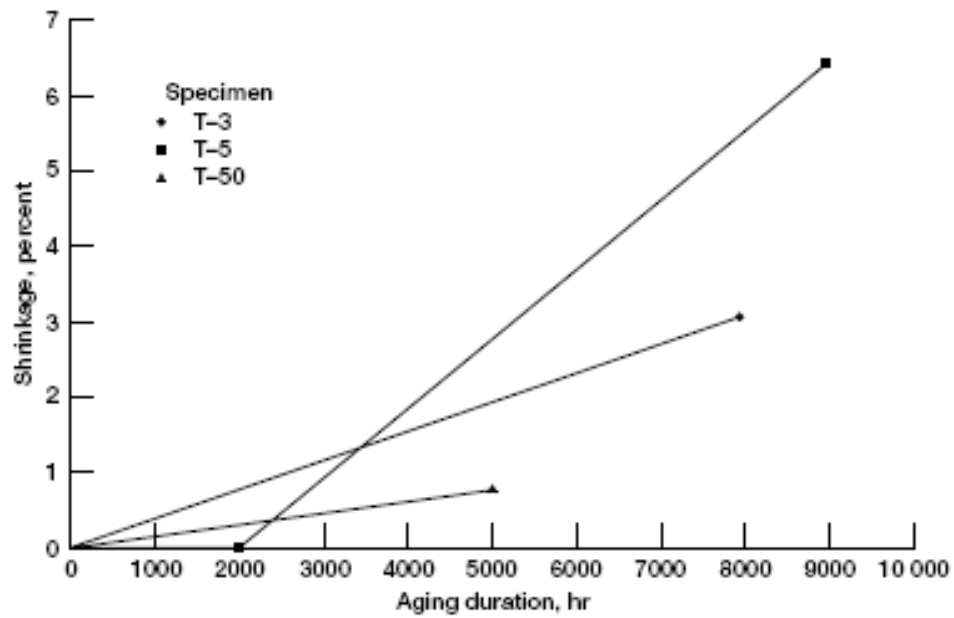


Figure 6: Shrinkage of T-650-35/PMR-15 composite specimens with aging at 288°C. Figure from Ref. [7].

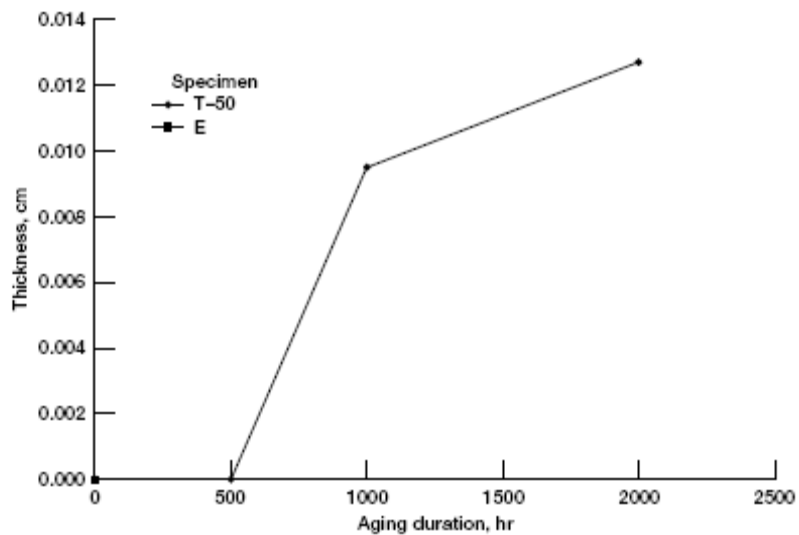


Figure 7: Surface layer thickness of T-650-35/PMR-15 composite specimens as a function of aging at 288°C. Figure from Ref [7].

Schoeppner et. al. [22] examined graphite/polyimide G30-500/PMR-15 composite specimens aged in air and argon at 288°C in order to measure volume and weight changes. The propagation of oxidation in the fiber (axial) direction and the transverse direction were also examined, and compared to the oxidation propagation rate in neat resin specimens. Time and temperature dependent surface weight loss rates are also presented and compared to the neat resin surface. In this review, the aging in argon will not be pertinent.

The specimens were cut from a 16 ply unidirectional cured panel. The panel was post-cured at 316°C for 16 hours in air. From the panel, four specimen geometries representing four different surface area ratios were cut. The dimensions for these specimens can be seen in Table 3. In addition, two specimens were cut from the panel in order to monitor the propagation rate of oxidation along the length of the fibers and transverse to the fibers. These two specimens had the dimensions: 60 mm x 7.6 mm x 2.54 mm.

Specimen	Width (mm) – axial	Length (mm) – transverse	Thickness (mm)
R1	37.77	7.57	2.47
R2	17.52	17.58	2.44
R3	25.09	25.08	2.39
R4	7.58	37.76	2.70

Table 3: Dimensions of the four specimen geometries. Table from Ref. [24].

In order to measure the oxidation, the samples were dry-sectioned from the larger specimen, potted in epoxy, and polished. The oxidation induced damage was examined using a scanning electron microscope (SEM) which provided evidence not only for resin

and fiber-matrix interphase degradation, but also for fiber degradation. The oxidation measurement procedure can be seen in Figure 8. From Figure 9, one can see that there is greater oxidation occurring in the axial direction [22]. Bowles et. al. [5] also examined this same phenomenon when studying specimen geometry effects on graphite/PMR-15 composites during thermo-oxidative aging. Using the same material, Skontorp et. al. [26] observed that the weight loss of on the axial surface is consistently larger than the weight loss on the transverse surface at a given temperature due to oxidation. Schoeppner et. al. [22] give a couple reasons why this may occur. First, resin cure shrinkage and mismatches in the coefficient of thermal expansion of the fibers and matrix during the cure process give rise to localized micromechanical residual stresses in the fiber-matrix interphase region. Secondly, the local stoichiometry of the polymer may be altered in the fiber-matrix interphase region by the presence of glass fiber reinforced coupling agents or graphite fiber reinforced sizing agents. In Figure 10, a close-up view of an oxidized fiber end is shown.

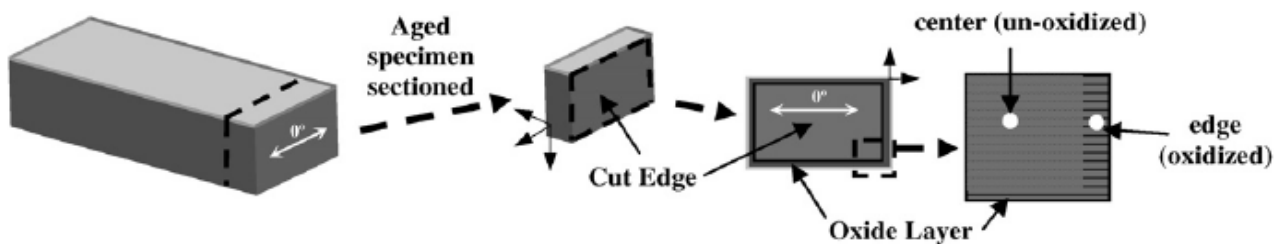


Figure 8: Oxidation measurement procedures. Figure from Ref. [22].

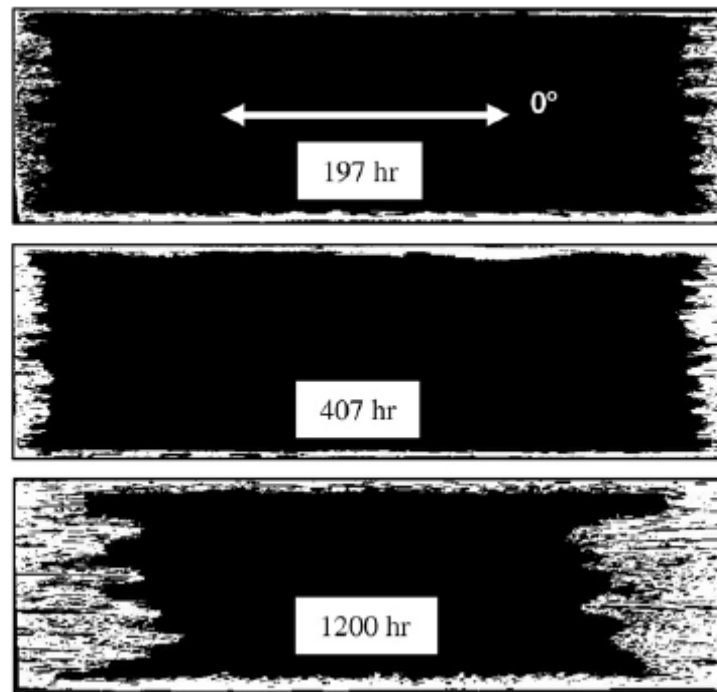


Figure 9: Oxidation of unidirectional G30-500/PMR-15 composites at 288°C. Figure from Ref. [22].

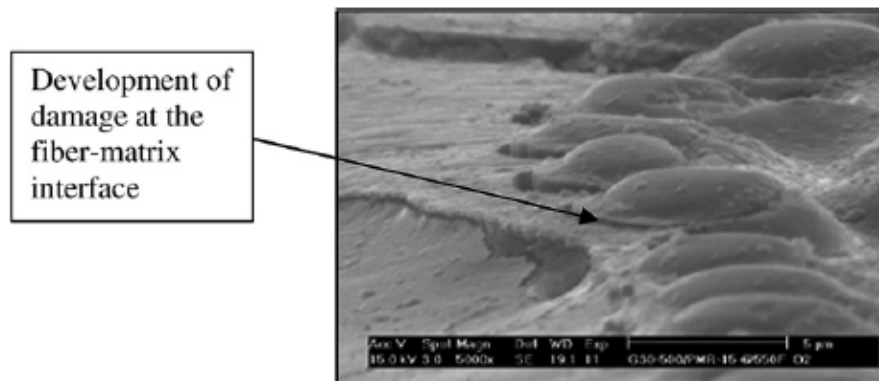


Figure 10: A close-up view of an oxidized fiber end. Figure from Ref. [22].

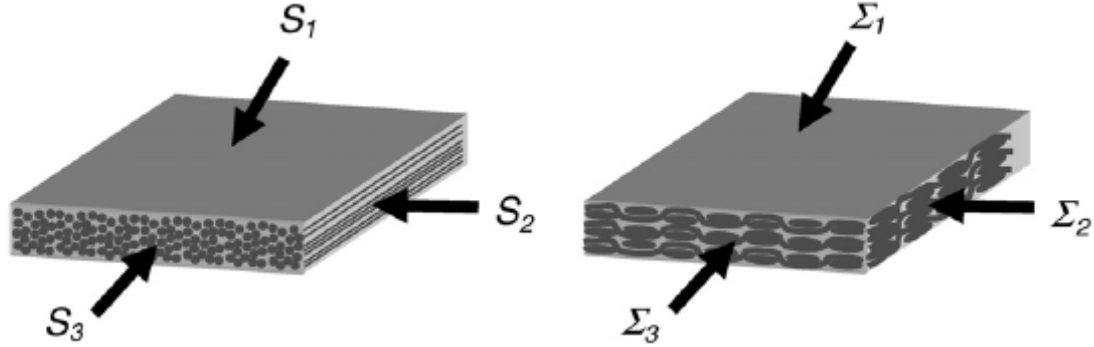


Figure 11: Surface area types for unidirectional and woven composites. Figure from Ref. [22].

There are three different surface types on the unidirectional and woven composites as seen in Figure 11 above. S_1 is the area of non-machined resin-rich surface (top and bottom of the tool surface). S_2 is the area cut parallel to the fibers and S_3 is the area cut perpendicular to the fibers. For the woven composites, Σ_1 is the area of the non-machined resin-rich surfaces, Σ_2 is the surface area cut perpendicular to the warp fibers, and Σ_3 is the surface area cut perpendicular to the fill fibers. In the Figures 12, and 13 below one can see the significant difference between the oxidative behaviors of the composite and the neat resin due to the influence of the fiber and fiber-matrix interphase region. Note that these graphs do not correspond to the surface geometries mentioned above, but for new dimensions brought about in the literature [22].

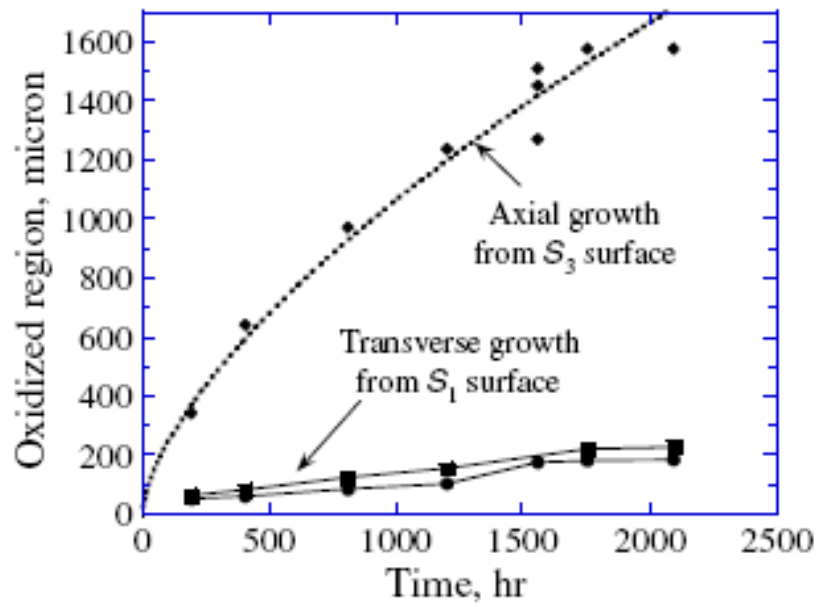


Figure 12: Comparison of oxidation growth in S_1 and S_3 directions of unidirectional composites. Figure from Ref. [22].

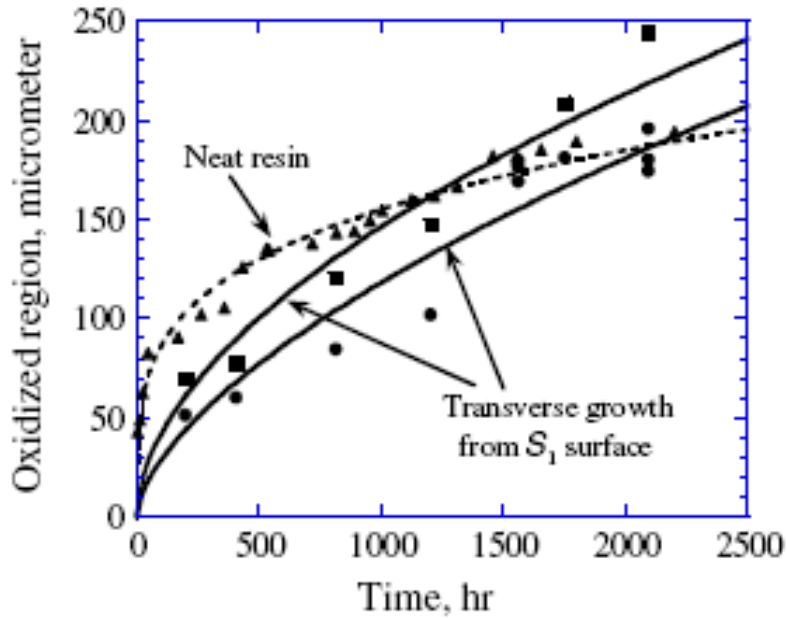


Figure 13: Comparison of oxidation growth in transverse direction S_1 of composite and in neat resin PMR-15. Figure from Ref. [22].

Oxidative weight loss was evident in the research done by Bowles et. al. [7]. Schoeppener et. al. [22] also proved that there is a strong dependence of the weight loss on the surface area ratio. This indicates that the weight loss is dependent on the surface type. The weight loss per unit surface area of the axial surface (S_3) is much greater than the weight loss rates in neat resin specimens. However, it was shown that the weight loss rate per unit surface area of the neat resin specimens was significantly different than the weight loss per unit surface of the transverse surfaces (S_1 and S_2).

Bowles [4] investigated the chemically induced physical changes of T650-35/PMR-15, 24 by 23, 8 harness satin-weave graphite fiber material at temperatures ranging from 204 to 343°C. The main focus of reviewing this piece of literature is to talk about discoloration and voids/crack propagation. Aging at the higher temperatures (288

to 316°C) produced a light-colored surface layer that grew inward and caused voids and microcracks to initiate and grow within the layer. This light color is caused by the formation of solid oxidation products at the elevated temperatures. On the other hand, at the lower temperatures, test specimens showed the same advance of voids and microcracks into the surface, but the oxidized light-colored surface layer was not visible. Results from the compression testing of composite layers that were machined parallel to the molded surface layer showed that after aging was completed at 204°C for 26,300 hours the compression strength of the visibly damaged layer was one half that of the apparently less damaged central core material. This proves that the growth of the cracked surface layer contributes to the degradation of the mechanical properties of PMR-15. Schoeppner et. al. [23] state that whereas fibers may mask some of the degradation mechanisms of the polymer (fiber dominated properties are less sensitive to polymer degradation) they tend to exacerbate some degradation mechanisms of the polymer (interfaces create pathways for diffusion of oxygen and moisture). Furthermore, Bowles [3] also states that more sites along a fiber are available for oxidative attack on the surfaces of the lower-modulus fibers than on the surfaces of the higher-modulus fibers. Figure 14, shows the surface oxidation of T650-35/PMR-15 composite specimens aged in air. Figure 15, shows matrix cracking perpendicular to fiber ends and a close-up view of a crack which creates a pathway for enhanced oxygen diffusion.

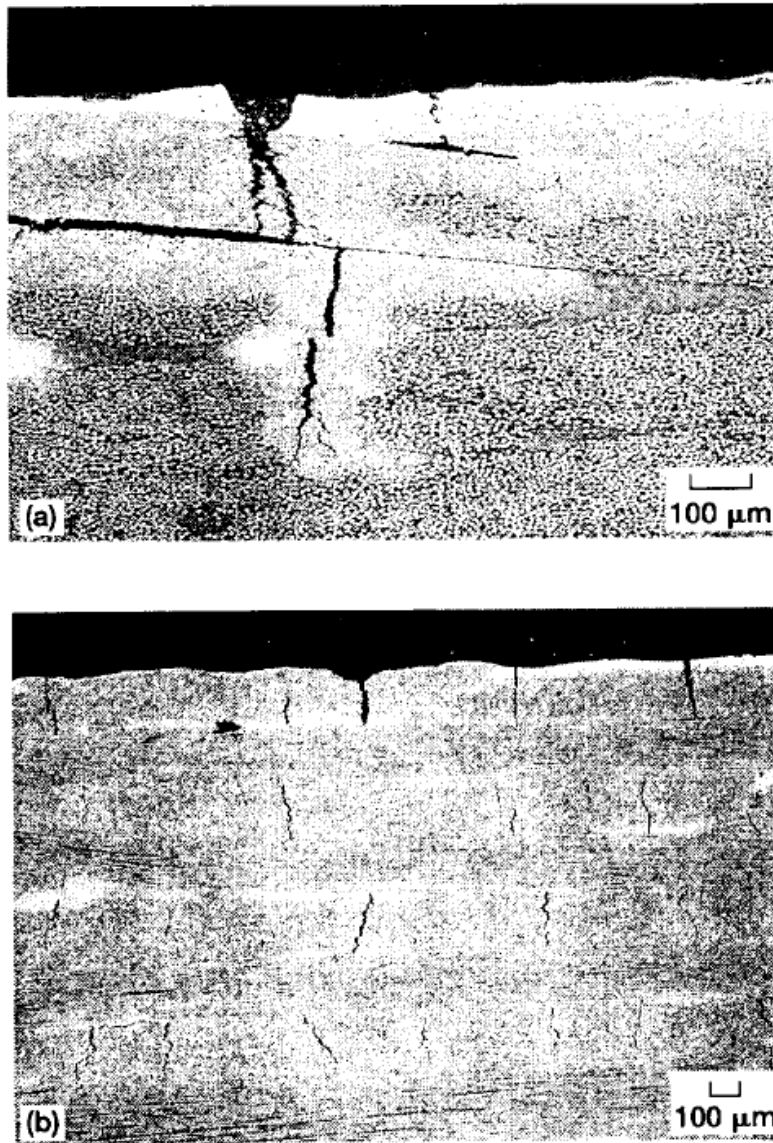


Figure 14: Surface oxidation of T650-35/PMR-15 composite specimens aged in air. (a) Aged 1000 hours at 316°C. (b) Aged 10,000 hours at 204°C. Figure from Ref. [4].

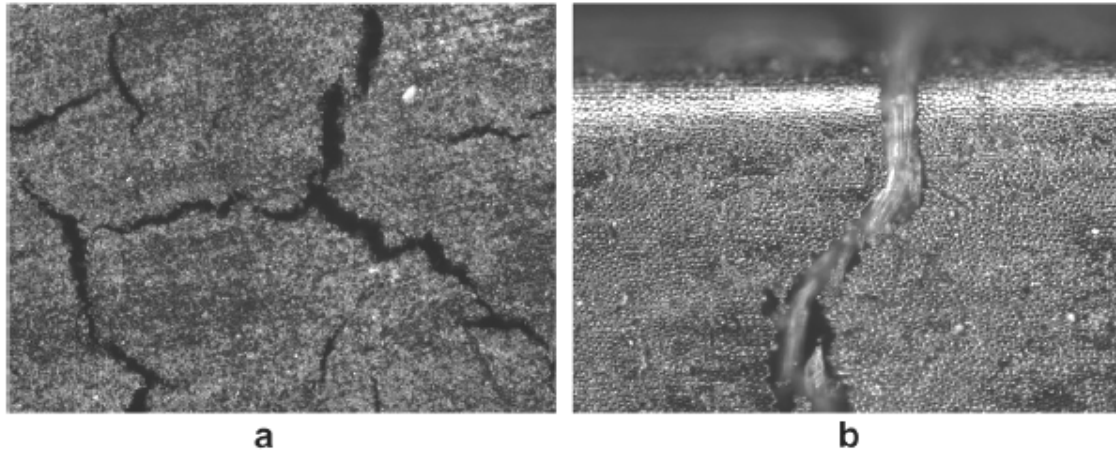
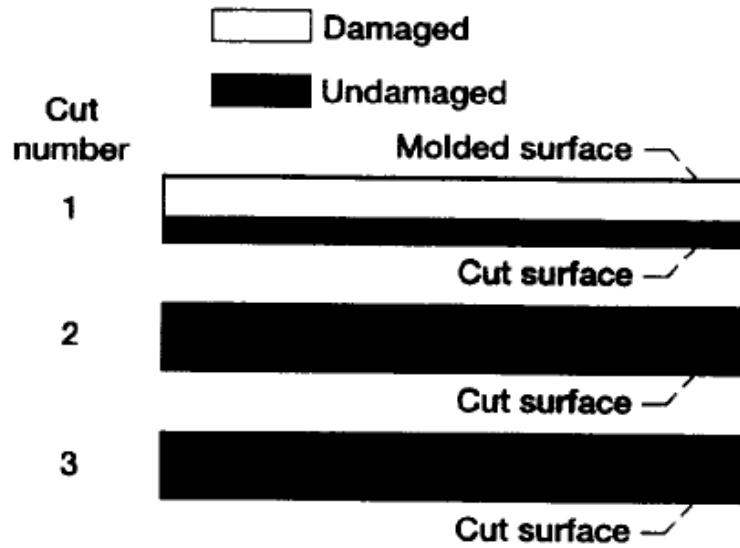


Figure 15: Photo micrographs of the axial surface of a unidirectional specimen aged for 1,864 hours at 288°C showing (a) matrix cracking perpendicular to fiber ends, (b) close-up view of a matrix crack providing a pathway for enhanced diffusion. Figure from Ref. [22].

Furthermore, Bowles and others [6] showed that mechanical properties vary with the distance from the surface of a T650-35/PMR-15 composite. Sections were cut out of an aged T650-35/PMR-15 composite (260°C for 20,000 hours) and then tested separately without additional aging. The compression strength and the modulus of each cut were measured. The moduli were measured using dynamic mechanical analysis (DMA). Figure 16, shows the different cuts, the compression strengths, and the moduli.



Cut number	Strength, MN/m ²	Modulus, GN/m ²
1	137.3	56.9
2	299.6	56.7
3	264.6	62.9

*Taken from different depths through the thickness of thick laminate aged at 260 °C for 20 000 hr.

Figure 16: Compression strengths and moduli of T650-35/PMR-15 sections cut from a single specimen. Figure from Ref. [6].

From the results above, Bowles et. al. [6] were able to show that the compression strength of the surface layer was much less (137.3 to 264.6 MN/m²) due to oxidation. However, there was not much of a difference between the modulus measurements. In the case of a T650-35/PMR-15 composite aged in air at 360°C for 2,090 hours, it was shown that the storage modulus was significantly lower at the surface than toward the center. The T_g also decreased when distance increased from the surface. In Figure 17, one can see a graph of the stored shear moduli for the different layers of the composite and notice

that while the surface is experiencing tremendous oxidation the center of the composite continues to degrade only by thermal mechanisms.

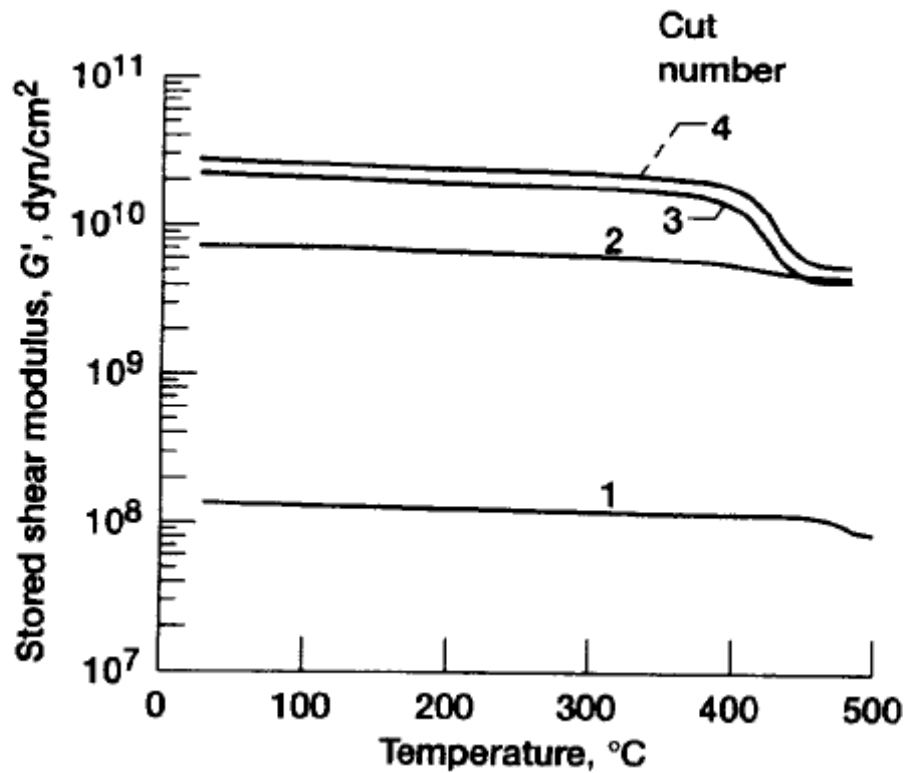


Figure 17: Stored moduli of a T650-35/PMR-15 composite aged in air at 360°C for 2,090 hours as a function of temperature for different depth cuts. Figure from Ref. [6].

Summary

This literature review was a brief summary of the current and on going research in the area of mechanical and chemical changes in fiber reinforced PMR-15 neat resin and composites due to exposure to elevated temperatures in an oxidizing environment.

III. Material and Specimen

Chapter Overview

This section will discuss in detail the material that is being subjected to testing. The test specimens will be described including: material processing, specimen geometry, specimen tabbing, aging, and relative humidity.

CYCOM 2237/PMR-15

This material was provided by HyComp incorporated located in Cleveland, Ohio. Given a company name of CYCOM 2237, this is Cytecs version of PMR-15. This materials micro-crack and thermo-oxidative stability makes it ideal for jet engine components and other fatigue load components like transmission housings, box covers, bypass ducts, nozzle flaps, vent tubes, core cowls, fan stator and vane assemblies, particle separator swirl frames, and compression molded bearings. Furthermore, CYCOM 2237 has the best balance of processing behavior, retention of properties in the 260°C to 280°C range, and thermo-oxidative stability. In addition, it has a dry glass transition temperature (T_g) of 640°F (338°C), a shelf life of 12 months at 0°F (-18°C), and a mechanical life of 20 days at 80°F (27°C) maximum and <70% relative humidity [11].

Specimen Fabrication

Material Processing

The fabrication of the carbon fiber reinforced PMR-15 neat resin molded panel is very important to the specimen preparation process. Failure to follow specific processing procedures could result in material defects which would hinder test results.

Unfortunately, the exact processing history of the panel was not provided by the manufacturer. Variability in the mechanical properties of each specimen cut from the panel will be determined by taking the initial elastic modulus of each test specimen. The geometry of the panel is: 11 in. x 16 in. x 3mm flat within .060 inches. The PMR-15 neat resin matrix is reinforced with T650-35 carbon fiber 8-harness satin fabric weave with a $\pm 45^\circ$ fiber orientation. The material was first subjected to an autoclave laminate cure cycle and then to a free-standing post cure cycle. These cure cycles are shown in tables 4 and 5 [11].

Table 4: Steps for HyComps laminate cure cycle	
1	Apply 2-6 in Hg vacuum
2	Raise temperature to $425 \pm 10^\circ\text{F}$ at a rate of $0.5 - 3.0^\circ\text{F}$ per minute
3	At $300 \pm 10^\circ\text{F}$ apply full vacuum
4	Hold for 180 – 210 minutes at $425 \pm 10^\circ\text{F}$ (temperature based on lagging thermocouple)
5	Raise temperature to $475 \pm 10^\circ\text{F}$ at a rate of $0.5 - 3.0^\circ\text{F}$ per minute
6	At 450 - 475°F apply 200 ± 10 psi pressure at a rate of 15 – 20 psi per minute
7	Hold at $475 \pm 10^\circ\text{F}$ for 30 – 55 minutes
8	Raise temperature to $600 \pm 10^\circ\text{F}$ at a rate of $0.5 - 3.0^\circ\text{F}$ per minute
9	Hold for 180 – 210 minutes at $600 \pm 10^\circ\text{F}$
10	At the end of hold, cool slowly under pressure
11	When temperature is below 400°F , release pressure and vent vacuum
12	Cool to 160°F prior to removing from autoclave

Table 5: Steps for HyComps free-standing post-cure cycle	
1	Post-cure in an oven starting at room temperature to $600 \pm 10^\circ\text{F}$ at $10 - 15^\circ\text{F}$ per minute
2	Hold at $550 \pm 10^\circ\text{F}$ for 5 hours
3	Raise temperature to $600 \pm 10^\circ\text{F}$ at a rate of $0.5 - 1.0^\circ\text{F}$ per minute
4	Hold at $600 \pm 10^\circ\text{F}$ for 10 hours
5	Cool to 160°F prior to removing from the oven

Specimen Geometry

The test specimens used in this study had a reduced gage section or dog bone shape. For the tensile tests, this shape ensured gage section failure. The test specimens were machined at the Air Force Institute of Technology machine shop from a PMR-15 neat resin panel with carbon-fiber reinforcement using a diamond saw. Prior research revealed that cutting the specimens using a diamond saw causes fewer defects than the water-jet process [10]. Specimens were not cut from the parts of the panel that showed defects. Defects in the gripping section of the specimens were acceptable. However, if there were defects in the gage section of the specimen, they were not used in mechanical testing. The panel was not C-scanned. The average thickness of the specimens was 2.98 mm with a range between 2.85 mm to 3.11 mm. Prior to aging and testing, all test specimens were washed using an everyday household soap and rinsed with distilled water to remove contaminants from the diamond saw process. The test specimens were then dried and placed in a vacuum oven at 105°C for 5 days to remove any moisture. All test specimens were then stored in a dry air purged dessicator before and after all mechanical testing.

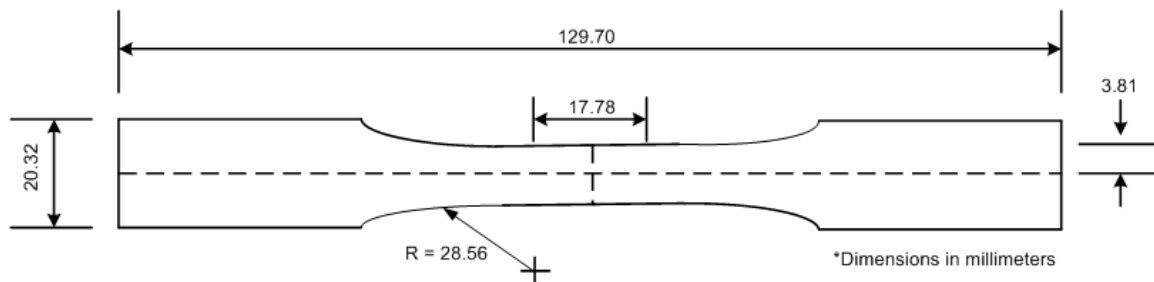


Figure 18: Dog bone test specimen with nominal dimensions. Figure from Ref. [14].

Specimen Tabbing

Before being subjected to mechanical testing, all of the test specimens were tabbed using a glass fabric/epoxy material to prevent contact between the specimens and the grips. The tabbing provides the load to be evenly transferred from the gripping wedge surface to the test specimen. Tabs on opposing faces of the test specimen should be evenly aligned so that localized stresses are minimized [1]. This material was chosen because it is able to absorb the surface damage created by the hydraulic wedge grips. The tabs were attached to the test specimens using M-Bond 200, a room temperature cure epoxy adhesive. Each tab was held for at least one minute to ensure a strong bond.



Figure 19: A test specimen before being tabbed

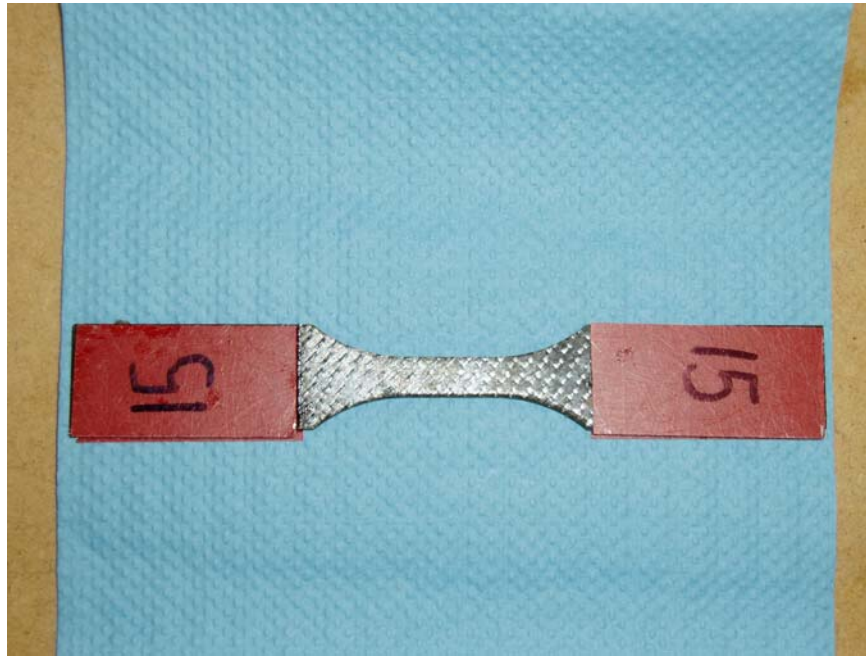


Figure 20: A test specimen after being tabbed

Aging

The test specimens were aged in an air environment for different periods of time. The temperature of the aging environment was held constant at 288°C. For the aging process, air was supplied to the Blue M oven through a compressed air line with an inline filter and desiccator. The trays which held the specimens in the oven were covered with quartz cloth to prevent contamination. Throughout the entire aging period, the measured relative humidity (RH) of the air fed to the chamber was less than 10%. The steady air flow rate was approximately 30 standard cubic feet per hour (SCFH) at steady state and 150 SCFH during the purge cycle. It is assumed that any moisture released into the aging environment was removed by the flowing air and that any moisture present in the chamber was caused by the air supply. When the oven was opened to take out specimens,

the chamber automatically went into a purge cycle when the door was shut. The purge cycle lasts for eighteen minutes and ensures that any ambient atmosphere that entered the chamber is depleted. When the oven was opened to take out the aging specimens, it was opened without cooling and closed immediately. It is assumed that the short exposure of the aging specimens to the outside atmosphere did not cause any additional effects that were not already present from the production process (mainly oxidation and humidity). When the samples were removed from the oven, they were placed in a dry air-purged desiccator prior to testing. To ensure the absence of moisture effects, the desiccator was kept at a constant relative humidity of less than 10%.



Figure 21: Aging chamber

Relative Humidity

One may wonder if the exposure of the test specimens to ambient air during long-term testing at 288° will affect the testing results. However, it was found in previous research that even in a very humid environment ($RH \geq 70\%$) the relative humidity around the sample is very low ($RH \leq 1\%$) due to the elevated test temperature [10]. Therefore, no moisture effects were introduced during long-term mechanical testing at 288°C.

IV. Experimental Setup and Testing Procedures

Chapter Overview

This section will provide a detailed description of the testing equipment and the testing procedures used in this research.

Test Equipment

The equipment used in this research consists of: the servo hydraulic machine, the cooling system, the extensometer, the computer software, and the high temperature equipment.

Servo Hydraulic Machine

Mechanical testing was completed using a vertically configured 810 Material Test System (MTS) servo hydraulic machine with a 3 KIP (13.3 KN) load cell. The servo hydraulic machine had MTS 647.02B hydraulic wedge grips capable of applying a pressure of up to 21 MPa (3000 psi) to each end of the test specimen. The grip pressure throughout the mechanical testing was 4.80 MPa. Each of the grips had a pair of flat wedges coated with surf alloy in order to allow for better gripping of the test specimen. Additionally, each wedge was equipped with an inlet and outlet to allow the flow of cool water through the grips to prevent overheating in the grip sections during high temperature testing.



Figure 22: 3 KIP MTS hydraulic machine

Cooling System

Both the grips and the extensometer required cooling equipment. The water for cooling was supplied by a NESLAB model HX-75 chilled water system. The temperature of the cooling water was kept between 9°C and 24°C. For the grips to operate properly, they must be kept in a -18°C to 65°C temperature range. The extensometer assembly was kept cool by using a cooling air flow and a heat shield.

Extensometer

Strain measurements were taken with an MTS model 632.53E-14 axial extensometer during high temperature testing. It is capable of measuring strains between -10% and +20%. The extensometer has two 3.5 mm diameter alumina extension rods with conical tips that allow it to be placed in the dimples of the test specimen to maintain continuous contact between the specimen and the rods to prevent slipping during testing. Dimples were made in the gauge section of the test specimen 12.7 mm (0.5 in) apart using an MTS dimpling tool. Dimple size was kept minimal in order to avoid possible induction of crack propagation. Each alumina rod extended 150 mm to ensure that the extensometer was far removed from the heat source. The extensometer was held in place using a spring-loaded assembly which places a 3 N contact force per rod onto the test specimen. This low contact force ensures that there is no more damage added to the specimen that may have been caused by dimpling. The extensometer can operate in temperatures up to 650°C without air cooling and up to 1200°C with air cooling. The strain measurements are very accurate; however, electrical noise in the strain measurement cannot be avoided.



Figure 23: MTS High temperature axial extensometer assembly with heat shield

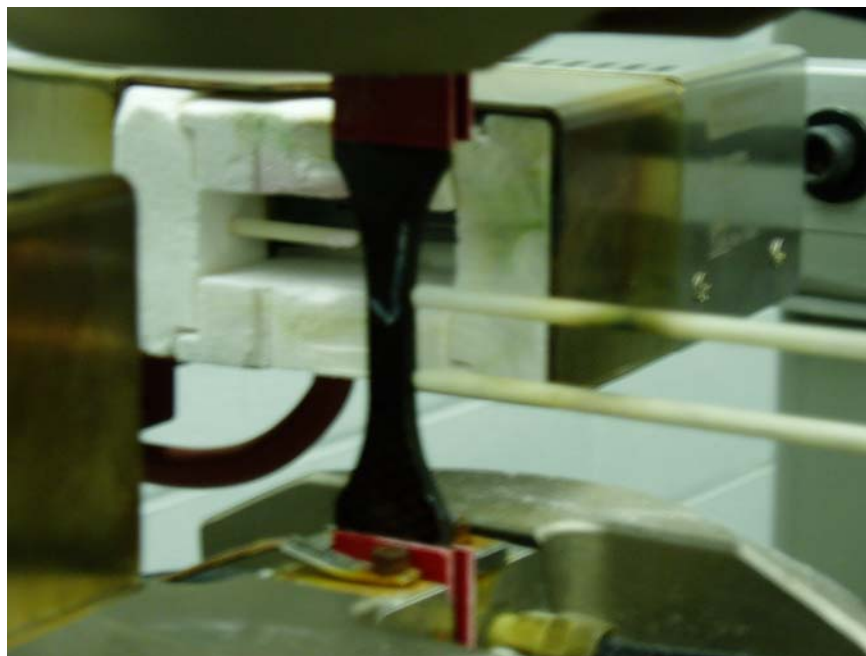
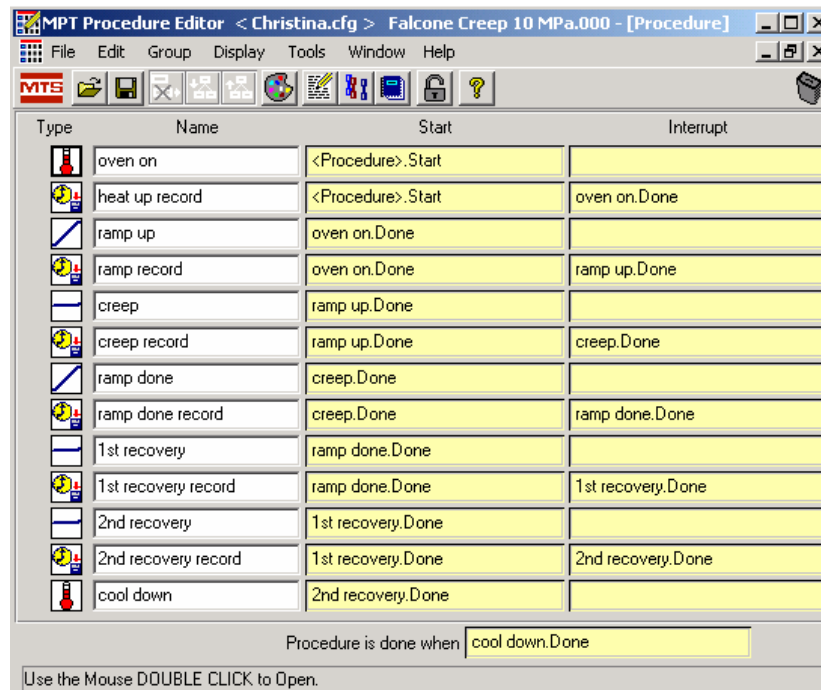


Figure 24: MTS High Temperature Axial Extensometer Attached to the Test Specimen

Computer Software

An MTS TestStar II digital controller was used for input signal generation and data acquisition. Using the MTS Station Builder application, a configuration file was specifically built for the test specimens. This allowed for the input of various tuning parameters. Next, the MTS Station Manager application allowed the user to perform test operations such as manually controlling displacement, temperature, or force, controlling hydraulic power, setting station interlock limits, monitoring input and output signals, and pushing play to run tests. The MultiPurpose Testware (MPT) was used to build computerized procedures. The careful construction of these procedures allowed for automated testing and data acquisition.



The screenshot shows the MPT Procedure Editor window with the title bar "MPT Procedure Editor < Christina.cfg > Falcone Creep 10 MPa.000 - [Procedure]". The menu bar includes File, Edit, Group, Display, Tools, Window, and Help. The toolbar contains icons for opening, saving, undo, redo, and other functions. The main area is a table with four columns: Type, Name, Start, and Interrupt. The table lists the steps of a creep test procedure, including oven on, heat up record, ramp up, ramp record, creep, creep record, ramp done, ramp done record, 1st recovery, 1st recovery record, 2nd recovery, 2nd recovery record, and cool down. Each step has a corresponding icon in the Type column and a sequence of events in the Start and Interrupt columns. At the bottom, there is a field "Procedure is done when" with the value "cool down.Done" and a note "Use the Mouse DOUBLE CLICK to Open."

Type	Name	Start	Interrupt
	oven on	<Procedure>.Start	
	heat up record	<Procedure>.Start	oven on.Done
	ramp up	oven on.Done	
	ramp record	oven on.Done	ramp up.Done
	creep	ramp up.Done	
	creep record	ramp up.Done	creep.Done
	ramp done	creep.Done	
	ramp done record	creep.Done	ramp done.Done
	1st recovery	ramp done.Done	
	1st recovery record	ramp done.Done	1st recovery.Done
	2nd recovery	1st recovery.Done	
	2nd recovery record	1st recovery.Done	2nd recovery.Done
	cool down	2nd recovery.Done	

Procedure is done when cool down.Done

Use the Mouse DOUBLE CLICK to Open.

Figure 25: MPT creep test procedure. Figure from Ref. [14].

High Temperature Equipment

An MTS 653 furnace was used to achieve the elevated temperature for mechanical testing. The operating temperature of the furnace ranges from 100°C to 1400°C. It has a center split design which closes around the test specimen and can be opened and shifted away from the testing area during specimen loading and extensometer setup. Each half of the furnace was equipped with a silicon carbide heating element surrounded by silica foam. The fibrous alumina inserts were filed down to make slots for both the specimen and extensometer rods to pass through. The temperature of the furnace was controlled with an MTS 409.83 Temperature Controller. During mechanical testing, a 19 mm section of the specimen was subjected to the elevated temperature. The MTS 409.83 Temperature Controller displayed the temperature of the furnace and the current input temperature. A feedback loop between the S-type thermocouple in the right side of the oven and the controller maintained the appropriate procedure temperature throughout the testing. The variation between both sides of the furnace did not exceed more than 5°C.



Figure 26: Temperature controller



Figure 27: Furnace

Experimental Procedures

Determining Test Temperature

In order to determine the desired testing temperature of 288°C, a temperature calibration was performed to determine the input temperature for the controller. Two K-type thermocouples were attached to a test specimen with Kapton tape and thin wire to give the temperature readings. The thermocouple tips were placed in the center of the specimen on both sides in order to get accurate temperature readings from each side of the furnace. The temperature of the specimen was monitored using an Omega OMNI-CAL-SA-110 two-channel temperature sensor. The whole procedure included manually increasing the temperature of the furnace at a rate of 1°C per minute until one thermocouple read 288°C and the other was within 5°C. A final input for the controller was determined to be 292°C. The specimen was allowed to dwell at this temperature for 10 hours to make sure that this was the correct temperature setting for testing. During this dwell period, the thermocouple readings did not fluctuate more than $\pm 5^\circ\text{C}$.

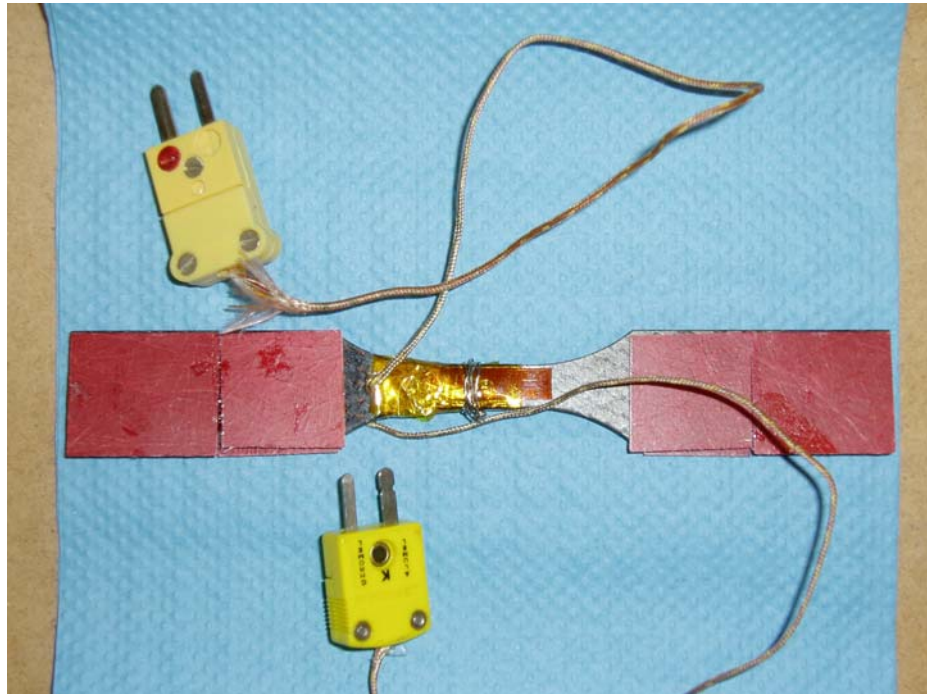


Figure 28: Temperature calibration specimen with two attached k-type thermocouples.

Test Procedures

Prior to beginning a test, many preparatory steps were completed. First, the hydraulic servo machine was warmed up for 30 minutes. This was accomplished by using the Function Generator application to cycle the actuator in displacement control. Next, the MPT procedure was updated with the specific specimen data. The thickness and width of each specimen was measured in order to obtain the cross-sectional area. Using the cross-sectional area and the desired stress level, the required force for the test could be calculated. The MPT procedure was updated for each specimen. Dimples were carefully hammered into each specimen, to ensure that the extensometer did not slip during testing. In manual command, the machine was put into displacement mode and

zeroed. The top grips were then closed on the centered specimen. The load cell was then zeroed and switched to force mode. Once switched to force mode, the bottom grips were quickly closed. After securing the test specimen and ensuring that no load was applied to the specimen, the extensometer rods were mounted onto the specimen. Once the extensometer assembly was complete, the furnace was closed around the specimen. The strain displacement was then zeroed and the interlocks were set. If triggered, the interlocks would automatically turn off the hydraulic power supply. During the heat up period, the machine was kept in force control at near zero force to ensure free expansion of the test specimen. Once the test temperature was reached, there was a 30 minute dwell period to ensure thermal equilibration and that thermal expansion had come to a stop.

Test Descriptions

Initial Elastic Modulus Measurements

In order to capture specimen-to-specimen variability, the initial room-temperature elastic modulus of each specimen was measured. This was done after the specimens were machined and prior to aging. Each test specimen was loaded to 3 MPa at a rate of 1 MPa/s and unloaded to zero stress at the same rate for 3 cycles. No permanent strain was introduced to the specimens during this process. A stress level of 3 MPa and a loading rate of 1 MPa/s were chosen to ensure a linear response. The test specimens did not vary significantly.

Monotonic Tensile Test

Multiple tensile tests to failure were carried out on the PMR-15 test specimens. These tests were performed at the elevated temperature of 288°C for aged and unaged test specimens. It can be noted from prior research, that the tensile tests may not have reached the ultimate tensile strength of the material due to fractures originating at one of the dimples [2]. The tensile test allowed for the finding of Young's modulus of elasticity and the Ultimate Tensile Strength (UTS).

Creep Tests

Creep and recovery tests were performed on both unaged and aged test specimens. Unaged specimens were crept at creep stress levels of 80 MPa, 60 MPa, and 30 MPa respectively for 50 hours and allowed to recover for 100 hours. Using the data from the unaged specimens, we could determine at what creep stress levels to use for the aged test specimens. Changes in the load-up and unloading rates are needed in order to observe the rate dependence of the material. Ultimately, creep stress levels of 30 MPa and 60 MPa were performed on the aged test specimens. The aged specimens crept for 25 hours and recovered for 50 hours at zero stress. The recovery period was followed by a cool down to room-temperature. Data collected during each stage of a creep test consisted of: load-up data, creep data, unloading to zero stress data, and recovery data. During the load-up and unloading periods, data was taken at a fast rate. Data was taken every 0.050049 seconds for the load-up and unloading periods. Data points taken during the long creep and recovery periods were separated by longer time intervals to reduce the

size of the data files. If a failure occurred during creep testing the fracture surfaces were observed using an optical microscope to view the morphology of the fracture surface. However, there were no failures during creep testing, but the microscope was used to examine fracture surfaces of the specimens that fractured during tensile testing.



Figure 29: ZEISS Discovery.V12 Model Stereo Microscope

Weight Measurements and Oxidation Layer Growth

A specimen from each particular aging time with a ± 45 fiber orientation ranging from 50 hours to 1000 hours was measured for oxidation layer growth. A separate rectangular specimen with a ± 45 fiber orientation was analyzed for weight measurements at 0, 10, 50, 100, 250, and 500 hours. The initial weight measurements of the specimen were taken after drying. All weight measurements were obtained with a Metler Toledo

AG245 microbalance with a resolution of 0.0001 grams. In order to maintain near zero moisture content, all of the test specimens were stored in a dry-air-purged dessicator before and after aging. The dessicator was kept at a relative humidity of less than 10%, while the average value was below 5% relative humidity. In order to measure the oxidation layer growth, a section of each specimen was cut, mounted, and polished for observation with a Nikon EPIPHOT digital microscope. The specimens were mounted in a room temperature cured epoxy, sanded with 320 and 600 grit sandpaper, and polished with 0.03 micron silica slurry by a Buehler PowerPro 5000 variable speed grinder-polisher. Staining of the specimens was not required to view the oxidation layer growth. The micrographs were obtained digitally and automatically dimensioned.

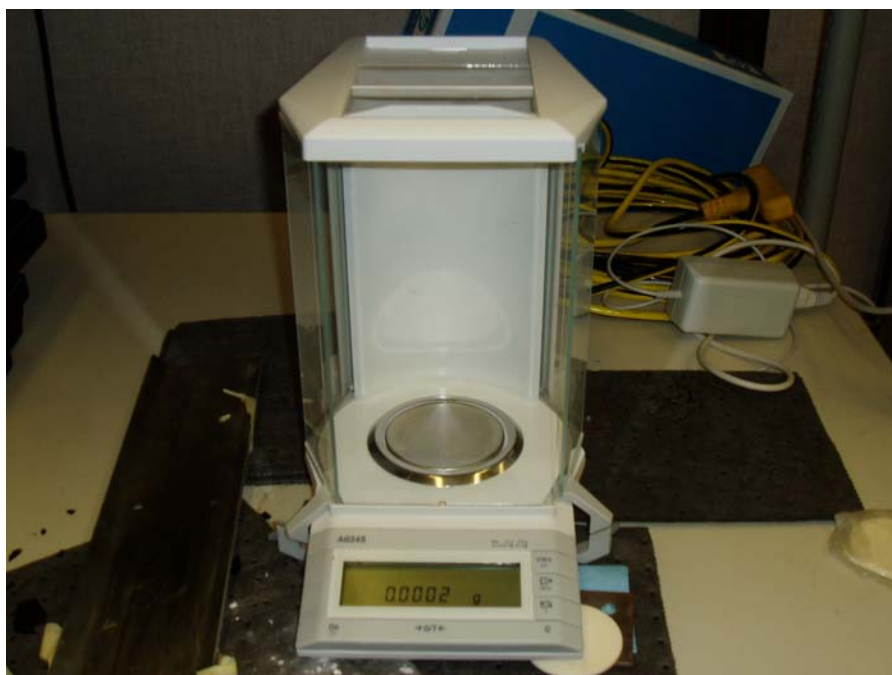


Figure 30: Metler Toledo AG245 Microbalance



Figure 31: Buehler PowerPro 5000 Variable Speed Grinder-Polisher



Figure 32: Sections of test specimens ready to be analyzed for oxidation growth after being mounted, sanded, and polished.

Summary

The elastic modulus for each specimen was measured at room temperature for every specimen to determine the variability from specimen-to-specimen. The test specimens were aged in air at 288°C in order to obtain oxidation layer growth. Oxidation layer thickness and weight measurements were taken at different times in order to analyze the dependence of oxidation layer growth and weight loss on exposure time at elevated temperature. Monotonic tensile tests and creep response tests were performed at 288°C in the laboratory air to determine mechanical properties of the carbon fiber reinforced PMR-15 neat resin.

V. Results and Discussion

Chapter Overview

This section documents the results and presents the analysis of the data collected during this thesis study. The results and the details of the individual experiments are reported. The discussion will make an attempt to correlate the data with theory.

Weight Loss Measurements

The weight of a ± 45 fiber oriented rectangular specimen aged in air was measured as a function of aging time. Weight loss during oxidative aging can be attributed to out-gassing of oxidation by-products from the resin, resulting in oxidative shrinkage which may account for opening of cracks at the fiber-matrix interface [22]. In the presence of an oxidizing environment the weight loss depends on the surface area of the test specimen. The change in surface area due to aging damage is effectively accounted for in the weight loss parameters. Therefore, weight loss should be normalized by the surface area of the individual test specimens [6, 7, 22]. The nominal surface area of the rectangular specimen was measured at every aging time interval of 10, 50 100, 250, and 500 hours. All weight measurements were obtained with a Metler Toledo AG245 microbalance with a resolution of 0.0001 grams. Figure 33 shows the weight loss factor as a function of

aging time in air at 288°C.

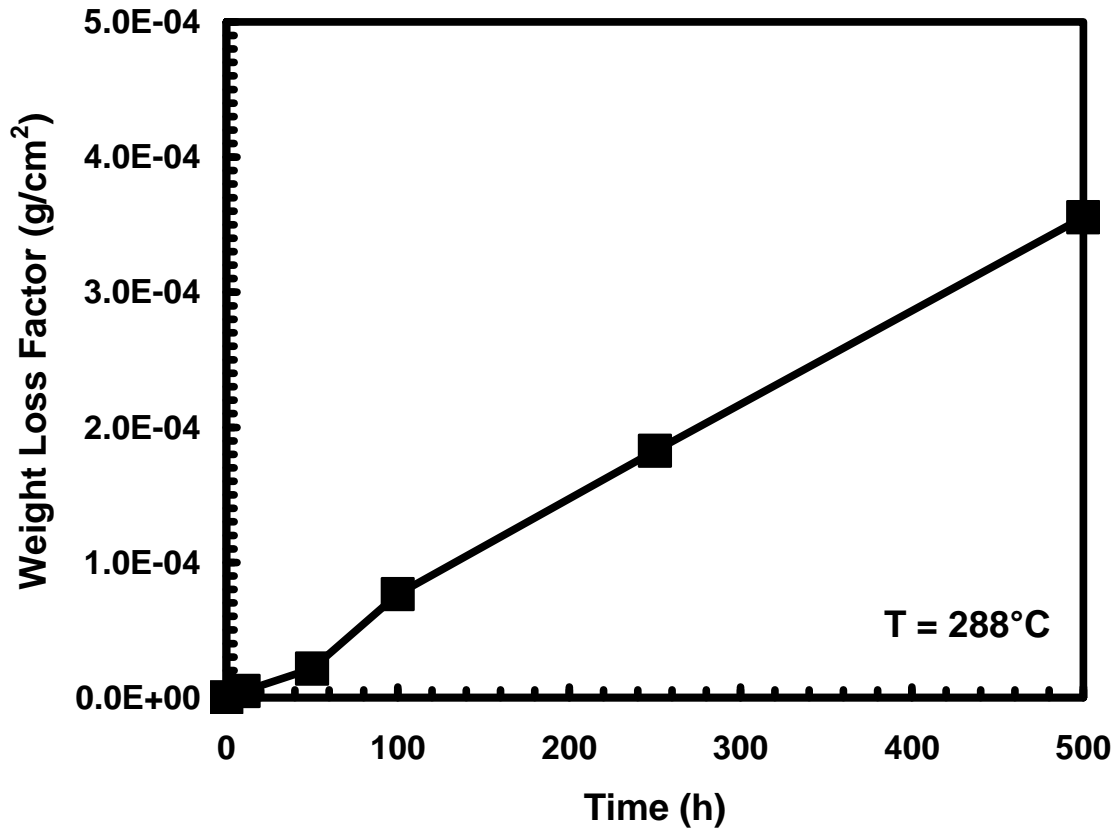


Figure 33: Weight loss factor as a function of aging time for carbon fiber reinforced PMR-15 neat resin at 288°C in air.

One can notice the difference between the initial fast rate of weight loss and the later rate for aging in air. This sudden increase is attributed to the diffusion of gaseous cure and postcure reaction products from the sample. The weight loss becomes linear between 100 and 500 hours and is attributed to normal thermal and oxidative reactions. After 500 hours, as seen in other studies, the weight loss rate is accelerated by reason of the increase in surface area caused by the initiation and growth of surface microcracks

that also allow easier penetration into the specimen by oxygen. This cracking occurs at a much faster rate than observed with neat resin specimens and continually increases in depth with increasing aging time [6]. Figure 34 shows percent weight loss for air as a function of aging time.

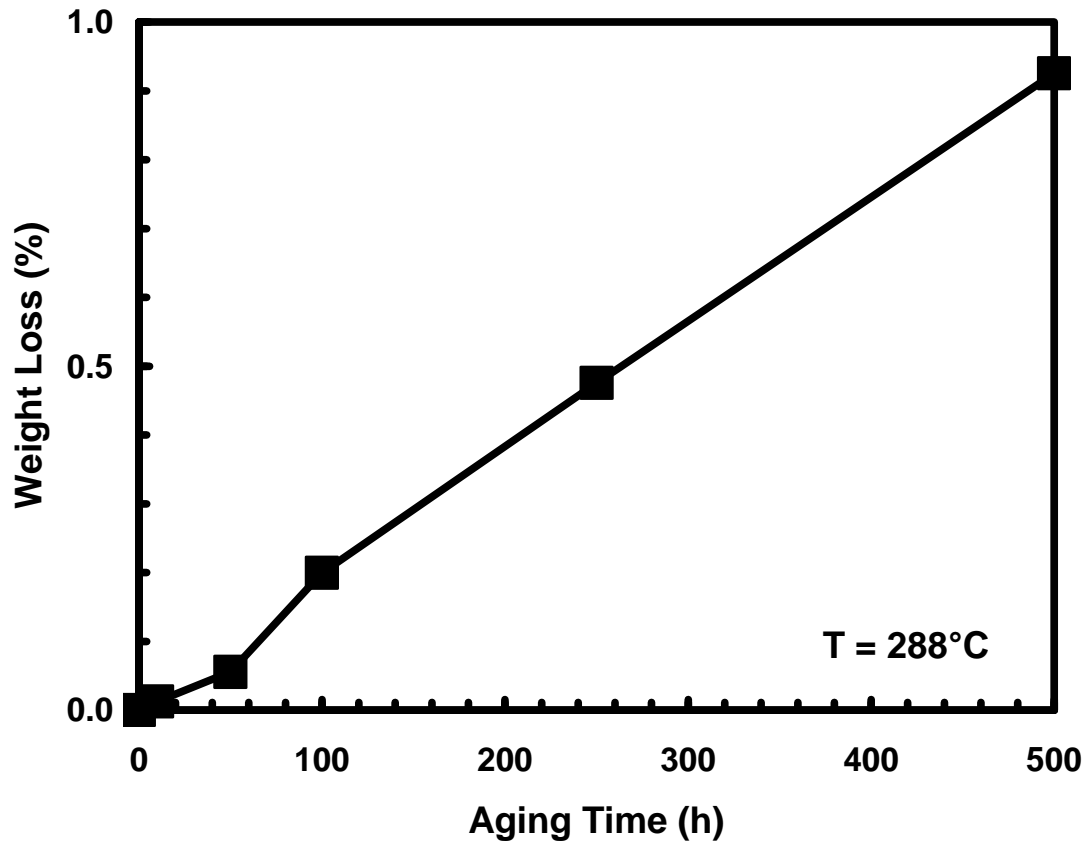


Figure 34: Percent weight loss as a function of aging time for carbon fiber reinforced PMR-15 neat resin aged in air at 288°C.

It is seen in Figure 34 that weight loss increases with increased aging time. Visual inspection of the test specimens after aging revealed a light brown color on the surface of the 1000 hour aged specimens. This light color is attributed to the formation of solid oxidation products at elevated temperature [4]. Sections of specimens at each aging time were cut using a diamond saw in order to view oxidation growth and any other micro structural changes. These results are discussed in detail in the next section.

Oxidation Layer Thickness

Test Specimens aged in air experienced chemical and physical changes at elevated temperature. These changes initiated at the outer surface of the test specimens and progressed inward following the oxygen as it proceeded by diffusion toward the central core. A cross sectional cut was taken from a specimen from each aging time using a diamond saw. The cross sectional cut came from a dog bone shaped specimen, so all edge effects were eliminated. The specimens were mounted in room temperature curing epoxy pucks, sanded with 320 and 600 grit sandpaper, and polished with 0.03 micron silica slurry by a Buehler PowerPro 5000 variable speed grinder-polisher. In order to maintain the structural integrity of the relatively soft specimen edges, an effort was made to minimize the amount of grinding and polishing. This is why there are many noticeable scratches shown on the micrographs. However, further grinding and polishing could affect the vulnerable oxidized edges and could lead to incorrect measurement of the actual oxidation layer. The ZEISS stereo microscope used to view the fractured surfaces of the failed specimens was not able to illuminate the oxidation layer, so the polished surface was observed under a Nikon EPIPHOT digital microscope. The digital microscope directed a light through the lens and onto the specimen which allowed for a bright field of viewing.

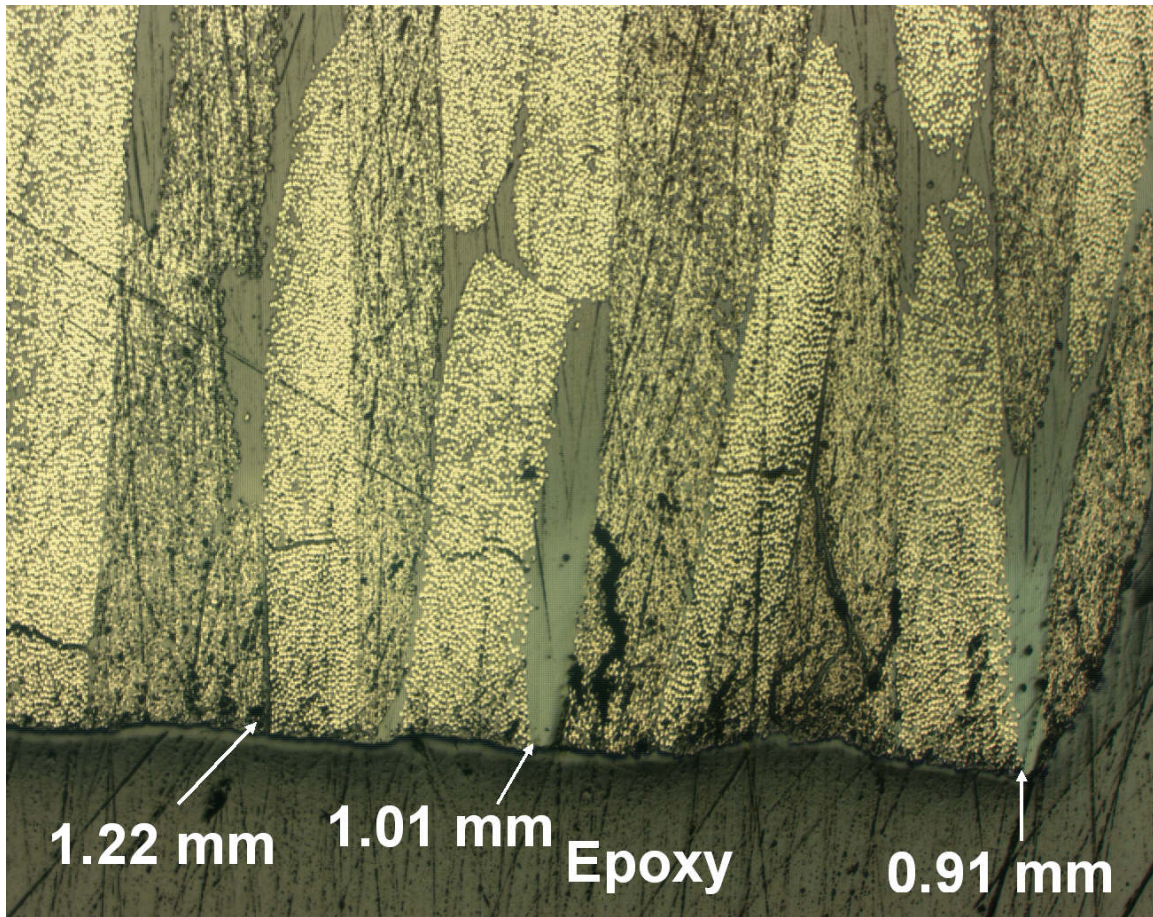


Figure 35: Optical micrograph showing the oxidation layer on the cut surface with the exposed fiber edges for the carbon fiber reinforced PMR-15 composite aged for 500 h at 288°C in air.

Figure 35 presents a micrograph of a cross sectional cut aged for 500 h at 288°C in air. Between the fibers one can notice the slight color change which depicts the oxidation layer growth. However, as seen above, the fibers obscure the view in which to observe all of the oxidation growth. Staining of the specimens was not necessary to see the oxidation layer. The micrographs were taken at a magnification of 50X, and measurements were carried out by using a traceable calibrated microslide. Figure 36

shows the oxidation growth on the molded side of a specimen aged for 500 h where the fibers are not directly exposed.

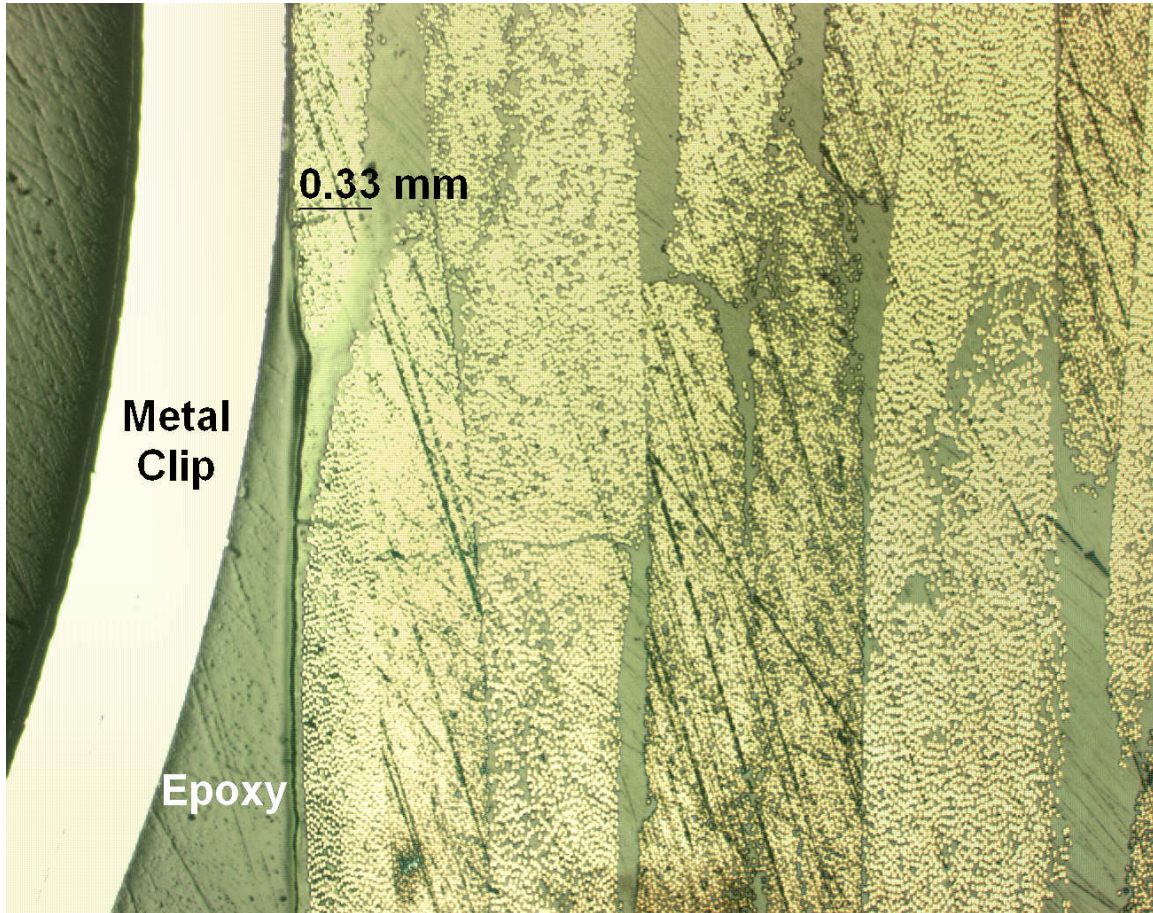


Figure 36: Optical micrograph showing the oxidation layer on the molded outer surface of a carbon fiber reinforced PMR-15 composite aged for 1000 h in air at 288°C.

From Figures 35 and 36 it can clearly be seen that the cut side in which the fiber surfaces are exposed is experiencing greater oxidation growth. This finding is well documented in other studies [22, 6, 3]. On the cut side the ± 45 oriented fibers are exposed and can create passageways for air to invade. Again, the fibers are blocking a great amount of the surface area in which to fully see the oxidation growth. In Figure 37

the effect of oxidation growth on the cut and molded sides of a specimen as a function of aging time can be seen.

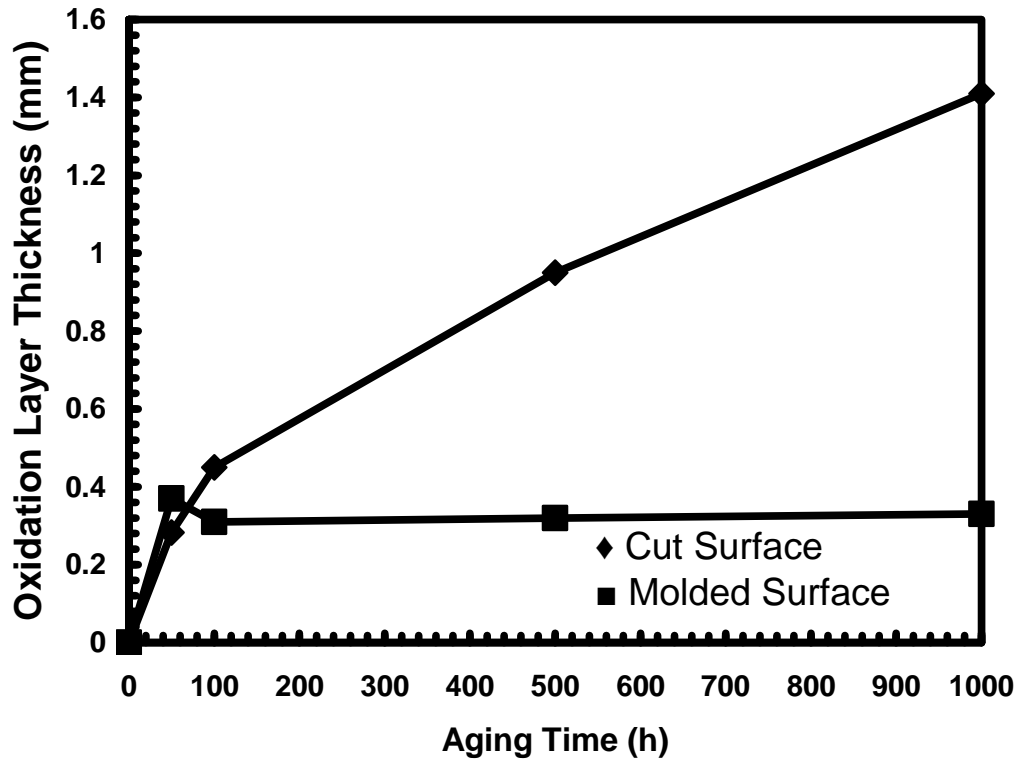


Figure 37: Oxidation layer thickness measure on both cross sectional cut and uncut surfaces as a function of aging time in air at 288°C for carbon fiber reinforced PMR-15 neat resin.

From Figure 37, it is apparent that oxidation layer thickness increases with increasing aging time. Clearly, when the fibers are exposed to the oxidizing environment the result is thicker oxidation layer growth. However, for the 50 h aging period the oxidation growth on the molded side is greater than on the cut side. One can see that the oxidation growth on the molded side did not significantly increase between 0 and 1000 h. It was hard to take accurate oxidation measurements on the molded surface due to so

many fibers obscuring oxidation growth visibility. One would think that there would be more oxidation growth on the molded side with increased aging time, but it can not be accurately determined because the fibers are in the way. In Appendix B, micrographs of cut and molded oxidation growth can be viewed. In Appendix B, note that for 50 h the molded oxidation growth is 0.7 mm while the molded oxidation growth for 1000 h is 0.33 mm. This is only because this large portion of the 50 h specimen was not obscured by fibers.

Elastic Modulus

Initial Room Temperature Modulus

In order to determine sample-to-sample variability, the initial room temperature elastic modulus of each specimen was measured. This testing was completed after machining and prior to any aging or elevated temperature testing. Each test specimen was loaded to 3 MPa at a rate of 1 MPa/s and unloaded to zero stress at the same rate for 3 cycles. No permanent strain was introduced to the specimens and there were no significant outlying specimens. The covariance for the elastic modulus for all 26 of the test specimens was calculated to be 0.094. The covariance was measured by dividing the standard deviation by the average modulus. The average modulus was calculated to be 16.3 GPa. Note, that all of these specimens were not used in testing, for some were supposed to be aged in argon. Due to time limitations this was not done. Figure 38 shows the output data of the statistical program, MiniTab, which was used to analyze the initial room temperature elastic modulus with a 95% confidence interval for each test specimen.

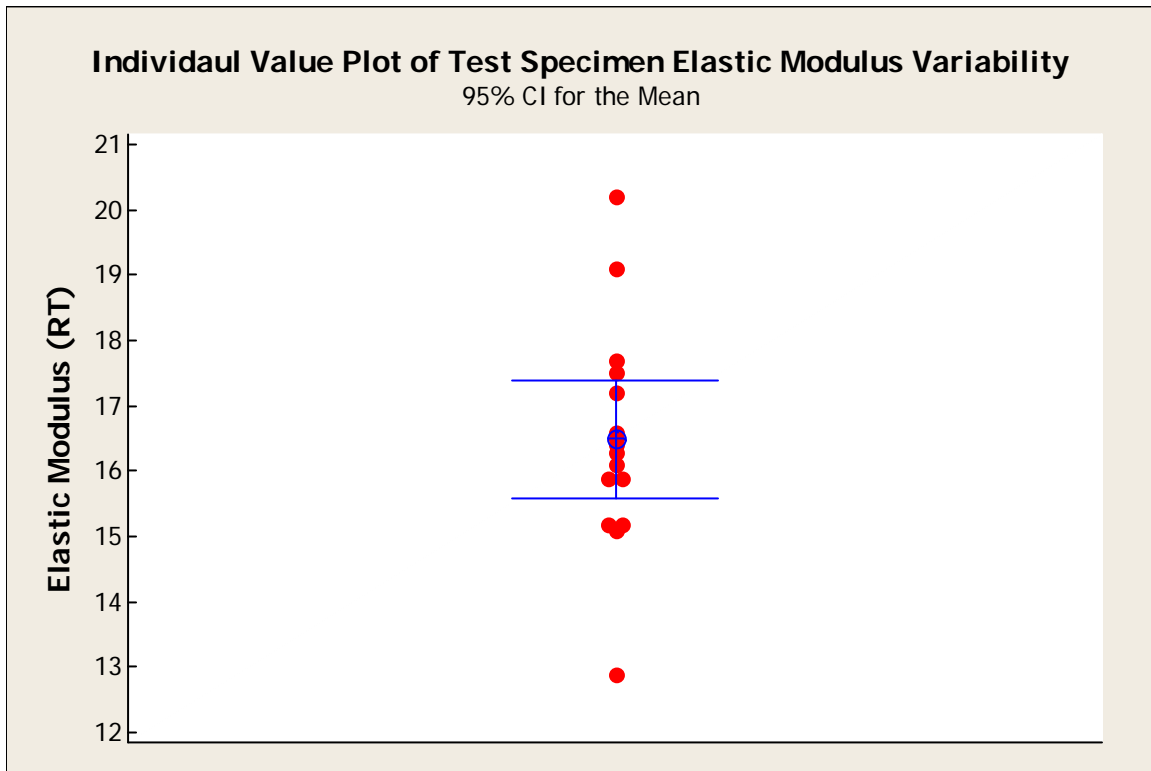


Figure 38: Initial room temperature elastic modulus data as a function of test specimens from a single panel, with a 95% confidence interval for each test specimen. This figure was produced using the MiniTab program.

Based on this room temperature elastic modulus measurement, it was decided that no test specimens would be eliminated from further investigation in the study. Figure 38 shows that there was some scatter within the samples, but very minimal. Each dot represents a specimen. From MiniTab, the average room temperature modulus was calculated to be 16.4875 GPa. This was very close to the average room temperature modulus calculated from testing (16.3 GPa). MiniTab was used to gain greater confidence in our testing results.

Aged Modulus versus Initial Modulus

In order to evaluate the effects of aging, the elastic modulus at elevated temperature was obtained during the loading and unloading segments of each creep and recovery test. The elastic modulus for each specimen was calculated from the stress portion of the curve between 0 and 7 MPa. The load rate of 1 MPa/s was used in all testing. The room temperature elastic modulus, in each case, was higher than the loading and the unloading elastic modulus of each specimen obtained at elevated temperature. Figure 39 shows a plot of aged loading and unloading moduli of aged specimens measured at 288°C versus the initial room temperature moduli.

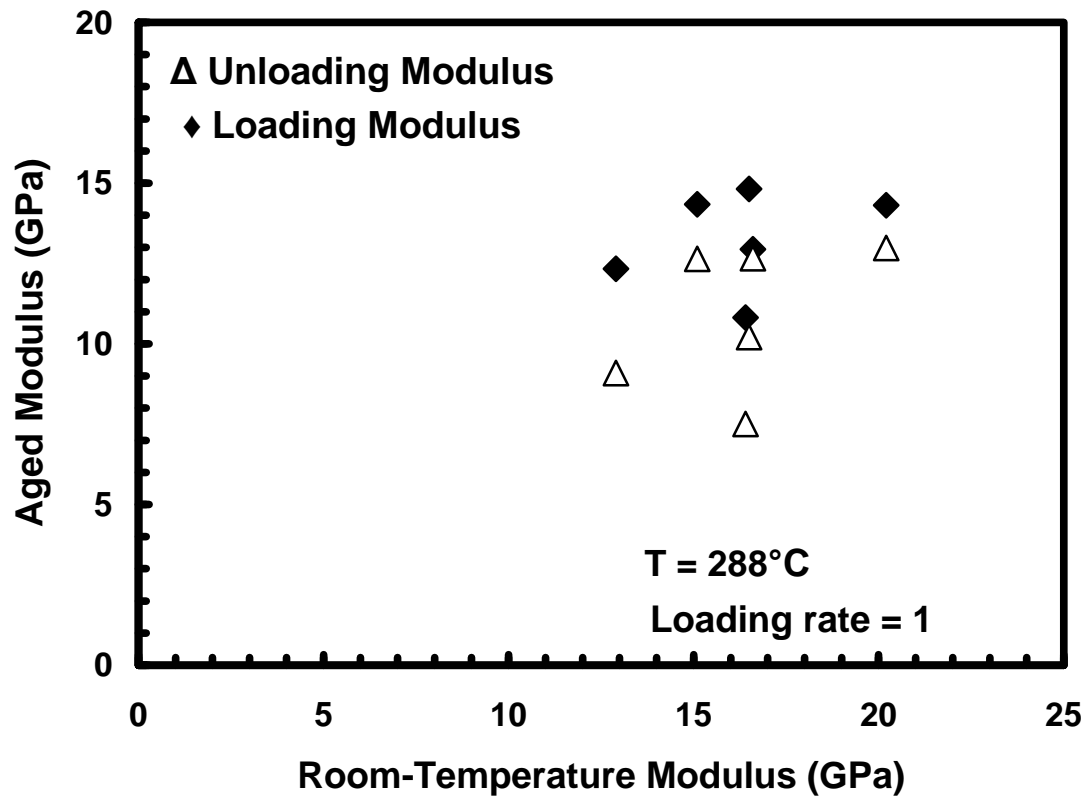


Figure 39: Elastic modulus of aged samples measured at 288°C versus initial room temperature elastic modulus for carbon fiber reinforced PMR-15 neat resin.

From Figure 39, it is evident that the unloading elastic modulus is usually lower than the loading elastic modulus regardless of the specimen's initial room temperature modulus. Having a lower unloading elastic modulus could be attributed to the accumulation of damage during mechanical testing.

Elastic Modulus upon Loading and Unloading

Upon loading and unloading, all test specimens produced stress-strain curves. The tensile stress-strain curves obtained during loading for the 13 tested specimens at 288°C in air can be seen in Figure 40.

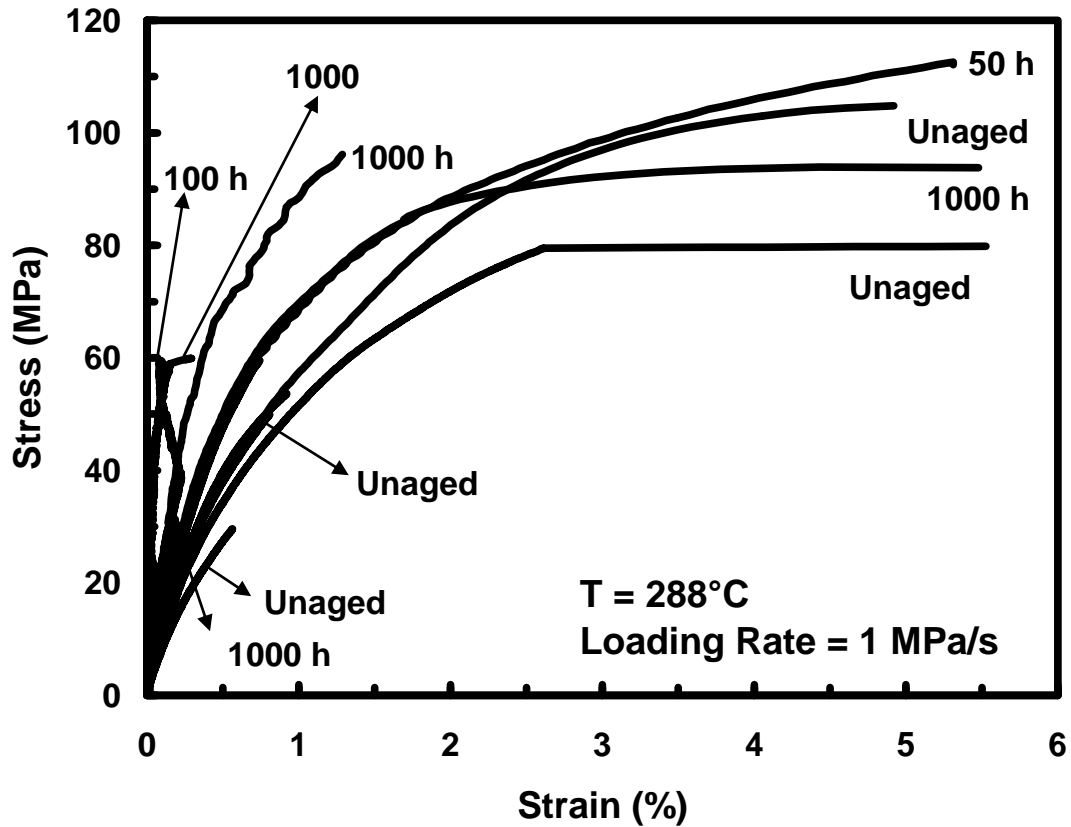


Figure 40: Tensile stress-strain curves during loading obtained in all tests at 288°C.

It was observed that increased aging time in air caused fluctuation in the loading and unloading moduli. For example, the unloading moduli were 7.507, 12.98, 9.09, and 12.64 GPa for 50, 100, 500, and 1000 h of prior aging time respectively. The elastic modulus was measured between 0 and 7 MPa. Figure 41 shows the loading elastic

modulus as a function of aging time in air. There is fluctuation, but the modulus of each specimen did ultimately increase from the 0 h measurement to the 1000 h measurement of aging. A trend line is drawn through the average values of the individual data points.

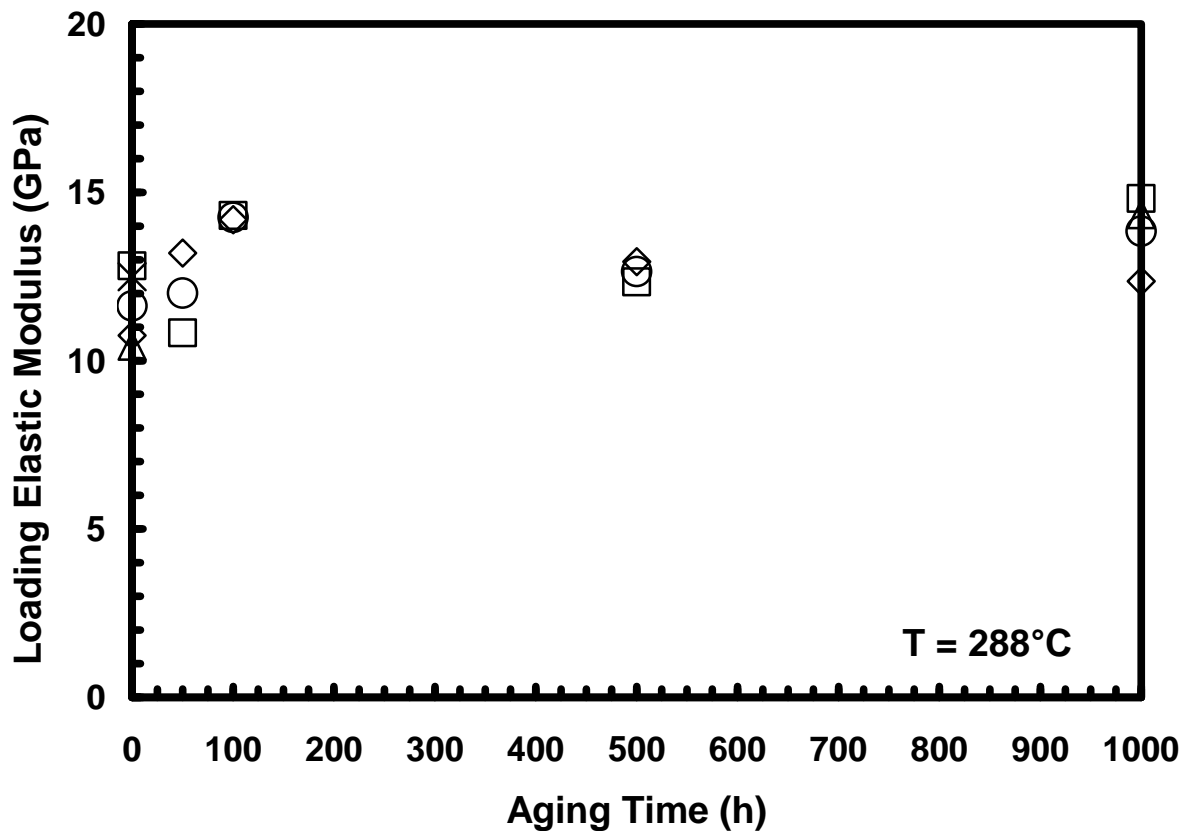


Figure 41: Elastic modulus upon loading versus aging time in air at 288°C for carbon fiber reinforced PMR-15 neat resin.

It is apparent that the elastic modulus upon loading shows little changes from aging times between 0 and 500 h, but an increase after 1000 h of aging. The general increase at 1000 h in the elastic modulus suggests that the bulk of the material is

stiffening and that the overall specimen elastic modulus is independent of the presence of an oxidation layer for prior aging time's ≤ 1000 h.

Figure 42 shows the elastic modulus measurements upon unloading as a function of aging time in air. The unloading modulus may be impacted by prior creep, so the results have been broken down by creep stress levels. It is shown that the unloading elastic modulus fluctuates with increased prior aging time. Lower modulus values could mean that there is structural damage occurring during the creep period. Each data point represents one specimen at that aging time.

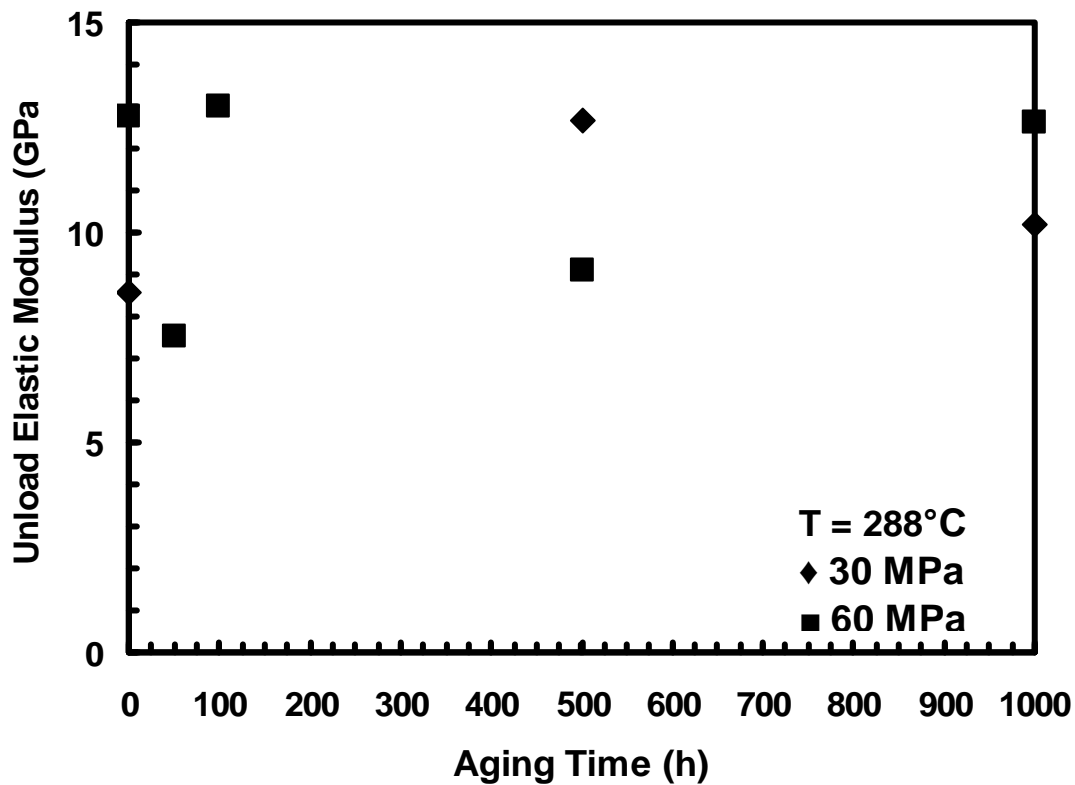


Figure 42: Elastic modulus obtained upon unloading versus aging time in air at various creep stress levels where carbon fiber reinforced PMR-15 composites were tested at 288°C .

Figure 43 below shows the % change in modulus as a function of aging time between loading and unloading moduli. This calculation is necessary to see if a specimens loading modulus is affecting its unloading modulus.

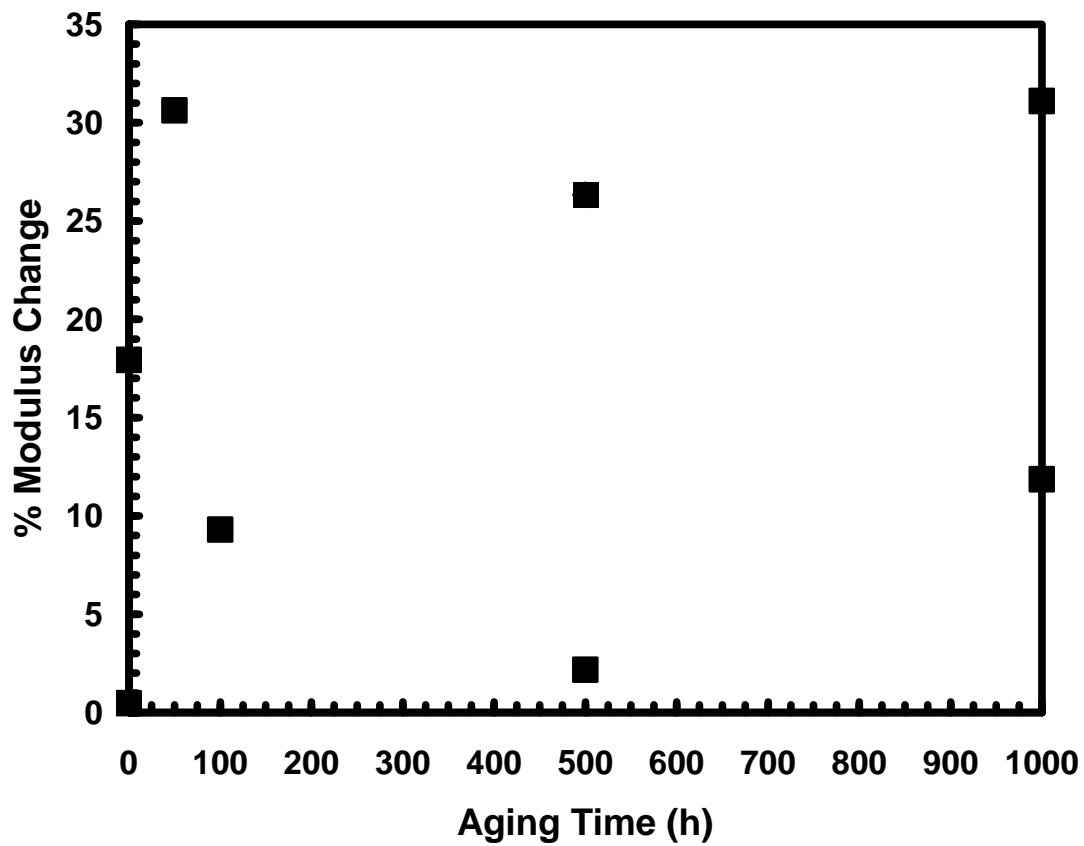


Figure 43: Change in elastic modulus between loading and unloading moduli as a function of aging time.

Figure 43 shows that no specimens had more than ~32 % difference in loading and unloading modulus. When there is a large % difference in modulus there is a decrease in the unloading modulus values.

Elastic Modulus Ratios

In order to identify any dynamic material changes due to aging and mechanical loading, the ratios of elastic moduli were measured before, during, and after mechanical testing. The ratio of the elastic modulus upon unloading (unloading modulus, E_U) to the elastic modulus measured upon loading (loading modulus, E_L) would mean that damage occurred within the material structure during the creep period. A ratio of the room temperature elastic modulus (initial modulus, E_O) to E_L at 288°C after aging shows that the elastic response is affected by both increasing temperature and aging time. The ratio of E_U to E_O may show material changes as a result of the entire testing and aging process. These elastic modulus ratios can be seen in Figure 43.

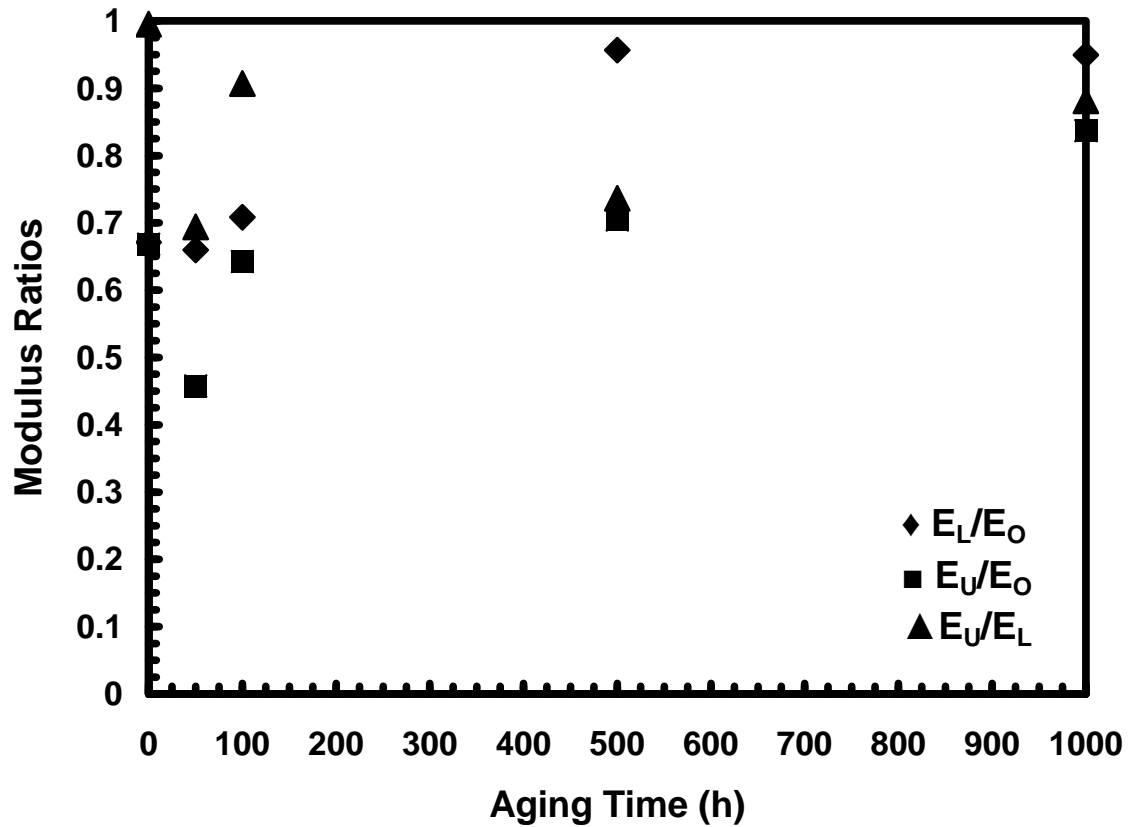


Figure 44: Elastic modulus ratios versus aging time in air for carbon fiber reinforced PMR-15 composites aged at 288°C and tested in creep at 60 MPa at 288°C.

One can notice in Figure 44 that the elastic modulus ratios had quite a bit of dispersion with increased aging time. For example, the E_U/E_L ratio went from ~1 at 0 h to ~0.7 at 50 h, and back to ~0.95 at 100 h of aging. Each point represents one test specimen.

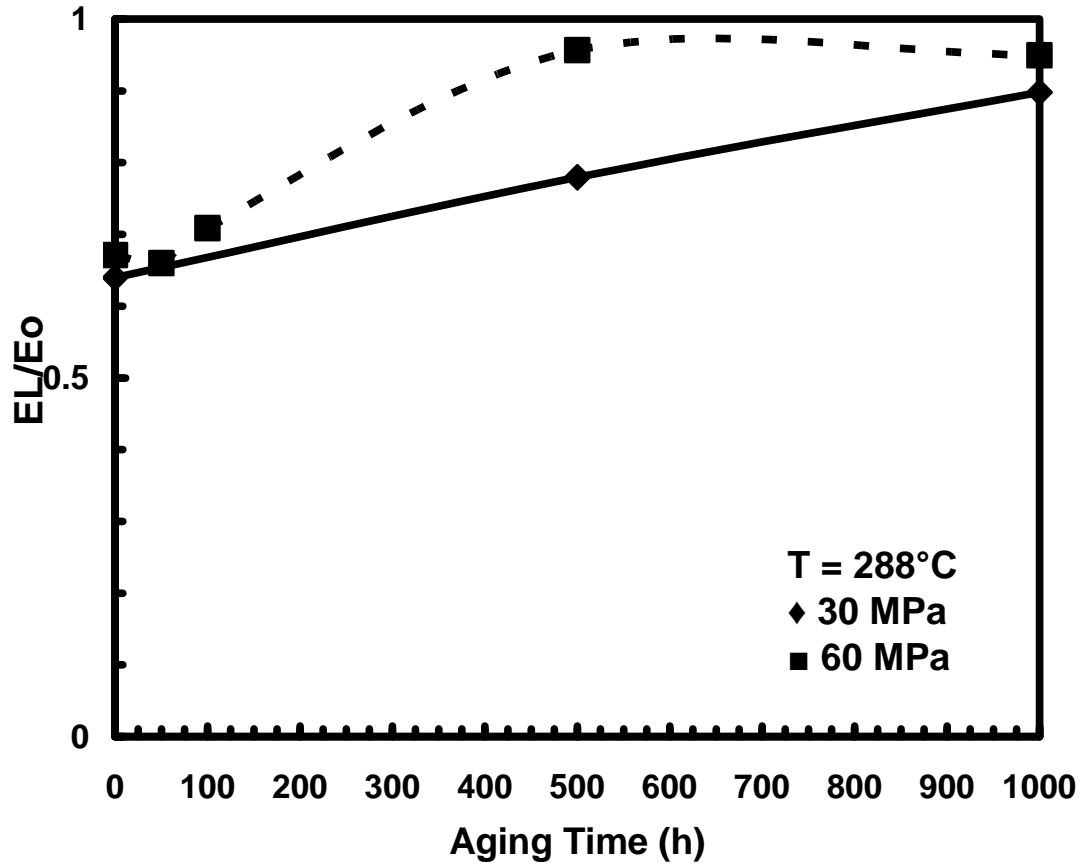


Figure 45: Ratio of elastic modulus measured upon loading to the initial room temperature elastic modulus as a function of aging time for carbon fiber reinforced PMR-15 composites tested in creep at 30 and 60 MPa.

Figure 45 shows the ratio of E_L/E_O as a function of aging time, which represents the effect of increasing temperature and aging time on elastic response. The E_L/E_O increases for all aging times at 30 MPa, but fluctuates at the start for 60 MPa. However, the E_L/E_O did increase significantly from 0 to 1000 h for both creep stress levels with a slight drop from 0 to 50h and from 500 to 1000 h for 60 MPa. This suggests that the aging time and elevated temperature have a considerable influence on the elastic

modulus. Each data point represents one test specimen. Figure 46 shows the E_U/E_L ratio as a function of aging time.

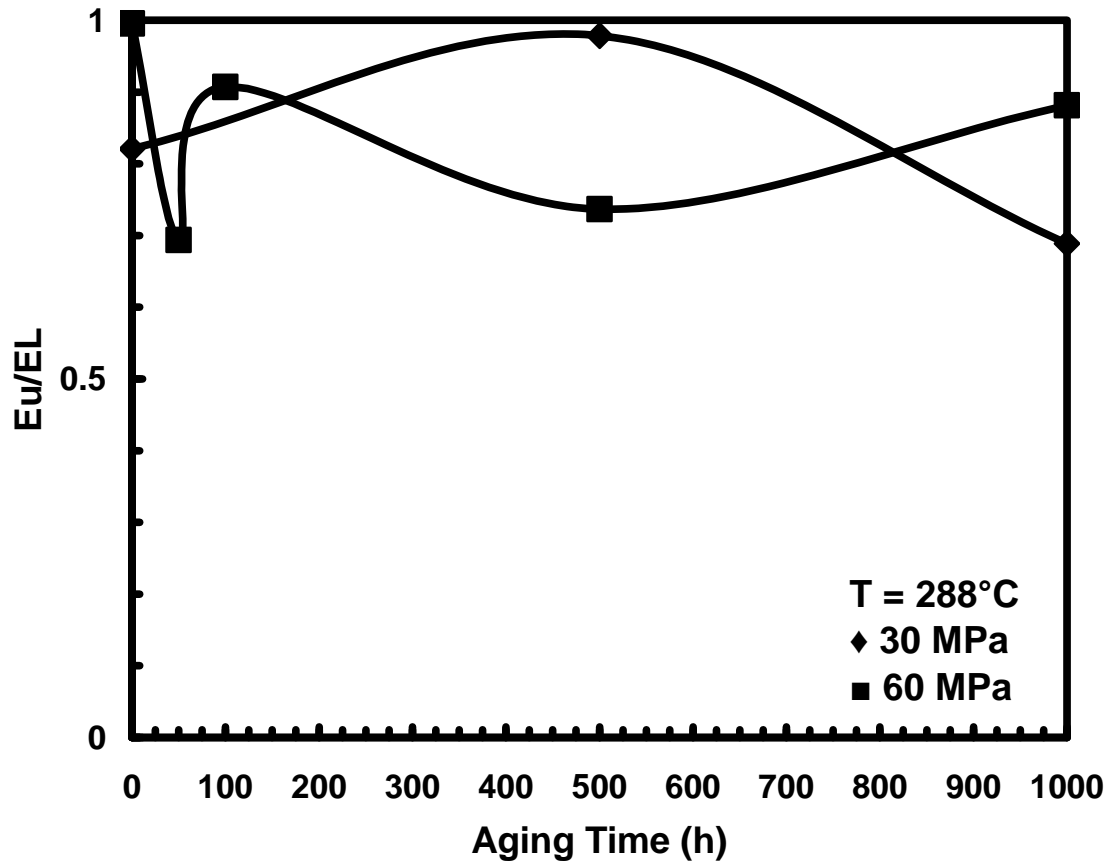


Figure 46: Ratio of elastic modulus measured upon unloading to the elastic modulus measured upon loading as a function of aging time for carbon fiber reinforced PMR-15 composites tested in creep at 30 and 60 MPa.

It can be seen in Figure 46 that the E_U/E_L is not dependent on the creep stress level. The opposite is true for PMR-15 neat resin [10]. It is evident that the modulus reduction represents that damage is occurring at both creep stress levels of 30 and 60 MPa. The specimens tested at 60 MPa have an average of 19% reduction in elastic

modulus while the specimens tested at 30 MPa show a 17.3% reduction in elastic modulus.

In Figure 47, the EU/EO ratio is shown as a function of aging time. The EU/EO ratio definitely shows the greatest amount of elastic modulus damage. This damage is due to prior aging, creep loading, and elevated temperature.

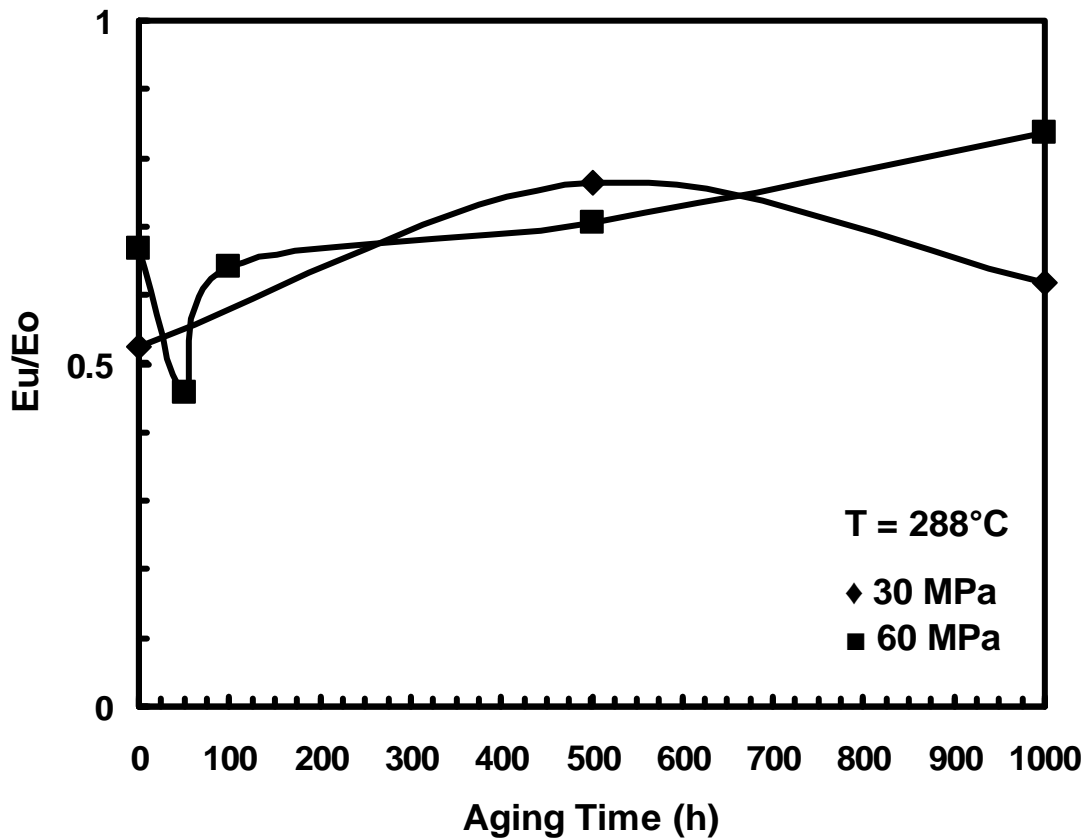


Figure 47: Ratio of elastic modulus measured upon unloading to the initial room temperature elastic modulus as a function of aging time for carbon fiber reinforced PMR-15 composites tested in creep at 30 and 60 MPa.

Elastic modulus loss due to testing at prior aging, elevated temperature and creep damage did not exceed 57%. The most drastic loss in elastic modulus was seen in the plot

of the E_U/E_O ratio as a function of aging time. These modulus ratios help to distinguish changes in the mechanical behavior of each specimen due to aging, those due to loading, and those due to elevated temperature. Furthermore, these modulus ratios may be more accurate in evaluating the degree of thermal or oxidative degradation of the specimen than the actual modulus values plotted in Figure 41 and Figure 42.

Monotonic Tensile Tests

Tensile Tests for Aged and Unaged Test Specimens

Multiple tensile tests to failure were carried out on the carbon fiber reinforced PMR-15 test specimens. These tests were performed at the elevated temperature of 288°C for aged and unaged test specimens. It can be noted from prior research, that the tensile tests may not have reached the ultimate tensile strength of the material due to fractures originating at one of the dimples [2]. The tensile test allowed for the finding of two material properties: the Young's modulus of elasticity and the Ultimate Tensile Strength. In Figure 48, the stress-strain curves are shown for all test specimens that were subjected to tensile testing.

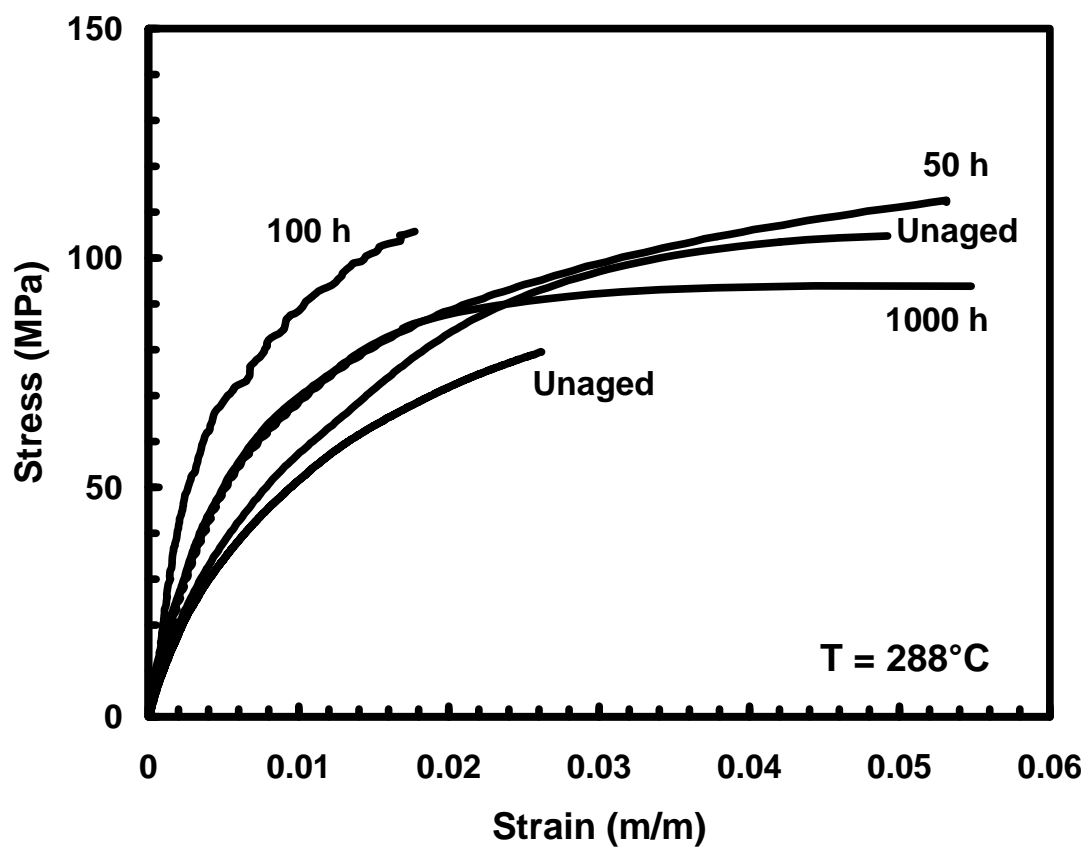


Figure 48: Stress-strain curves for aged and unaged specimens at 288°C during tensile testing.

Aging History	Modulus (GPa)	Ultimate Tensile Strength (MPa)
Unaged	12.49	104.82
Unaged	10.75	79.84
50 h	13.2	112.15
100 h	14.19	105.77
1000 h	12.36	93.80

Table 6: Elastic modulus and UTS measurements for test specimens subjected to tensile testing at 288°C.

As seen in Table 6, it is apparent that there is fluctuation in the loading modulus. The modulus was calculated from the early portion of the stress-strain curve for all specimens between 0 and 7 MPa. The Ultimate Tensile Strength is decreasing as a function of aging time at 288°C. There is significant variation in UTS between the two unaged test specimens. They had similar room temperature moduli, so there is little explanation for this decrease. Failure of every specimen occurred in the gage section of each specimen. Fiber scissoring preceded failure and accounted for large failure strain.

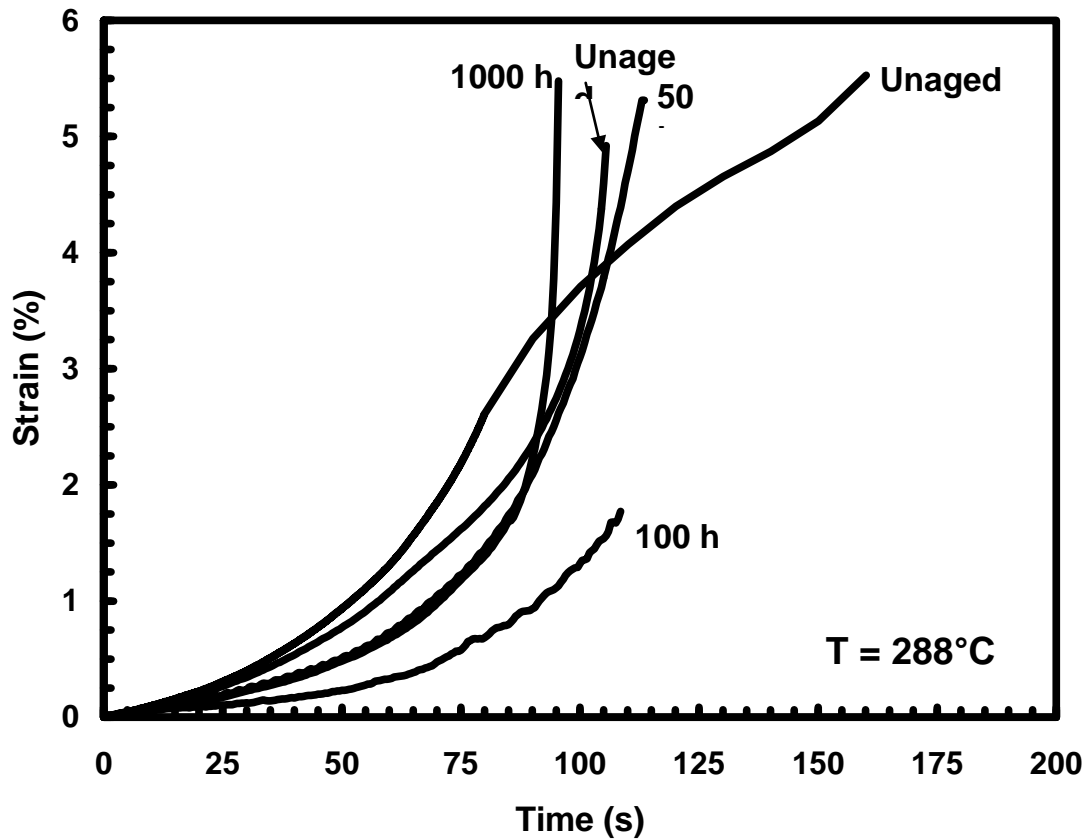


Figure 49: The strain as a function of time that it took the aged and unaged carbon fiber reinforced PMR-15 neat resin specimens to fracture at 288°C.

All fracture surface pictures can be seen in Appendix A.

Creep Tests

Creep Tests of Unaged Specimens

Creep tests at 30 and 60 MPa stress levels lasting for at least 25 h were followed by unloading to zero stress and a recovery period of at least 50 h. Notice that the recovery period is twice that of the creep period. Creep results are plotted in the form of creep

strain versus creep time curves. During creep, stress remains constant, but strain increases.

The creep curves of the unaged specimens at 30 and 60 MPa at 288°C are presented in Figure 50.

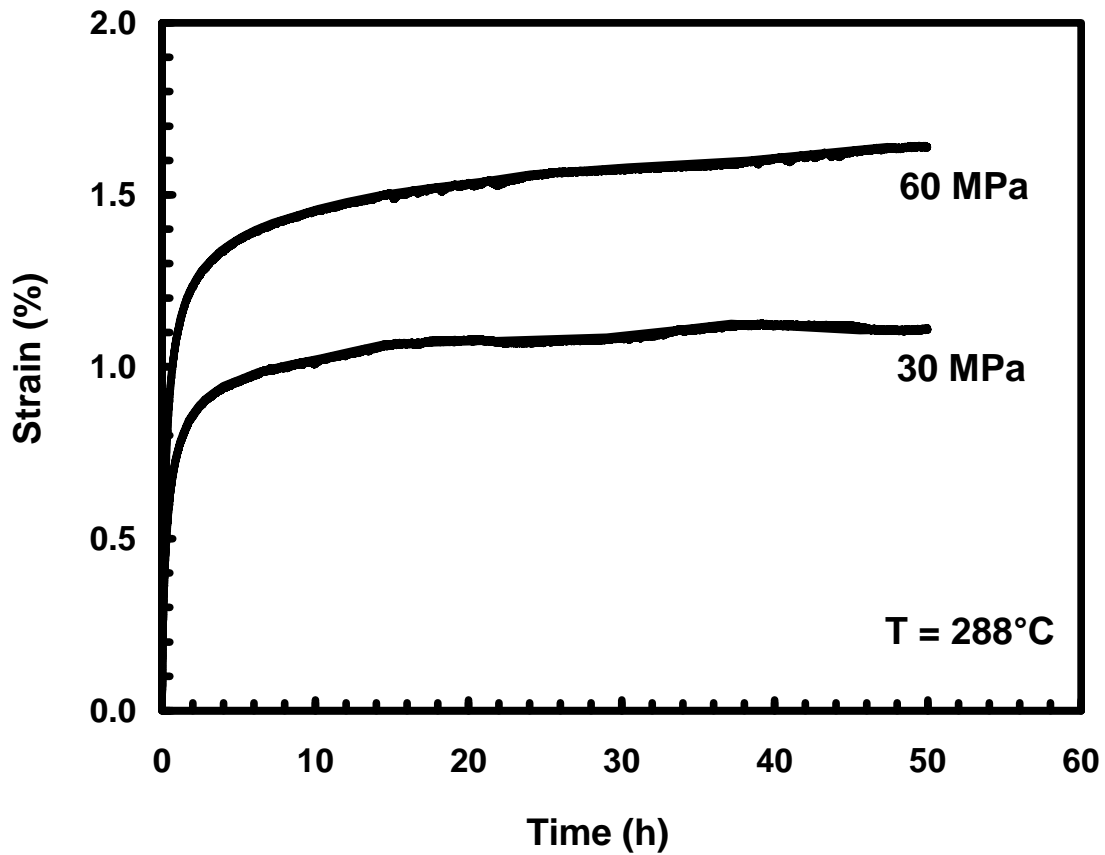


Figure 50: Creep stress versus strain curves for the unaged (as-processed) carbon fiber reinforced PMR-15 neat resin at 288°C.

For unaged specimens it can be seen that higher creep strains are produced at a higher creep stress level with increasing aging time and elevated temperature. Both creep

curves exhibit primary and secondary creep regimes. The transition from primary creep to secondary creep takes place at about 4 h. Steady-state or secondary creep rates increase with creep stress level. These unaged test specimens were subjected to 50 hours of creep duration followed by 100 hours of recovery at zero stress.

Creep Tests at 60 MPa

Test specimens were aged in air at 288°C for up to 1000 h and subjected to creep and recovery tests. The creep stress level was 60 MPa, and the duration of the creep period was at least 25 h. Recovery was at zero stress and lasted for at least 50 h.

One would suspect from prior research that creep strain would decrease with increased aging time. However, this is not the case with the 50 h aged specimen which accumulated ~2% creep strain compared to that of the unaged specimen which accumulated ~1.8% creep strain. This could be due to the fact that the unaged specimen had a higher room temperature elastic modulus. This 50 h specimen is an anomaly and may have had a defect not noticeable before testing. However, the rest of the experimental data agrees with prior research. The specimen aged at 100 h accumulated a creep strain of ~1.3%, while the specimen aged at 500 h accumulated a creep strain of ~0.7%. It is clear that as the aging time increases at 288°C the creep strain accumulation obtained by the specimen decreases. The specimen aged for 1000 h accumulated a creep strain of ~0.5%. These creep strain measurements were taken from Figure 51 on the next page. It shows that creep strain accumulation decreases with increasing prior aging time.

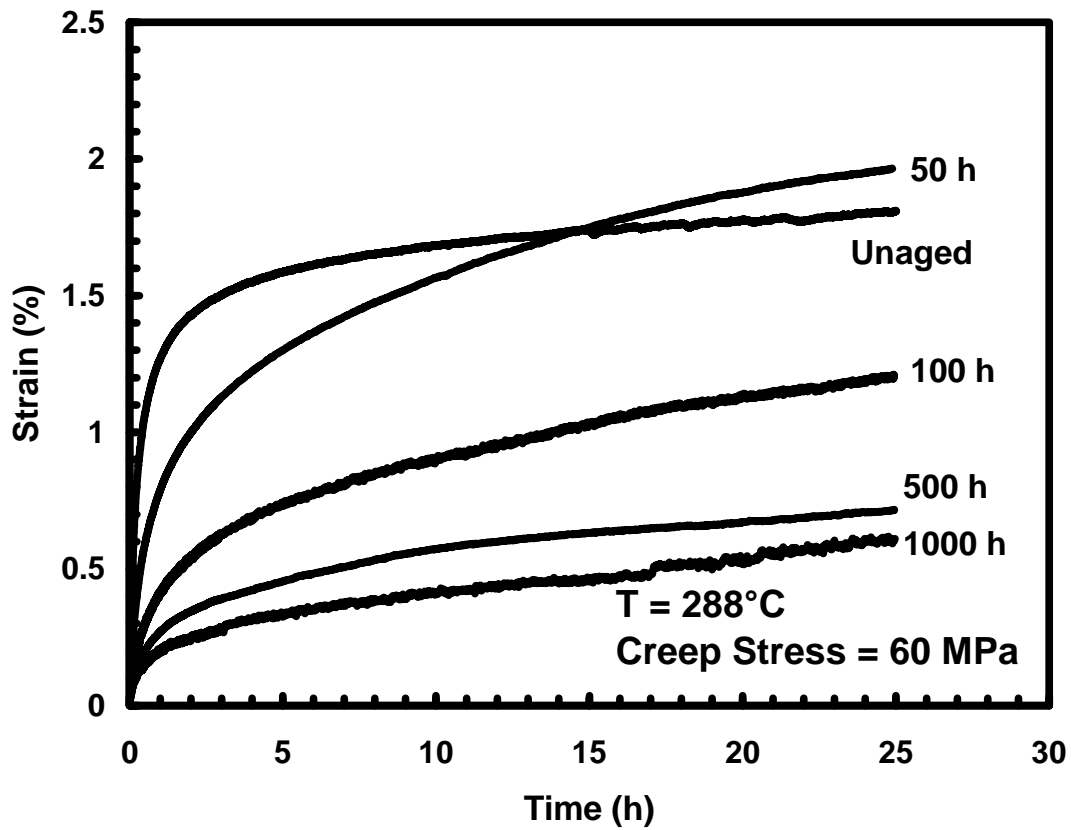


Figure 51: Creep stress versus strain curves for carbon fiber reinforced PMR-15 neat resin aged in air at 288°C at a creep stress level of 60 MPa.

Creep Tests at 30 MPa

Test specimens were aged in air at 288°C for up to 1000 h and subjected to creep and recovery tests. The creep stress level was 30 MPa, and the duration of the creep period was at least 25 h. Recovery was at zero stress and lasted for at least 50 h.

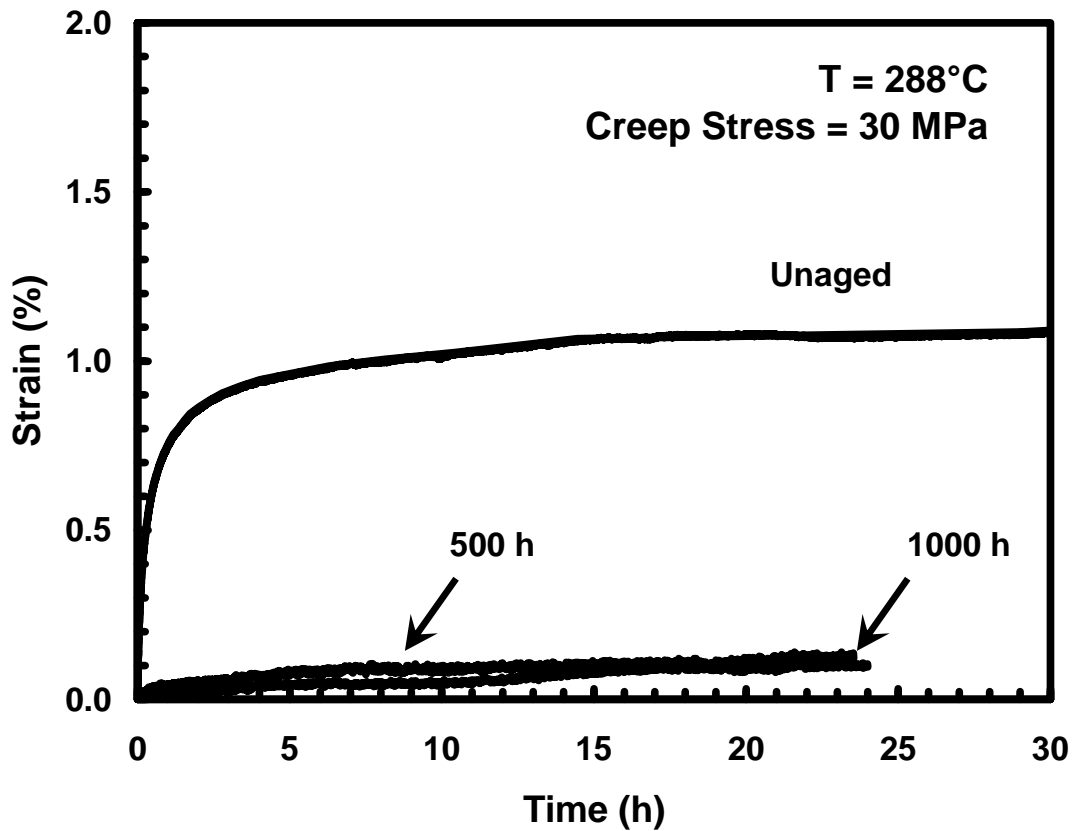


Figure 52: Creep stress versus strain curves for carbon fiber reinforced PMR-15 neat resin aged in air at 288°C at a creep stress level of 30 MPa.

From Figure 52 it is evident that accumulation of creep strain decreases with increasing prior aging time at 288°C. It appears that at a lower creep stress level the accumulation of creep strain is also lower. Overlapping or very close proximity of the 500 h and 1000 h creep curves is also evident. It should be mentioned that not a single specimen failed during creep tests at 30 or 60 MPa.

While in the process of examining creep curves, it may also be useful to examine creep strain accumulation after 25 h of creep as a function of prior aging time. Creep strain accumulation after 25 h versus aging time for all specimens is shown in Figure 53.

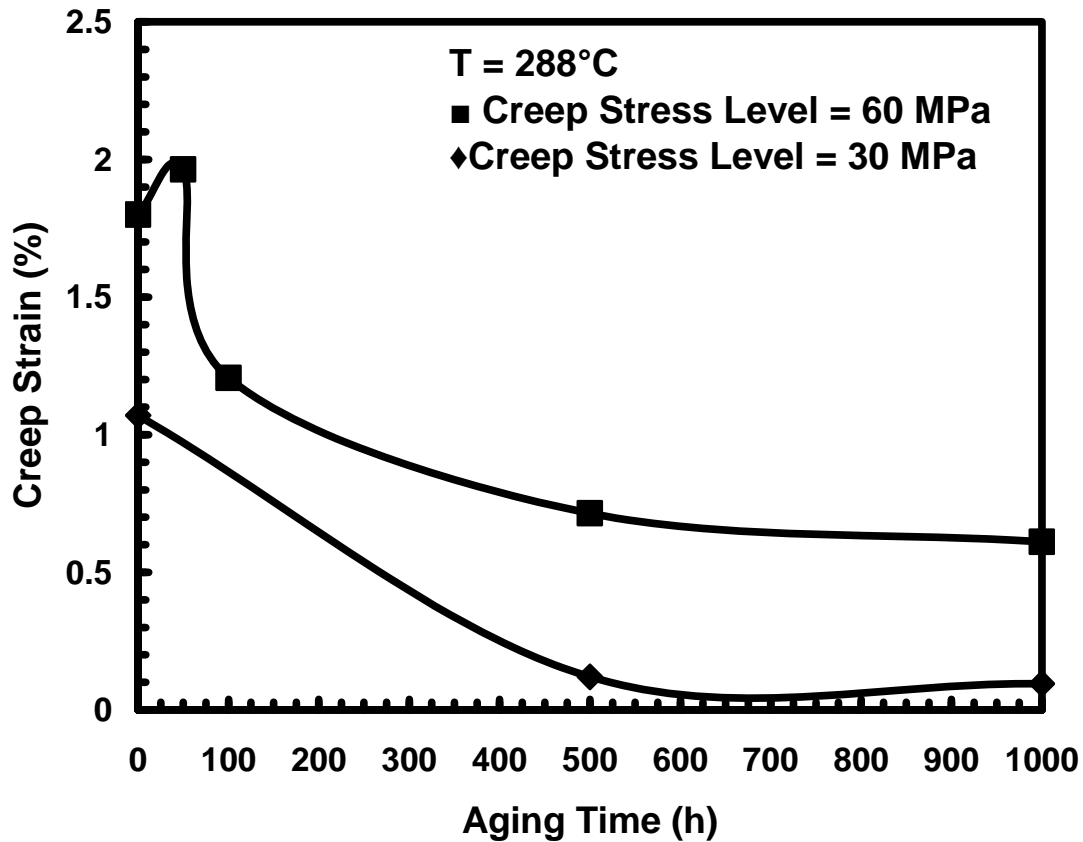


Figure 53: Creep strain accumulated in 25 h as a function of aging time for carbon fiber reinforced PMR-15 neat resin.

For the most part, creep strain accumulation decreases with increasing prior aging time. This is not the case at a creep stress level of 60 MPa for the unaged and 50 h aged specimens, but prior studies show the general trend of decreasing creep strain accumulation with increasing aging time [10]

Recovery at Zero Stress after 60 MPa Creep Test

Test specimens in a creep stress level of 60 MPa were held in this creep stress level for at least 25 h and then recovered at zero stress for at least 50 h. In Figure 54, it is evident that recovery period strain decreases rapidly during the initial recovery period and then levels off and remains nearly constant until the end of the recovery period. The amount of creep strain recovered may emphasize the amount of permanent damage that was accumulated during the creep period or any other physical or chemical damages.

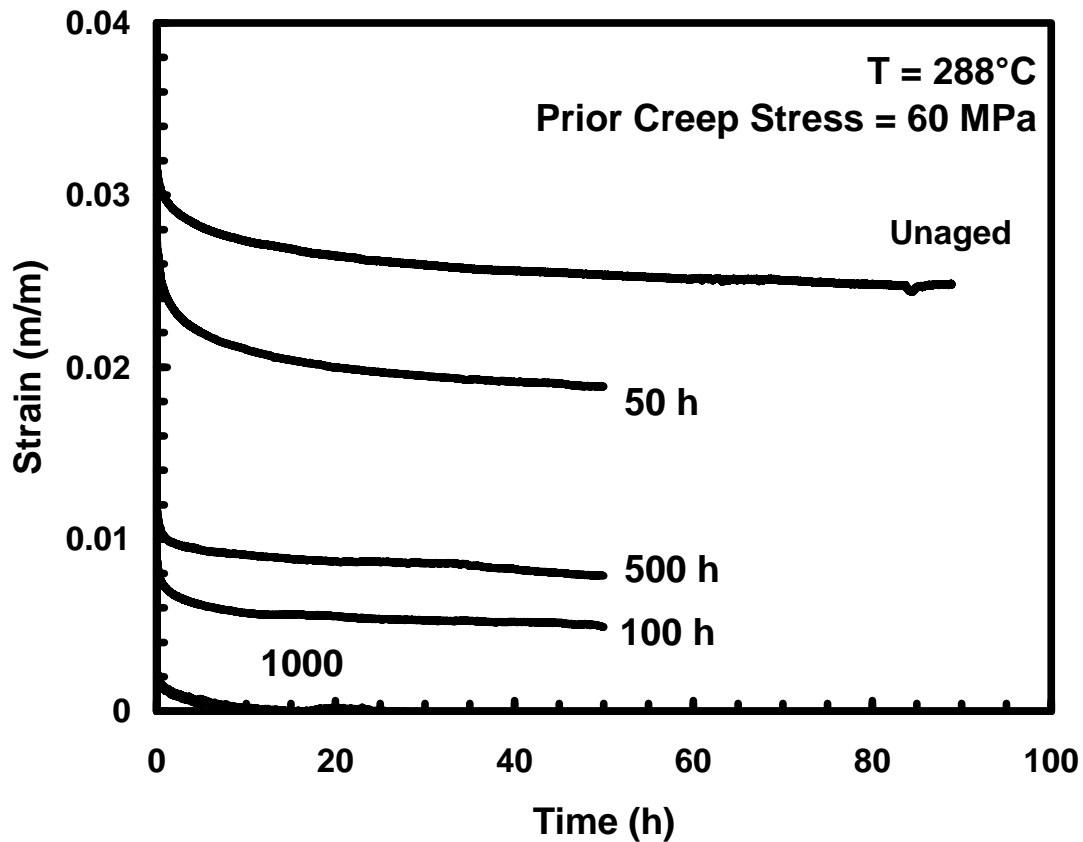


Figure 54: Recovery curves for carbon fiber reinforced PMR-15 neat resin aged in air at 288°C with a prior creep stress of 60 MPa at 288°C.

Comparing the creep strain curves in Figure 54 may be difficult due to the fact that their placement depends on the creep strain accumulated prior to recovery. Therefore, it is imperative to look at the amount of creep strain recovered. The recovered strain is defined as $\varepsilon^r = \varepsilon' - \varepsilon^*$, where ε' and ε^* are the strain after the beginning of the recovery period and at some time t during the recovery period, respectively. These strains are shown in Figure 55.

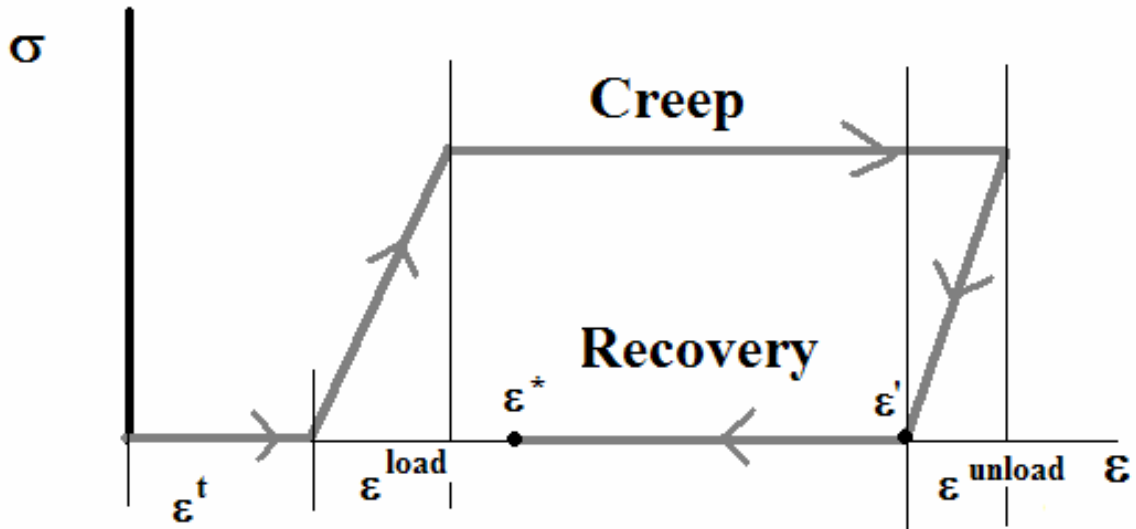


Figure 55: Schematic stress-strain curve for a constant stress creep period followed by recovery period at zero stress. Figure from Ref. [10].

The recovered strain as a function of time is depicted in Figure 56 for specimens tested at a creep stress level of 60 MPa. The recovered strain as a function of time at a creep stress level of 30 MPa will not be shown graphically. The data is meaningless due to the fact that the strain recovered was very small and was within the range of the noise inherent in the system. The recovered strain was between 0.05 and 0.01% which is

pushing the accuracy limit of the extensometer. The results were so close to the accuracy of the extensometer that the data becomes obscured by electrical noise. Overall, the graphical analysis is misleading.

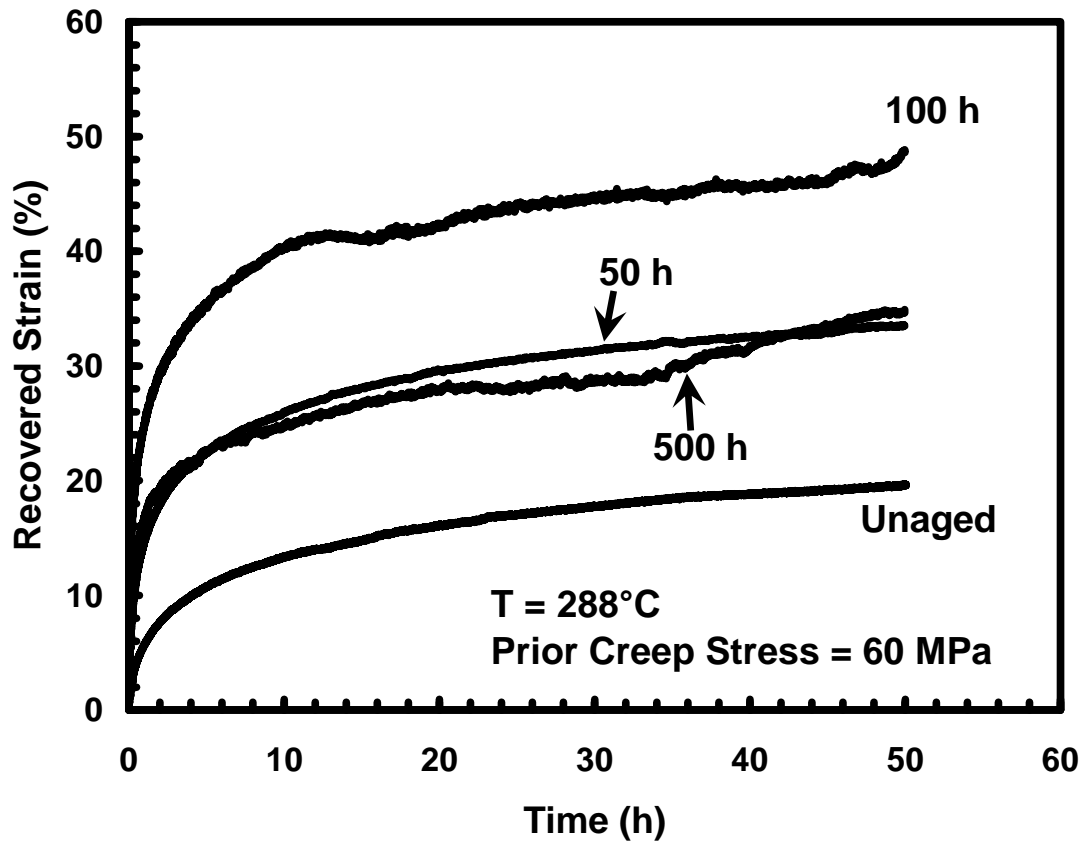


Figure 56: Recovered Strain versus time curves for carbon fiber reinforced PMR-15 neat resin aged in air at 288°C and exposed to a prior creep stress of 60 MPa at 288°C.

In Figure 56, prior aging time does not appear to significantly influence recovery at zero stress as was seen in the PMR-15 neat resin [10]. The PMR-15 neat resin showed that recovered strain decreases with prior aging time in air at 288°C. In Figure 56, the test

specimen with a prior aging time of 100 h was found to recover about 50% of its strain whereas the unaged specimen only recovered about 20% of its strain.

In addition to calculating percent of recovered strain, the percent of creep strain recovered was also calculated. Using the schematic in Figure 55, the percent of creep strain recovered was calculated. From Figure 55, ϵ^t is the thermal strain accumulated during heating of the specimen, ϵ^{load} is the strain accumulated during loading, ϵ^{unload} is the strain recovered during unloading, ϵ' is the strain value immediately upon reaching zero stress, and ϵ^* is the instantaneous strain at any point in time during the recovery period. Creep strain or ϵ^{creep} is defined as the amount of strain accumulated during the creep period, and is given by $\epsilon^{\text{creep}} = \epsilon' - \epsilon^t + \epsilon^{\text{unload}} - \epsilon^{\text{load}}$. Typically, ϵ^{unload} was close to or almost equal to ϵ^{load} , so the expression for ϵ^{creep} becomes $\epsilon^{\text{creep}} = \epsilon' - \epsilon^t$. The ratio of recovered strain ($\epsilon^r = \epsilon' - \epsilon^*$) to creep strain ($\epsilon^{\text{creep}} = \epsilon' - \epsilon^t$) will determine the percent of creep strain recovered. Results in Figure 57 show the percent of creep strain recovered for specimens tested at a creep stress level of 60 MPa aged in air at 288°C.

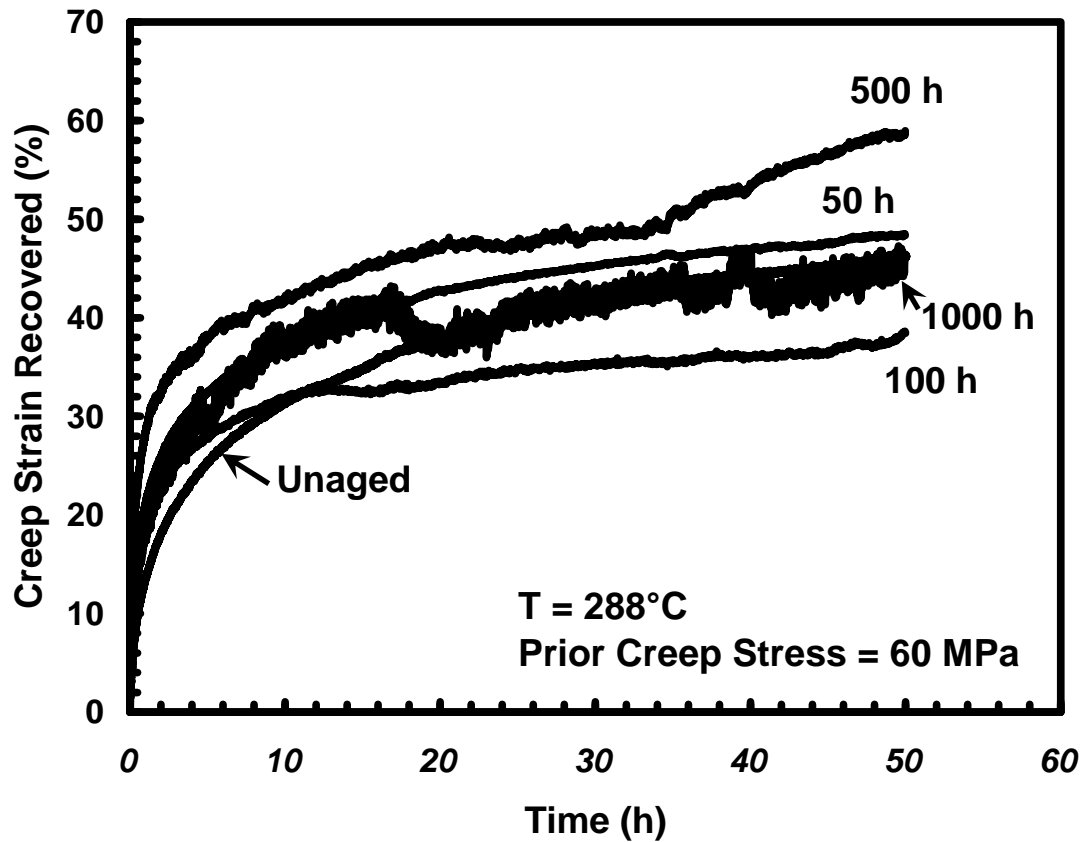


Figure 57: Creep recovery curves for carbon fiber reinforced PMR-15 neat resin aged in air at 288°C with a prior creep stress of 60 MPa.

In Figure 57, prior aging time does not appear to significantly influence recovery at zero stress. Again, the graph depicting the creep recovery curves for carbon fiber reinforced PMR-15 neat resin aged in air at 288°C with a prior creep stress of 30 MPa will not be shown due to the small measured strains which become obscured by electrical noise.

VI. Concluding Remarks

Chapter Overview

This section will help to draw conclusions from the experimental data gathered from testing.

Concluding Remarks

Carbon fiber reinforced PMR-15 neat resin with a 8-harness satin fabric weave \pm 45 fiber orientation was aged in air at 288°C for 0, 50, 100, 500, and 1000 h. Test specimens were subjected to tensile and creep testing at 288°C. Creep tests were conducted at 30 and 60 MPa. All creep tests were followed by recovery at zero stress. The duration of the creep period was at least 25 h followed by a recovery period of at least 50 h, or twice the creep period. In addition, a rectangular test specimen was measured for weight loss measurements at 0, 10, 50, 100, 250, and 500 h. The test specimens subjected to tensile testing to failure were used from each respective aging time to view oxidation layer growth. Elastic modulus measurements were made before, during, and after mechanical testing at 288°C.

Results indicate that prior aging time in air for most of the testing significantly impacted the creep response behavior of the carbon fiber reinforced PMR-15 neat resin composites. Unaged test specimens accumulated creep strains of ~1.7% at 60 MPa and ~1.1% at 30 MPa. After 1000 h of aging the test specimens accumulated creep strains of ~0.5% at 60 MPa and ~0.1% at 30 MPa. It is clear that with prior aging time, there is a reduction in creep strain accumulation. A lower creep stress level also produces less creep strain accumulation. Decrease in creep strain accumulation with prior aging time

was also evident in the PMR-15 neat resin [10]. It appeared that prior aging time did not significantly influence recovery at zero stress. With the PMR-15 neat resin, it was clear that recovered creep strain increased with increasing prior aging time [10]. However, the fibers may have an affect on the creep strain recovered in carbon fiber reinforced PMR-15 neat resin.

The weight loss and the oxidation layer growth as a function of aging time at 288°C were measured. In the presence of an oxidizing environment the weight loss depends on the surface area of the test specimen. The change in surface area due to aging damage is effectively accounted for in the weight loss parameters [6, 7, 22]. The experimental data revealed that weight loss and oxidation layer growth increase with increasing aging time at elevated temperature. After 500 h of aging, the ± 45 rectangular composite saw ~0.95% weight loss compared to ~0.50% at 250 h. The oxidation layer growth at 500 h was ~0.97 mm for the cut surface and ~0.32 mm for the molded surface. After 1000 h the oxidation layer growth was ~1.5 mm for the cut surface and ~0.33 mm for the molded surface. It is apparent that the cut side of the specimen with the fibers exposed to the oxidizing environment experiences a thicker oxidation layer growth. However, much of the oxidation growth on the molded sides of the composite was obscured by the fibers. All weight measurements were obtained with a Metler Toledo AG245 microbalance with a resolution of 0.0001 grams. Oxidation layer growth was observed under a Nikon EPIPHOT digital microscope.

Before prior aging and testing at elevated temperature, the room temperature elastic modulus of each test specimen was measured to account for any specimen-to-

specimen variability. The average modulus was calculated to be 16.3 GPa with a covariance of 0.094. The elastic moduli were also measured during elevated temperature testing at the loading and unloading periods. It was found that the room temperature elastic modulus was higher than the loading and the unloading elastic modulus of each test specimen at elevated temperature. In addition, the unloading modulus was typically lower than the loading modulus which could be attributed to damage accumulated by test specimens during mechanical testing.

In order to increase the effectiveness of this study, it would be imperative for follow on studies to test multiple specimens at each test condition. Due to the limited amount of time and material available, one test was performed for each aging condition. With multiple tests run at each condition, one can determine if the test run the first time around had any errors. Creep tests can also have longer periods of duration to assess whether long term creep response can be predicted from short term creep data. Test specimens can also be aged for a longer periods of time to see a greater decay of the overall composite. It would also be interesting to conduct longer recovery tests to see whether the specimens stop recovering and how much permanent damage occurred. While some of the tests conducted in this study did not match the results of those experienced by the PMR-15 neat resin alone, it is assumed that the carbon fiber reinforcement caused these differences. Aging in argon would also be valuable to see if a change in environment will cause chemical or physical changes in mechanical structure. Additionally, dynamic modulus analysis (DMA) could be performed to check changes in the T_g to check for changes in crosslink density. DMA analysis in the PMR-15 resin

showed that there was an increase in crosslink density with aging time at 288°C, causing a change in mechanical properties and in creep response [10]. Overall, this study made an effort to broaden the current understanding on the mechanical response for carbon fiber reinforced PMR-15 neat resin under sustained loading at 288°C. This study was completed in hopes that this information will be valuable in determining if carbon fiber reinforced PMR-15 composites can be used in future aircraft component applications.

Bibliography

- [1] Ashraf, Badir, Shonkwiler, Brian, Talreja, Ramesh. "Fatigue Property Characterization of T650-35/AMB21 Laminates under Room and Elevated Temperature", *American Institute of Aeronautics and Astronautics*, AIAA 2002-1679 (2002).
- [2] Balconis, John G. *Some Aspects of the Mechanical Response of BMI-5240-4 Neat Resin at 191°C*. MS Thesis, AFIT/GAE/ENY/06-M03. Graduate School of Engineering and Management, Air Force Institute of Technology, Wright-Patterson Air Force Base, OH, March 2006.
- [3] Bowles, K.J., "Effect of Fiber Reinforcements on Thermo-Oxidative Stability and Mechanical Properties of Polymer Matrix Composites", *NASA/Lewis Research Center*, NASA TM-103648 (January 1991).
- [4] Bowles, K.J., "Thermal and Mechanical Durability of Graphite-Fiber-Reinforced PMR-15 Composites", *NASA/Lewis Research Center*, NASA TM-113116 (September 1997).
- [5] Bowles, Kenneth J., Meyers, Anne, "Specimen Geometry Effects on Graphite/PMR-15 Composites During Thermo-Oxidative Aging", *NASA/Lewis Research Center*, NASA TM-87204 (April 1986).
- [6] Bowles, K.J., Papadopoulos, Demetrios S., Linda, Ingraham L., Linda, McCorkle S., Klan, Ojars V., "Longtime Durability of PMR-15 Matrix Polymer at 204, 260, 288, and 316°C", *NASA/Glenn Research Center*, NASA TM-2001-210602 (July 2001).
- [7] Bowles, K.J., Luis, Tsuji, Kamvouris, John, Roberts, Gary D., "Long-Term Isothermal Aging Effects on Weight Loss, Compression Properties, and Dimensions of T650-35 Fabric-Reinforced PMR-15 Composites—Data", *NASA/Lewis Research Center*, NASA TM-2003-211870 (February 2003).
- [8] Bowles, K.J., Nowak, Gregory, "Thermo-Oxidative Stability Studies of Celion 60000/PMR-15 Unidirectional Composites, PMR-15, and Celion 6000 Fiber", *Journal of Composite Materials*, 22:966-985 (1987).
- [9] Brinson, Catherine L, and others, "Going to Extremes Meeting the Emerging Demand for Polymer Matrix Composites", Washington DC, *The National Academies Press*, 2005.

- [10] Broeckert, Joseph L., *Effects of Prior Aging at Elevated Temperature in Air and in Argon Environments on Creep Response of PMR-15 Neat Resin*. MS Thesis, AFIT/GMS/ENY/07-M01. Graduate School of Engineering and Management, Air Force Institute of Technology, Wright-Patterson Air Force Base, OH, March 2007.
- [11] Cytec Engineered Materials. "CYCOM 2237 Polyimide."
<http://www.cytec.com/engineered-materials/products/Datasheets/CYCOM2237.pdf>
- [12] Conreur, C., Francillette, J., Laupretre, F., "Synthesis and Processing of Model Compound of PMR-15 Resin", *Journal of Polymer Science Part A: Polymer Chemistry*, 23:123-136 (1997).
- [13] "DMBZ Polyimides Provide an Alternative to PMR-15 for High-Temperature Applications", *NASA/Lewis Research Center*, 2005.
- [14] Falcone, Christina M. *Rate Dependence and Short-Term Creep Behavior of PMR-15 Neat Resin at 23 and 288°C*. MS Thesis, AFIT/GAE/ENY/05-S07. Graduate School of Engineering and Management, Air Force Institute of Technology, Wright-Patterson Air Force Base, OH, September 2005.
- [15] Gentz, M., Armentrout, D., Rupnowski, P., Kumosa, L., Shin, E., Sutter, J.K., Kumosa, M., "In-Plane Shear Testing of Medium and High Modulus Woven Graphite Fiber Reinforced/Polyimide Composites", *Composites of Science and Technology*, 64:203-220 (2004).
- [16] Green, John A.S. and others, "New Materials for Next Generation Commercial Transports", Washington DC, *The National Academies Press*, 1996.
- [17] Odegard, G., Searles, K., Kumosa, M., "Nonlinear Analysis of woven Fabric-Reinforced Graphite/PMR-15 composites under Shear-Dominated Biaxial Loads", *Mechanics of Composite Materials and Structures*, 7:129-152 (2000).
- [18] "Polyimide Composites", Aeronautics Learning Laboratory for Science, Technology, and Research. NASA All Star Network, 2004. 4 April 2007.
<http://www.allstar.fiu.edu/aero/polycomp.htm>
- [19] Preston, Peter N., Jigajinni, Veerappa B., Soutar, Ian, Woodfine, Barry, Stewart, Nevin J., Hay, John N., "Structure-Property Relationships in PMR-Type Polyimide Resins: 4. Investigatin of Matrials Derived From Diamino(diaryl)methanes", *Polymer*, Vol. 35, No.11 (1994).

- [20] Ripberger, E.R., Tandon, G.P., Schoeppner, G.A., “Characterizing Oxidative Layer Development in AFR-PE-4-Resin”, In: *Proceedings of the SAMPE 2004 symposium/exhibition*, May 16-20, Long Beach, California.
- [21] Schoeppner, Gregory, Tandon, G.P., “Aging and Durability of PMR-15 High Temperature Polyimide”, In: *Proceedings of the 35th international SAMPE technical conference*, Dayton, OH, September 2003.
- [22] Schoeppner, G.A., Tandon, G.P., Ripberger, E.R., “Anisotropic Oxidation and Weight Loss in PMR-15 Composites”, *Composites: Part A*, 38:890-904 (2007).
- [23] Schoeppner, G.A., Curliss, D.B., “Model-Based Design for Composite Materials Life Management”, In: *Proceedings of the 9th AIAA/ISSMO Symposium on Multidisciplinary Analysis and Optimization Conference*, 4-6 September, Atlanta, GA, AIAA-2002-5516.
- [24] Schoeppner, G.A., Tandon, G.P., Pochiraju, K.V., “Predicting Thermo-Oxidative Degradation and Performance of High Temperature Polymer Matrix Composites”, Multiscale Modeling and Simulation of Composite Materials and Structures, Y Kwon, DH Allen, R Talreja (Eds) Springer-Verlag (in press), 2007.
- [25] Sheppard, Clyde H., “Thermal and Oxidative Stability of Carbon Fibers and Composites”, *SAMPE Quarterly*, Vol. 18, No. 2, pp 14-17 (1987).
- [26] Skontorp, Arne, Wong, Ming-Shih, Wang, Su-Su, “High-Temperature Anisotropic thermal Oxidation of Carbon-Fiber Reinforced Polyimide Composites: Theory and Experiment”, *Proceedings of ICCM-10*, IV 375-382, Whistler B.C., Canada (1995).
- [27] Xie, Wei, Pan, Wei-Ping, Chuang, Kathy C., “Thermal Characterization of PMR Polyimides”, *Thermochimica Acta* 367-368 (2001) 143-153.

Appendix A – Fracture micrographs for test specimens subjected to tensile testing at 288°C

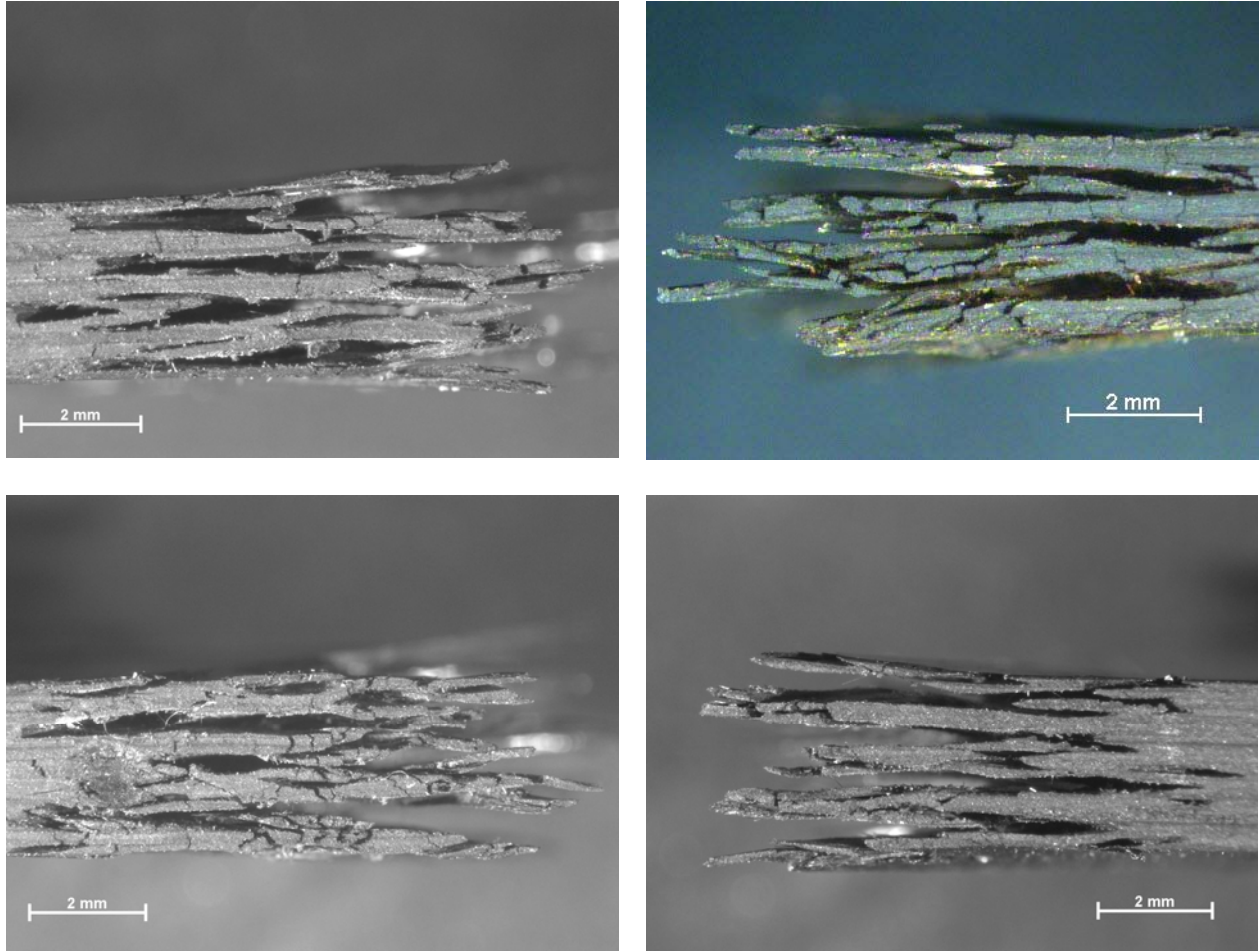


Figure 58: Carbon fiber reinforced PMR-15 neat resin unaged specimen 1 (side view).

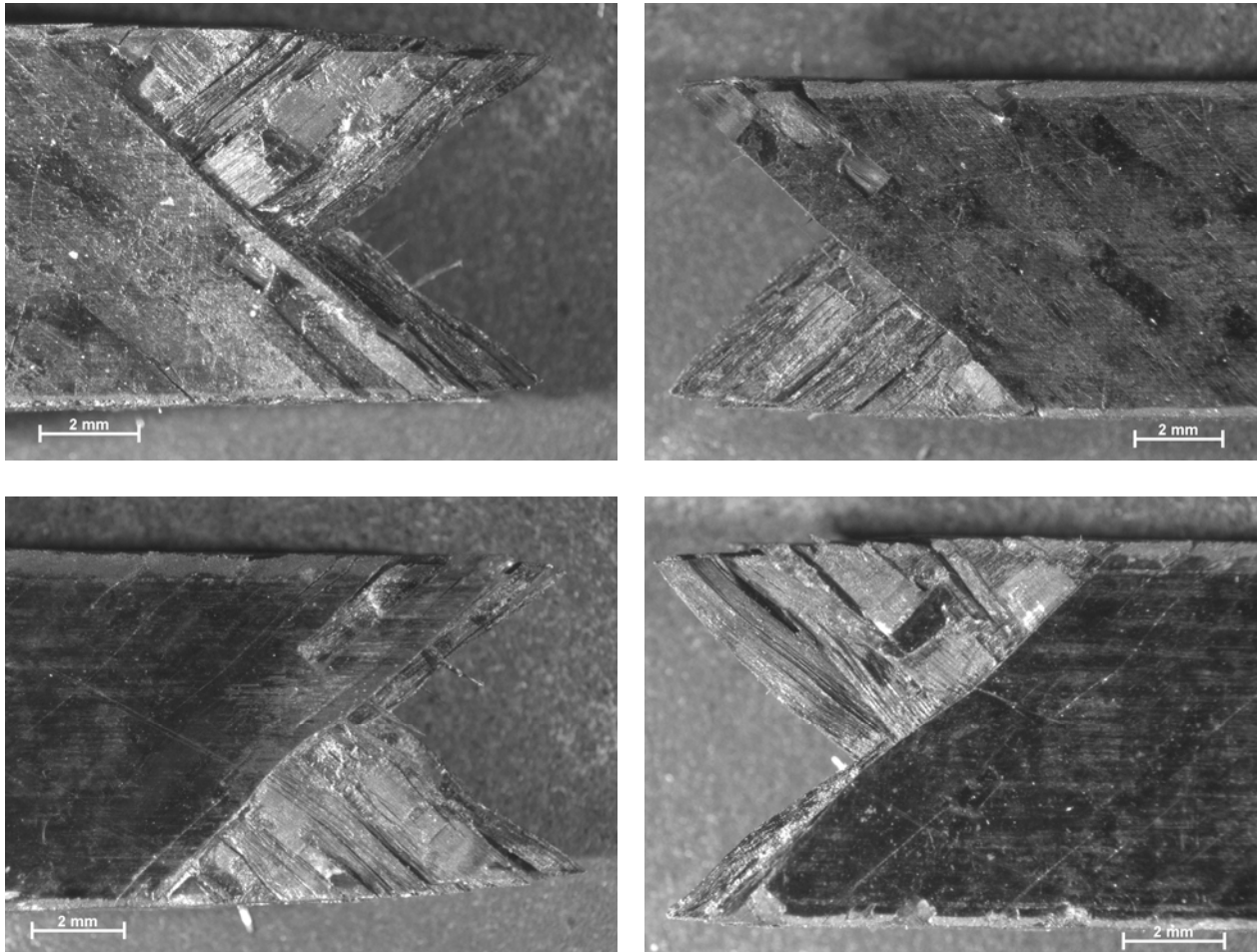


Figure 59: Carbon fiber reinforced PMR-15 neat resin unaged specimen 1 (top view).

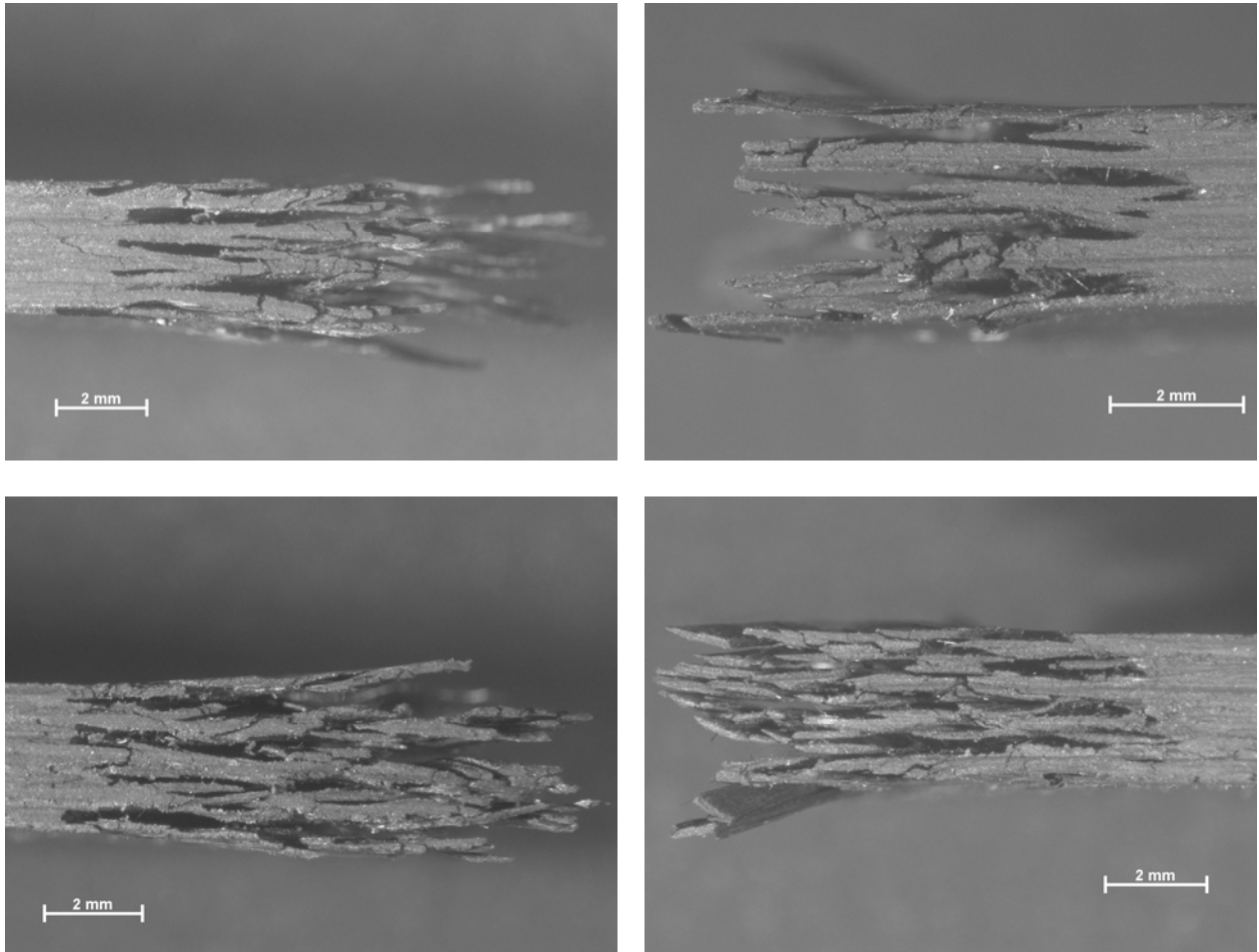


Figure 60: Carbon fiber reinforced PMR-15 neat resin unaged specimen 4 (side view).

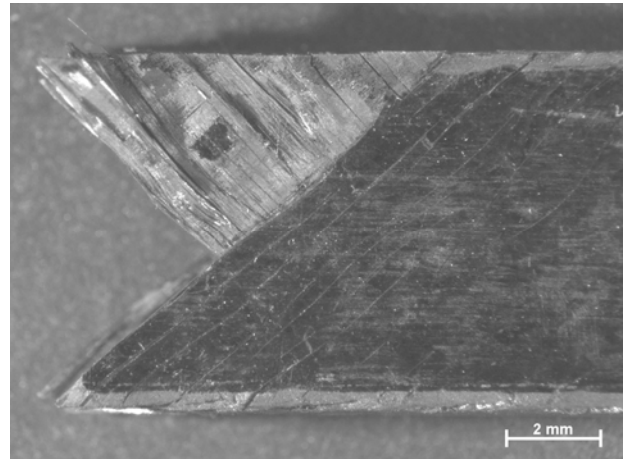
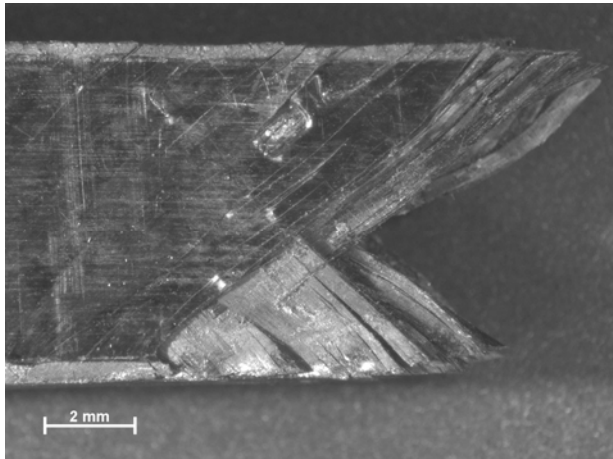
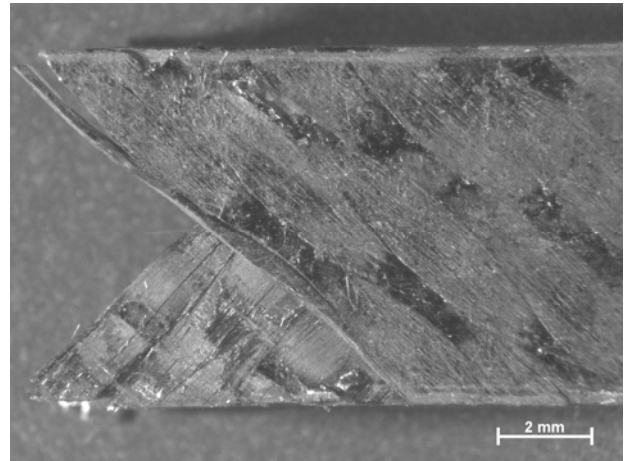
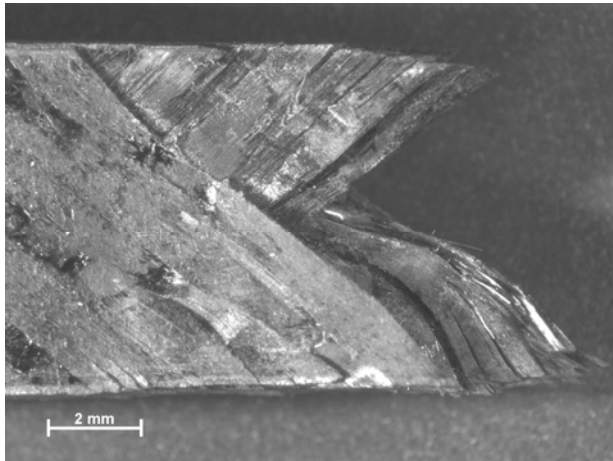


Figure 61: Carbon fiber reinforced PMR-15 neat resin unaged specimen 4 (top view).

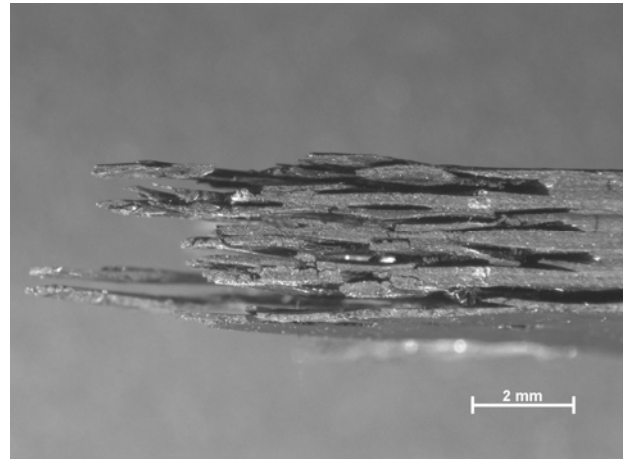
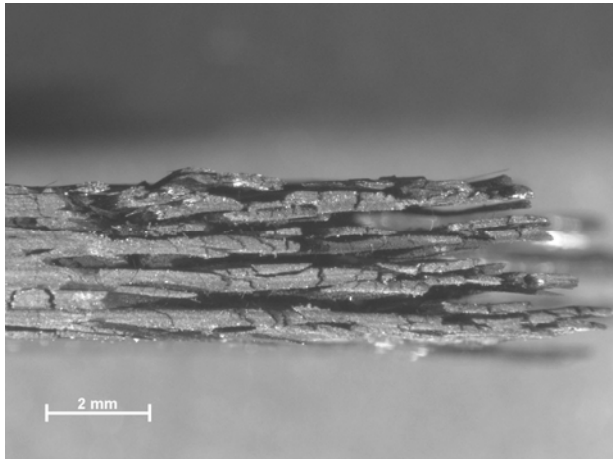
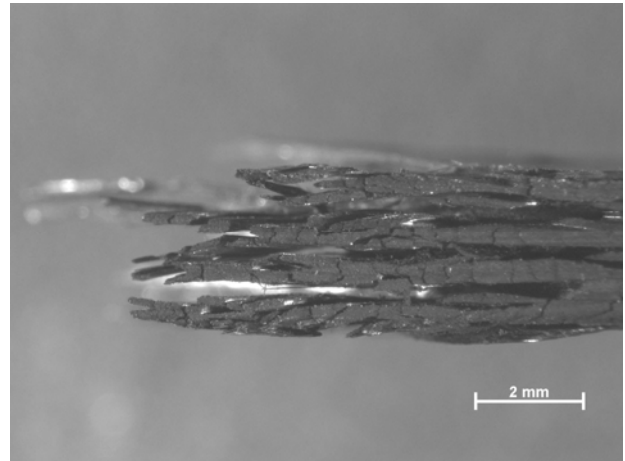
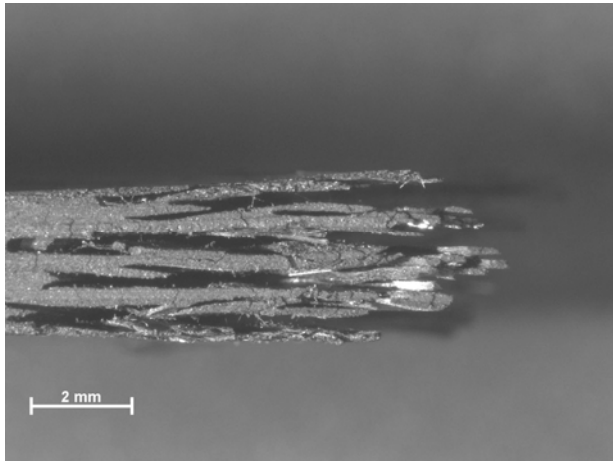


Figure 62: Carbon fiber reinforced PMR-15 neat resin specimen 7 aged in air for 50 h at 288°C (side view).

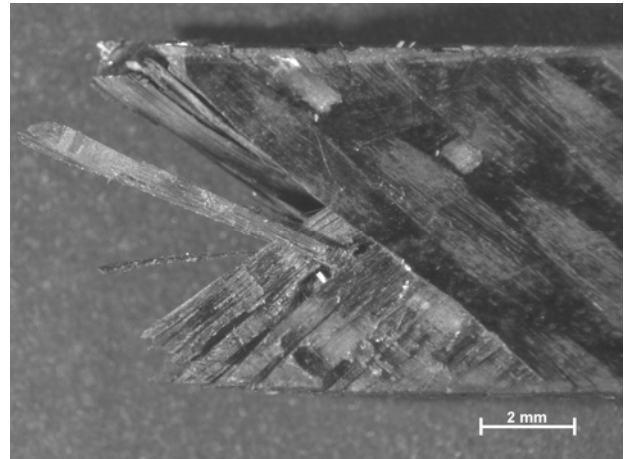
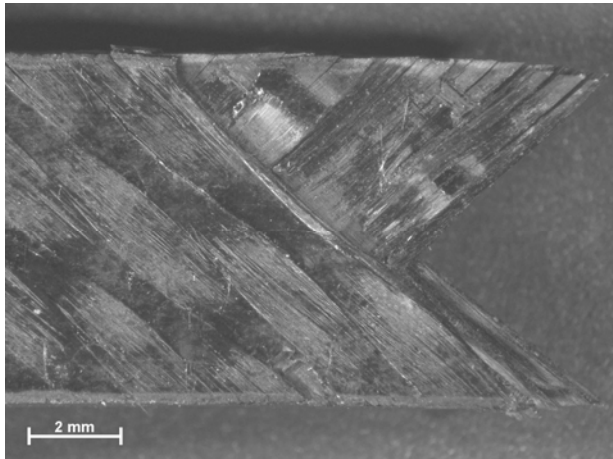
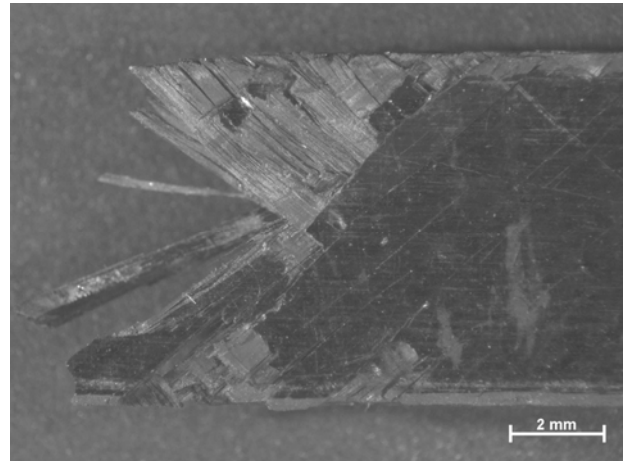
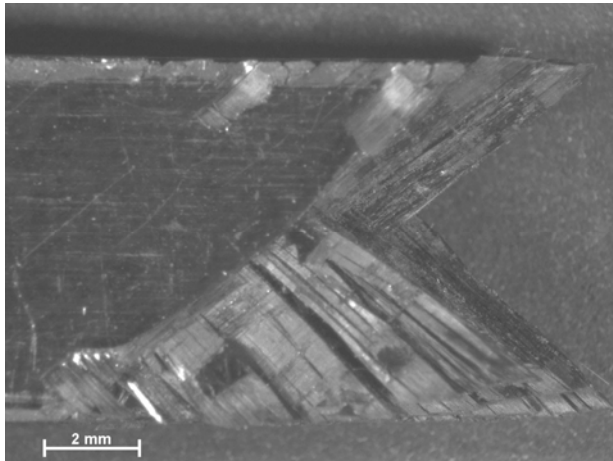


Figure 63: Carbon fiber reinforced PMR-15 neat resin specimen 7 aged in air for 50 h at 288°C (top view).

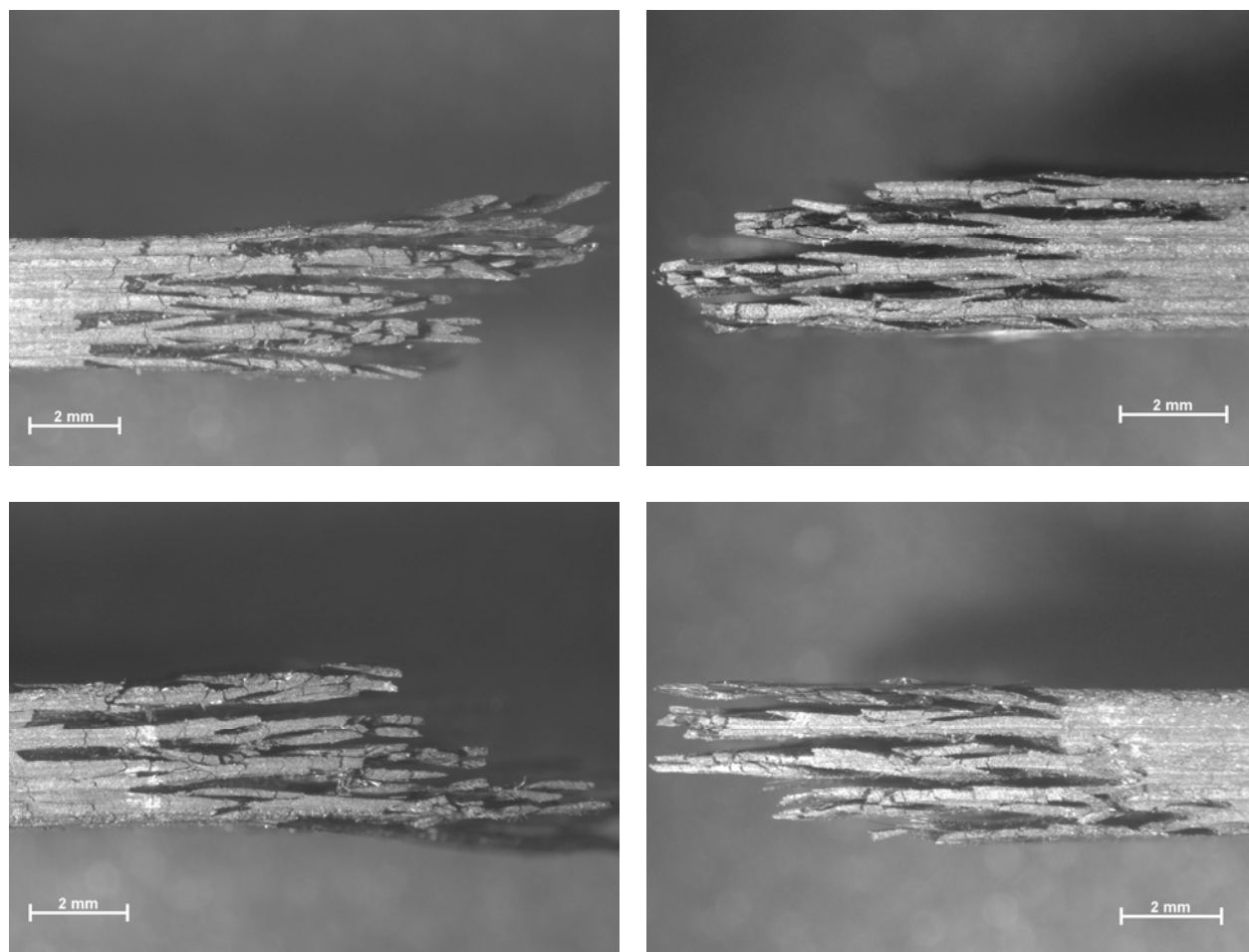


Figure 64: Carbon fiber reinforced PMR-15 neat resin specimen 9 aged in air for 100 h at 288°C (side view).

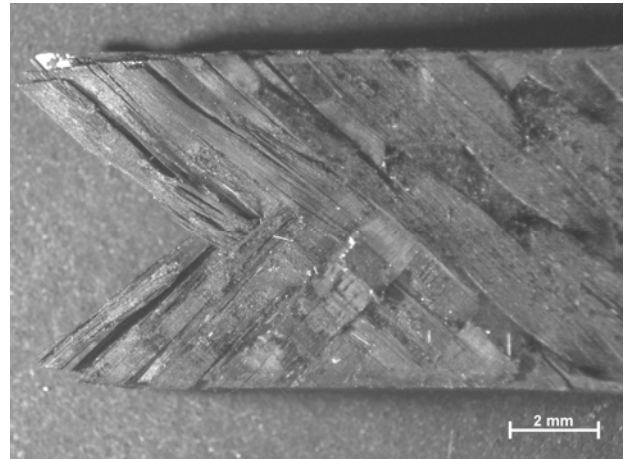
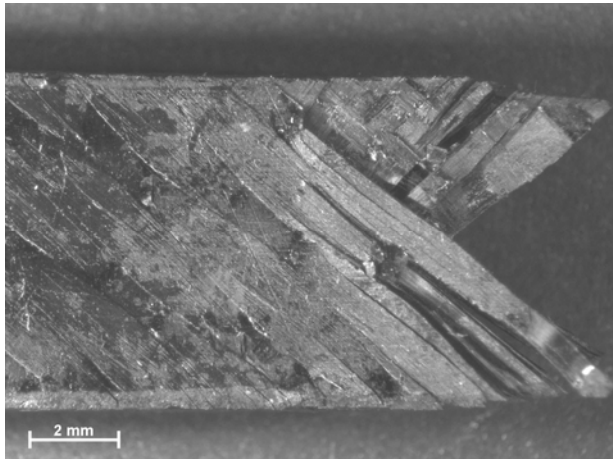
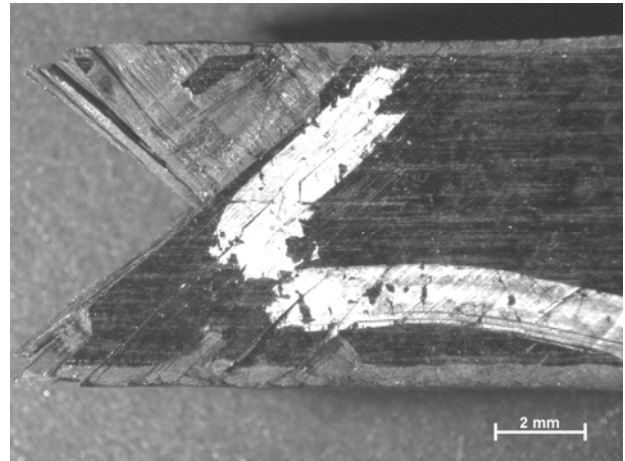
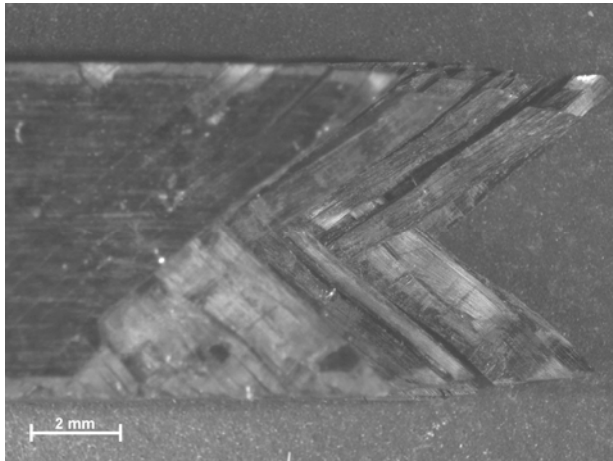


Figure 65: Carbon fiber reinforced PMR-15 neat resin specimen 9 aged in air for 100 h at 288°C (top view).

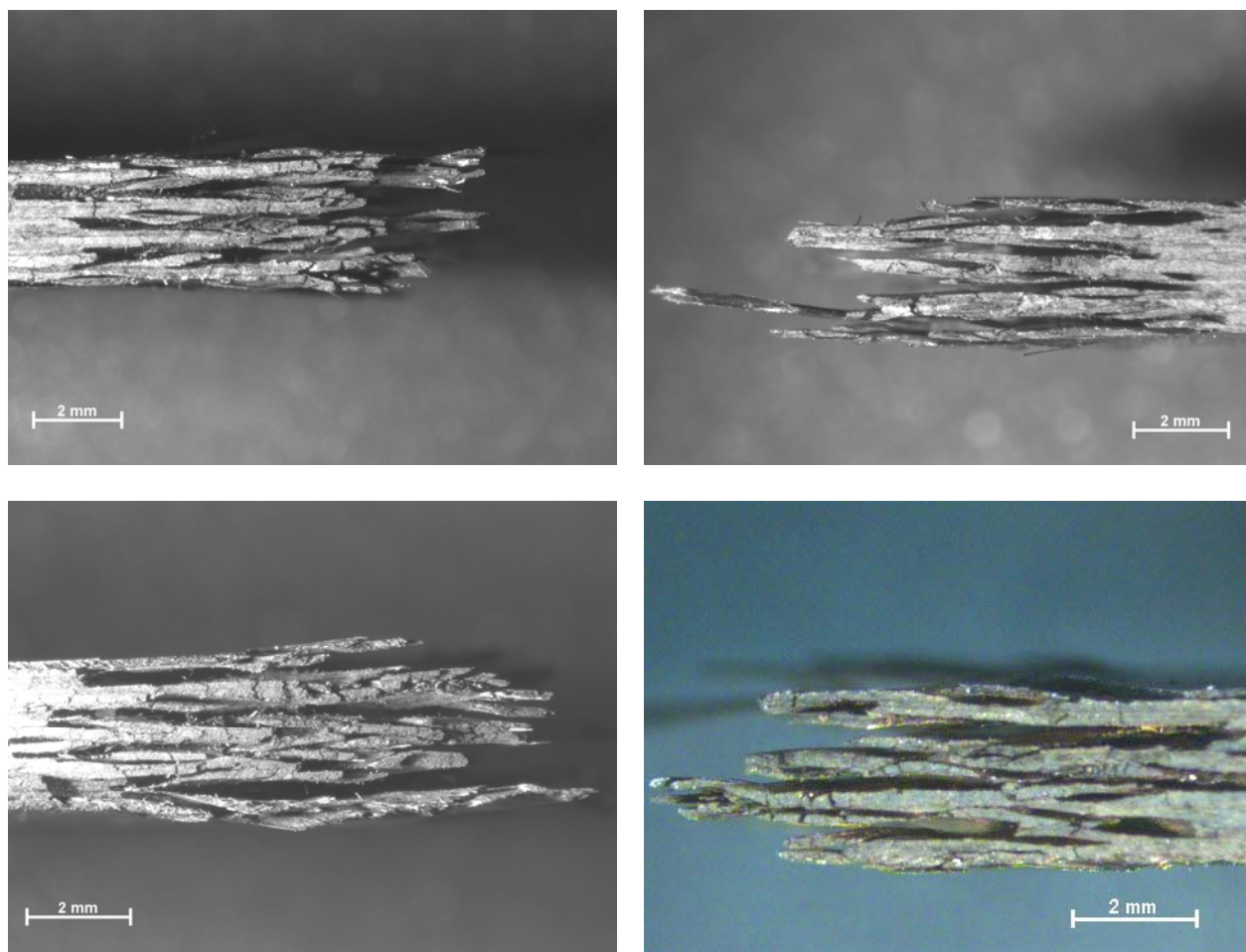


Figure 66: Carbon fiber reinforced PMR-15 neat resin specimen 17 aged in air for 1000 h at 288°C (side view).

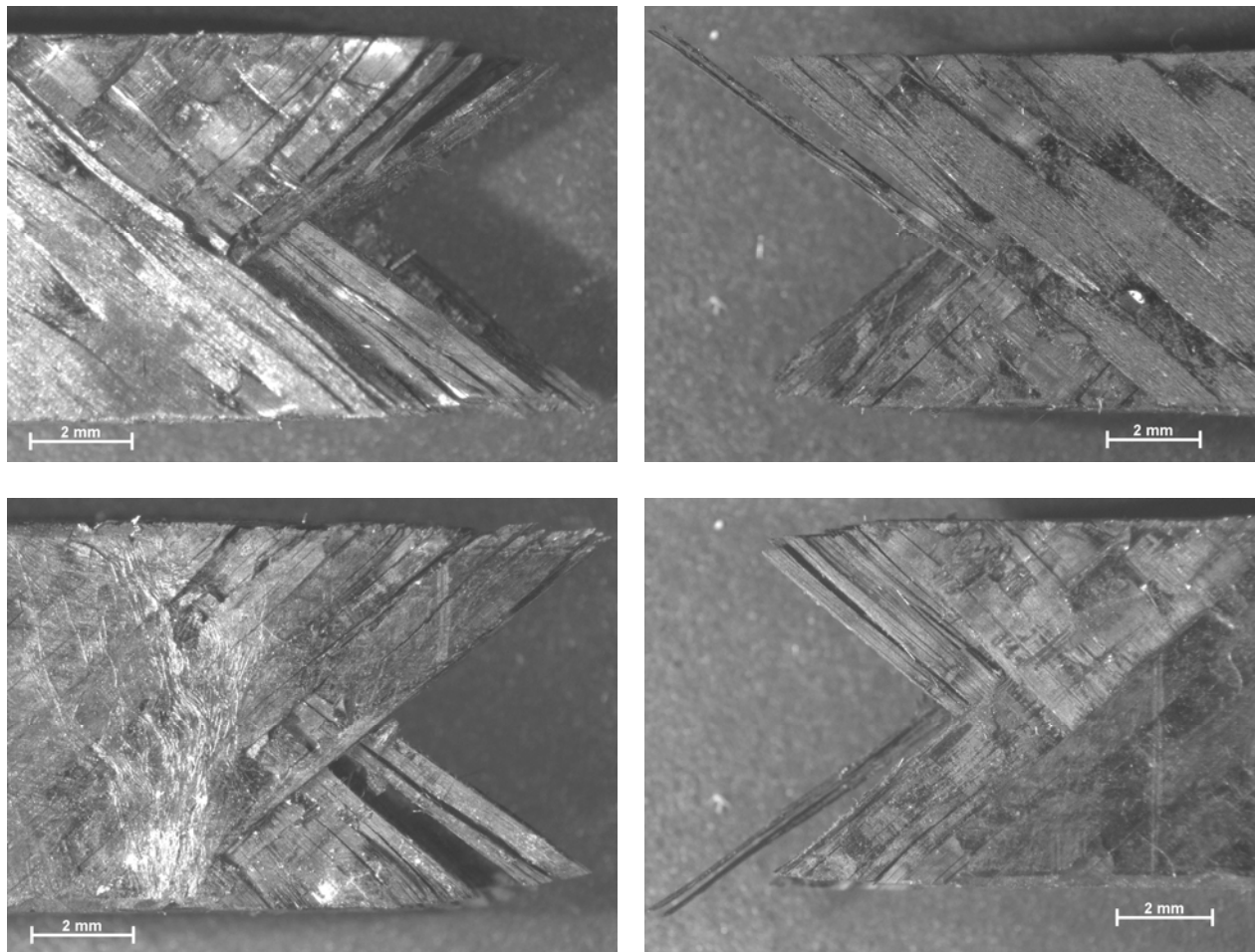


Figure 67: Carbon fiber reinforced PMR-15 neat resin specimen 17 aged in air for 1000 h at 288°C (top view).

Appendix B – Oxidation Layer Growth on Cut and Uncut Surfaces of Test Specimens Aged in Air at 288°C

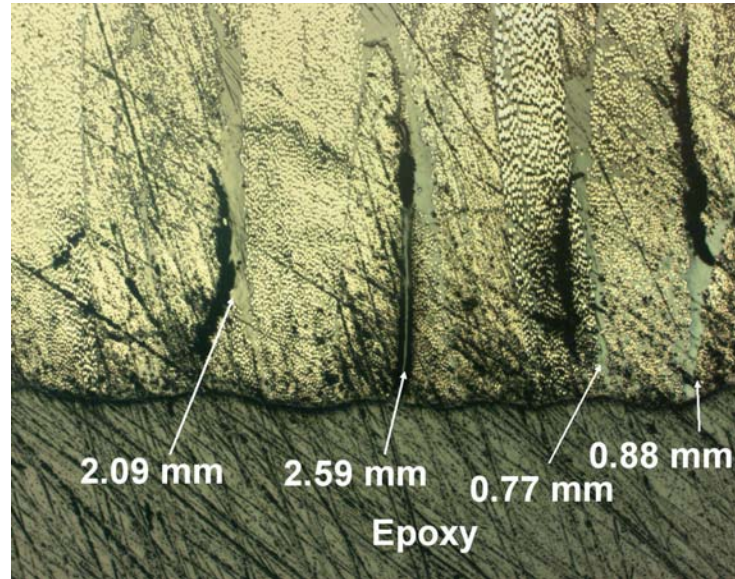


Figure 68: Oxidation layer growth on a specimen aged for 1000 h at 288°C (cut surface). This shows an average oxidation layer of 1.58 mm thick.

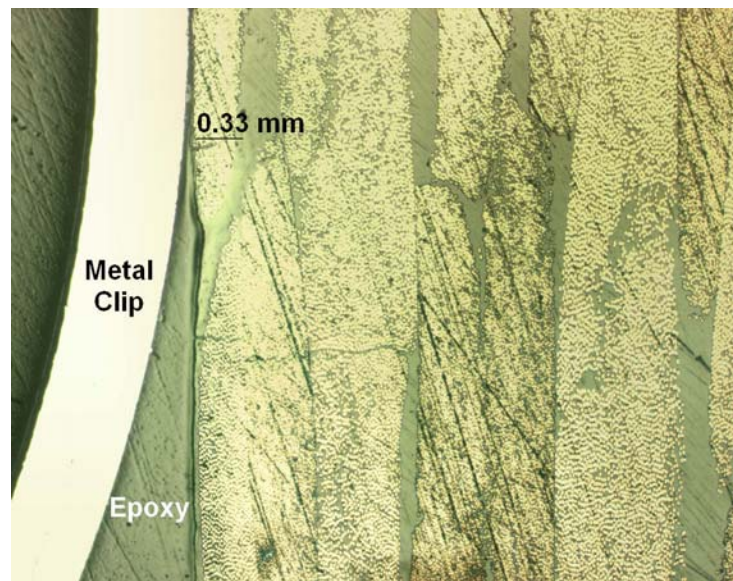


Figure 69: Oxidation layer growth on a specimen aged for 1000 h at 288°C (uncut surface).

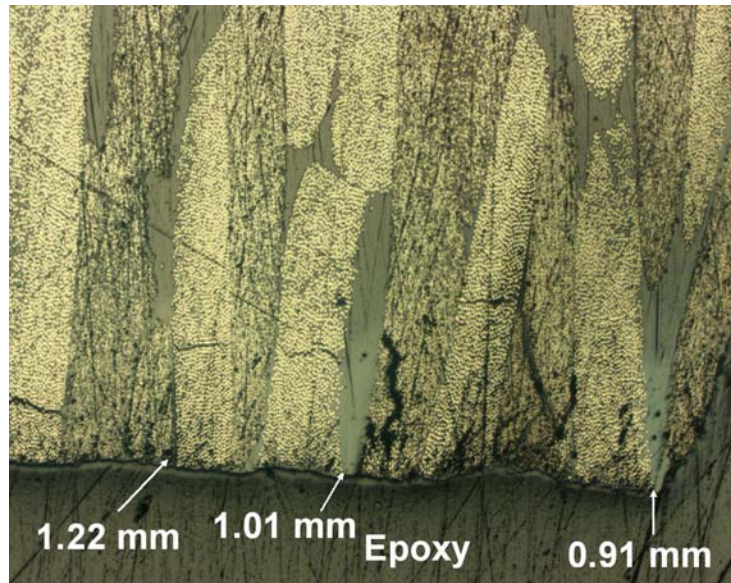


Figure 70: Oxidation layer growth on a specimen aged for 500 h at 288°C (cut surface). This shows an average oxidation layer of 1.04 mm thick.

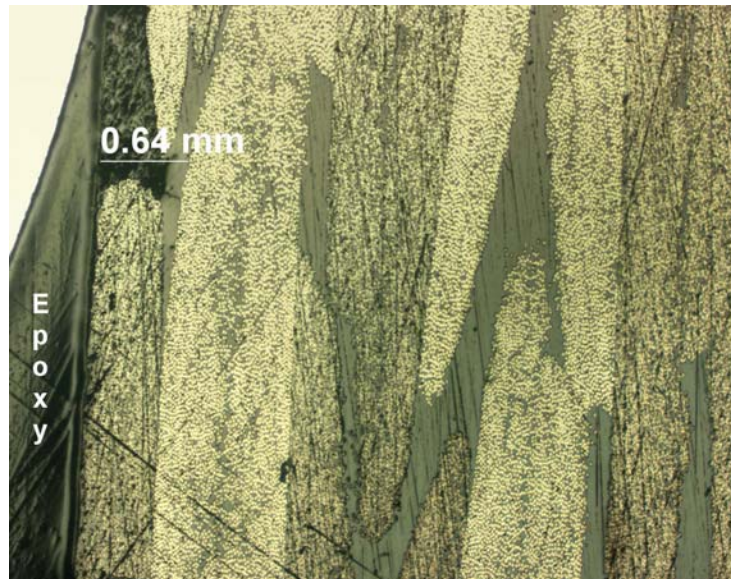


Figure 71: Oxidation layer growth on a specimen aged for 500 h at 288°C (uncut surface).

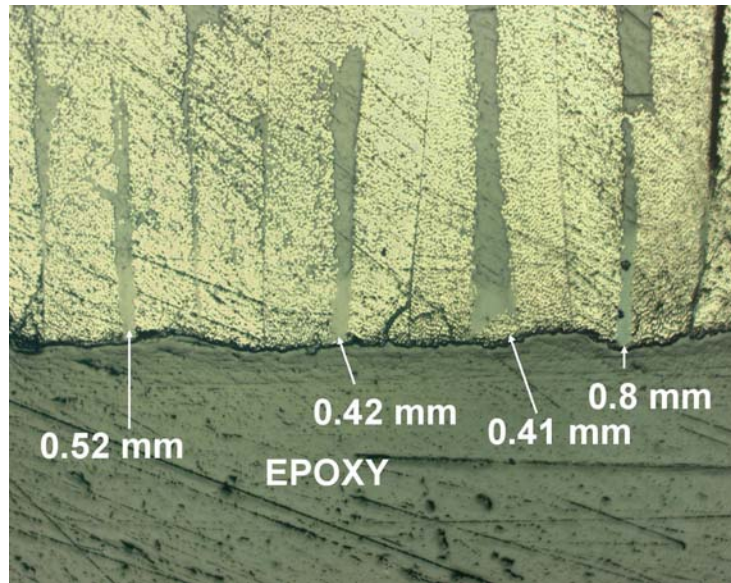


Figure 72: Oxidation layer growth on a specimen aged for 100 h at 288°C (cut surface). This shows an average oxidation layer of 0.42 mm thick.

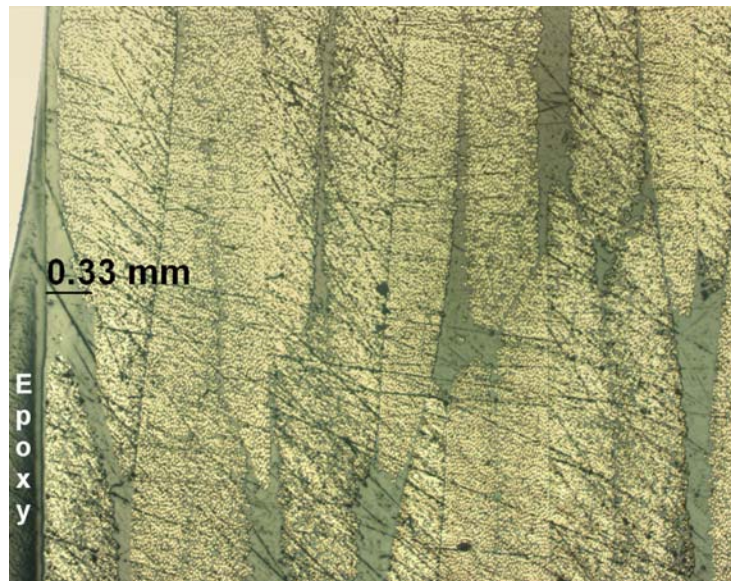


Figure 73: Oxidation layer growth on a specimen aged for 100 h at 288°C (uncut surface).

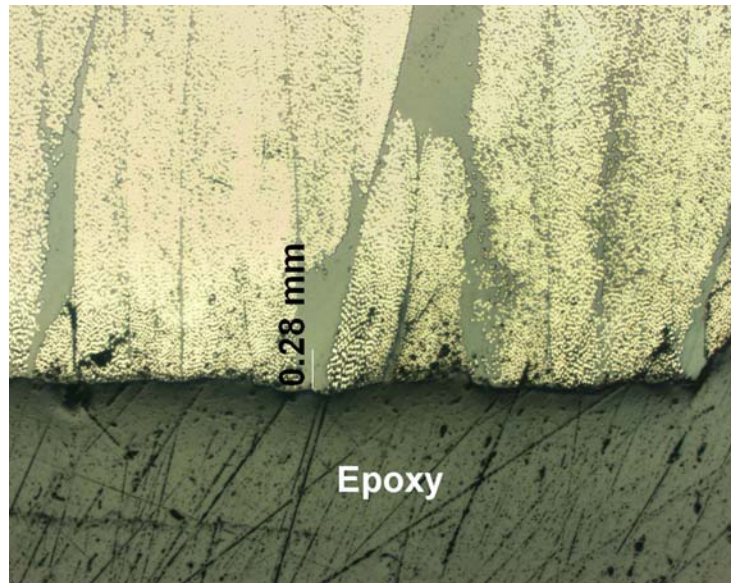


Figure 74: Oxidation layer growth on a specimen aged for 50 h at 288°C (cut surface). This shows an oxidation layer of 0.28 mm thick.

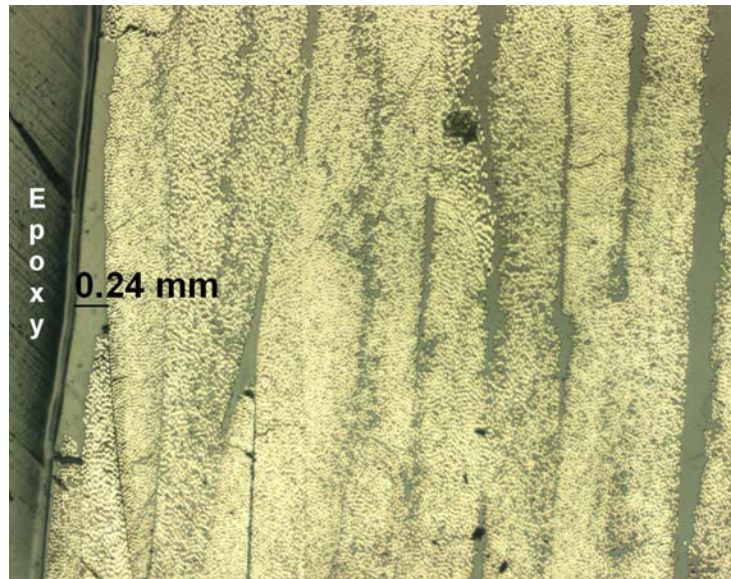


Figure 75: Oxidation layer growth on a specimen aged for 50 h at 288°C (uncut surface).

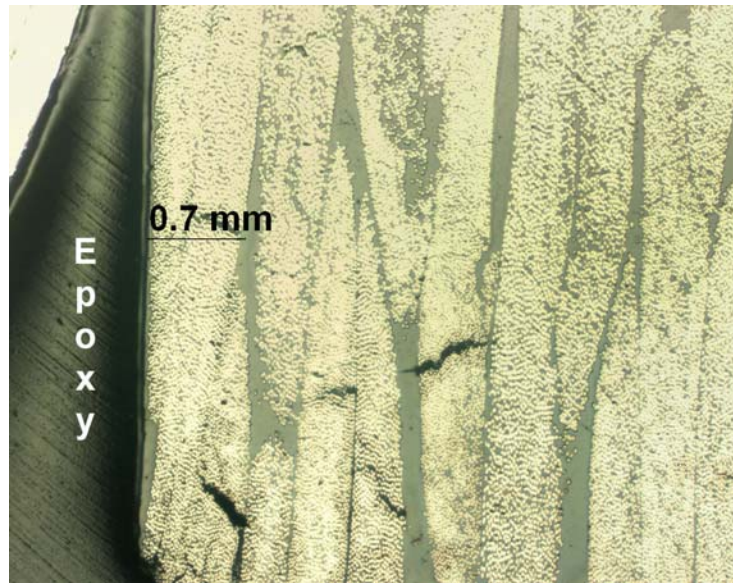


Figure 76: Oxidation layer growth on a specimen aged for 50 h at 288°C (uncut surface).

Vita

Ensign Christopher A. Back graduated from West Springfield High School in Springfield, Virginia. He entered undergraduate studies at the Virginia Military Institute in Lexington, Virginia where he graduated with a Bachelor of Science degree in Mechanical Engineering in May 2006. He was commissioned through the Naval Reserved Officer Training Corps (NROTC) unit at the Virginia Military Institute where he was recognized as a Distinguished Graduate and nominated for a Regular Commission.

His first assignment was at Wright-Patterson Air Force Base as a student at the Air Force Institute of Technology Graduate School of Engineering and Management June 2006 where he is pursuing a Masters Degree in Aeronautical Engineering. Upon graduation, he will be reporting to Pensacola, FL for Naval flight training.

REPORT DOCUMENTATION PAGE				Form Approved OMB No. 074-0188	
<p>The public reporting burden for this collection of information is estimated to average 1 hour per response, including the time for reviewing instructions, searching existing data sources, gathering and maintaining the data needed, and completing and reviewing the collection of information. Send comments regarding this burden estimate or any other aspect of the collection of information, including suggestions for reducing this burden to Department of Defense, Washington Headquarters Services, Directorate for Information Operations and Reports (0704-0188), 1215 Jefferson Davis Highway, Suite 1204, Arlington, VA 22202-4302. Respondents should be aware that notwithstanding any other provision of law, no person shall be subject to a penalty for failing to comply with a collection of information if it does not display a currently valid OMB control number.</p> <p>PLEASE DO NOT RETURN YOUR FORM TO THE ABOVE ADDRESS.</p>					
1. REPORT DATE (DD-MM-YYYY) 14-06-2007		2. REPORT TYPE Master's Thesis		3. DATES COVERED (From – To) Jun 06 – Jun 07	
4. TITLE AND SUBTITLE EFFECTS OF PRIOR AGING ON THE CREEP RESPONSE OF CARBON FIBER REINFORCED PMR-15 NEAT RESIN AT 288°C IN AN AIR ENVIRONMENT				5a. CONTRACT NUMBER	
				5b. GRANT NUMBER	
				5c. PROGRAM ELEMENT NUMBER	
				5d. PROJECT NUMBER	
6. AUTHOR(S) Back, Christopher, A., ENS, USN				5e. TASK NUMBER	
				5f. WORK UNIT NUMBER	
7. PERFORMING ORGANIZATION NAMES(S) AND ADDRESS(S) Air Force Institute of Technology Graduate School of Engineering and Management (AFIT/EN) 2950 Hobson Way, Building 640 WPAFB OH 45433-8865				8. PERFORMING ORGANIZATION REPORT NUMBER AFIT/GAE/ENY/07-J02	
9. SPONSORING/MONITORING AGENCY NAME(S) AND ADDRESS(ES) AFOSR/NL AFRL/MLBCM AFRL/MLBCM Attn: Dr. Charles Y-C Lee Attn: Greg Schoeppner Attn: Richard Hall 875 Randolph St 2941 P Street 2941 P Street Arlington, VA 22203-1954 WPAFB, OH, 45433, WPAFB, OH, 45433, Comm No: (703)696-7779 (937)255-9072 (937)255-9097				10. SPONSOR/MONITOR'S ACRONYM(S)	
				11. SPONSOR/MONITOR'S REPORT NUMBER(S)	
12. DISTRIBUTION/AVAILABILITY STATEMENT APPROVED FOR PUBLIC RELEASE; DISTRIBUTION UNLIMITED.					
13. SUPPLEMENTARY NOTES					
14. ABSTRACT <p>The mechanical response of carbon fiber reinforced PMR-15 neat resin with a ± 45 fiber orientation was investigated at 288°C. Mechanical testing was performed on unaged specimens and specimens that were aged up to 1000 hours in an air environment. Tensile tests were performed to determine Young's modulus of elasticity and Ultimate Tensile Strength. Creep tests were performed at creep stress levels of 30 and 60 MPa. Creep periods of at least 25 h in duration were followed by recovery at zero stress. Duration of the recovery period was at least twice the time of the creep period. Oxidation layer growth and weight loss measurements were also taken as a function of aging time. Unaged test specimens accumulated creep strains of ~1.7% at 60 MPa and ~1.1% at 30 MPa. After 1000 h of aging the test specimens accumulated creep strains of ~0.5% at 60 MPa and ~0.1% at 30 MPa. It is clear that with prior aging time, there is a reduction in creep strain accumulation. Prior aging did not appear to significantly influence recovery at zero stress. The experimental data revealed that weight loss and oxidation layer growth increase with increasing aging time at elevated temperature. After 500 h of aging, the rectangular ± 45 carbon fiber reinforced PMR-15 composite had ~0.95% weight loss compared to ~0.5% at 250 h. The oxidation layer growth at 500 h was ~0.97 mm for the cut surface and ~0.32 mm for the molded surface. After 1000 h the oxidation layer growth was ~1.5 mm for the cut surface and ~0.33 mm for the molded surface. It is apparent that the cut side of the specimen with the fibers exposed to the oxidizing environment experiences a thicker oxidation layer growth.</p>					
15. SUBJECT TERMS Composite, T650-35 Carbon Fiber/PMR-15, creep, recovery, weight loss, oxidation growth, prior aging history					
16. SECURITY CLASSIFICATION OF:		17. LIMITATION OF ABSTRACT UU	18. NUMBER OF PAGES 124	19a. NAME OF RESPONSIBLE PERSON Dr. Marina B. Ruggles-Wrenn	
REPORT U	ABSTRACT U			c. THIS PAGE U	19b. TELEPHONE NUMBER (Include area code) (937) 255-3636, ext 4641 (marina.ruggles-wrenn@afit.edu)